Methods[1]

Expedition 311 Scientists[2]

Chapter contents

Introduction

Information assembled in this chapter will help the reader understand the basis for our preliminary conclusions and also enable the interested investigator to identify data and select samples for further analysis. This information concerns only shipboard operations and analyses described in the site chapters. Methods used by various investigators for shore-based analyses of Expedition 311 data will be described in individual publications in various professional journals and the "Research results" section of this *Proceedings* volume. This introductory section provides an overview of operations, curatorial conventions, and general core handling and analysis.

Site locations

At all Expedition 311 sites, Global Positioning System (GPS) coordinates from precruise site surveys were used to position the vessel on site. The only seismic system used during the cruise was the 3.5 kHz profiler, which was monitored on the approach to each site to determine water depth prior to spudding. Once the vessel was positioned at a site, the thrusters were lowered and a reference beacon was deployed. Although the automated stationkeeping system of the vessel usually uses GPS data, the beacon provides a backup reference in case of problems with the transmission of satellite data. The final site position was the mean position calculated from the GPS data collected over the time that the site was occupied.

Drilling operations

Two standard coring systems were used during Expedition 311: the advanced piston corer (APC) and the extended core barrel (XCB). These standard coring systems and their characteristics are summarized in the "Explanatory Notes" chapters of various Ocean Drilling Program (ODP) *Initial Reports* volumes. Most APC/XCB cored intervals were ~9.6 m long, which is the length of a standard core barrel. In a few cases, the drill string was "washed ahead" without recovering sediments to advance the drill bit to a target depth, where core recovery was resumed. In addition to these conventional coring tools, several pressure coring systems were used (see **"Pressure coring"**). In situ temperature was measured at prescribed depth intervals at each site (see **"Physical properties"**). Logs of geophysical parameters were obtained dur-

[1] Expedition 311 Scientists, 2006. Methods. *In* Riedel, M., Collett, T.S., Malone, M.J., and the Expedition 311 Scientists. *Proc. IODP,* 311: Washington, DC (Integrated Ocean Drilling Program Management International, Inc.). doi:10.2204/iodp.proc.311.102.2006
[2] **Expedition 311 Scientists' addresses.**

doi:10.2204/iodp.proc.311.102.2006

ing logging while drilling (LWD) and measurement while drilling (MWD) and using wireline tools (see "Downhole logging").

Drilled intervals are referred to in meters below rig floor (mbrf), which is measured from the kelly bushing on the rig floor to the bottom of the drill pipe, and meters below seafloor (mbsf), which is calculated. When sediments of substantial thickness cover the seafloor, the meters below rig floor depth of the seafloor is determined with a mudline core, assuming 100% recovery for the cored interval in the first core. Water depth is calculated by subtracting the distance from the rig floor to sea level from the mudline measurement in meters below rig floor. This water depth usually differs from precision depth recorder measurements by a few to several meters. The meters below seafloor depths of core tops are determined by subtracting the seafloor depth (meters below rig floor) from the core top depth (meters below rig floor). The resulting core top data in meters below seafloor are the ultimate reference for any further depth calculation procedures.

Drilling-induced core deformation

When cores are split, many show signs of significant sediment disturbance, including the concave-downward appearance of originally horizontal bedding, haphazard mixing of lumps of different lithologies (mainly at the tops of cores), fluidization, and flow-in. Core deformation may also occur during retrieval because of changes in pressure and temperature as the core is raised and during cutting and core handling on deck. These changes were particularly important during Expedition 311 because temperature and pressure variations induce exsolution of gas from interstitial water (IW) and dissociation of gas hydrate, which also releases large amounts of gas. The "Lithostratigraphy" section in each site chapter discusses characteristics of cores that indicate this type of disturbance and can, therefore, serve as proxies for the presence of gas hydrate.

Curatorial procedures and sample depth calculations

Numbering of sites, holes, cores, and samples follows standard Integrated Ocean Drilling Program (IODP) conventions (Fig. F1). A full curatorial identifier for a sample consists of the expedition, site, hole, core number, core type, section number, and interval in centimeters measured from the top of the core section. For example, a sample identification of 311-U1325A-1H-1, 10–12 cm, represents a sample removed from the interval between 10 and 12 cm below the top of Section 1 of Core 1 (H designates that this core was taken with the APC system) in Hole U1325A during Expedition 311. Cored intervals are also referred to in "curatorial" meters below seafloor. The mbsf of a sample is calculated by adding the depth of the sample below the section top and the lengths of all higher sections in the core to the core top datum measured with the drill string.

In general, sediment core from less than a few hundred meters below seafloor may, in some cases, expand upon recovery (typically 10% in the upper 300 m), and its length may not necessarily match the drilled interval. Such core expansion can be greater for gassy cores like the ones recovered during Expedition 311. In addition, a coring gap is typically present between cores. Thus, a discrepancy may exist between the drilling mbsf and the curatorial mbsf. For instance, the curatorial mbsf of a sample taken from the bottom of a core may be larger than that of a sample from the top of the subsequent core, whereas the latter corresponds to the drilled core-top datum.

If a core has incomplete recovery, all cored material is assumed to originate from the top of the drilled interval as a continuous section for curation purposes. The true depth interval within the cored interval is not known. This should be considered as a sampling uncertainty in age-depth analysis and correlation of core data with downhole logging data.

Core handling and analysis

Cores were generally handled according to ODP/IODP standard core handling procedures as described in previous ODP *Initial Reports* volumes and the *Shipboard Scientist's Handbook* (ODP Science Services, 2006), with modifications required to quickly identify intervals containing gas hydrates and to maintain approximately aseptic conditions for microbiological sampling. Precautions were also taken to identify and safely deal with hydrogen sulfide gas.

To identify gas hydrates, cores were scanned with both handheld and track-mounted infrared (IR) cameras to identify intervals with significant thermal anomalies. This is explained further in "Physical properties" and in individual site chapters. Some suspected gas hydrate–bearing intervals were cut and immediately stored in liquid nitrogen–filled dewars on the catwalk. In addition, some gas hydrate samples that self-extruded from the liner were collected for various shipboard geochemical analyses.

Cores identified for microbiological sampling were cored with drilling fluid spiked with contamination tracers (see "Microbiology"). When these cores were brought on board, appropriate sections for microbiological studies were taken on the catwalk and then

transferred immediately to the microbiology laboratory on the forecastle deck. In intervals of more intense microbiological interest, an entire 1.5 m section was identified on the catwalk for rapid microbiological processing. Once the section was selected, it was labeled with a red permanent marker with orientation and section number and removed from the core. Ends of the removed section were covered with plastic caps, but not sealed, and the section was carried into the hold refrigerator, which was set to ~4°C and served as a microbiology cold room for microbiology and geochemistry sampling.

Gas samples for routine shipboard safety and pollution-prevention purposes were collected on the catwalk for shipboard and shore-based studies (see **"Organic geochemistry"**). Whole rounds (10–30 cm long) were taken for interstitial water analysis (see **"Interstitial water geochemistry"**). Additional whole-round samples were also collected for shore-based physical properties and organic geochemistry studies. The cores were then compressed with a plunger to remove large voids and cut into 1.5 m sections. The remaining cut sections were transferred to the core laboratory for further processing.

Whole-round core sections not used for microbiological sampling were run through the multisensor track (MST), and thermal conductivity measurements were performed (see **"Physical properties"**). The cores were then split into working and archive halves (from bottom to top). Investigators should be aware that older material may have been transported upward on the split face of each section.

The archive-half sections were scanned on the digital imaging system (DIS) and measured for color reflectance on the archive multisensor track (AMST). Select intervals also were measured with the AMST point susceptibility meter. Visual core descriptions (VCDs) of the archive halves were prepared, augmented by smear slides and thin sections (see **"Lithostratigraphy"**). The archive halves were then run through the cryogenic magnetometer (see **"Physical properties"**) and photographed with color film one whole core at a time. Digital close-up photographs were taken of particular features for illustrations in site summary reports, as requested by scientists.

P-wave velocity, shear strength, and electrical resistivity were measured on split-core sections of the working half. The working half was then sampled both for shipboard analyses, such as physical properties, carbonate, and bulk X-ray diffraction (XRD) mineralogy, and for shore-based studies (see **"Physical properties"**). Both halves of the core were then put into labeled plastic tubes, sealed, and placed in cold storage space aboard the ship.

Two 20 ft refrigerated containers were mounted on the vessel (on the lab stack roof and on top of the core technician shop) during Expedition 311 for pressure core processing and analyses. The lab stack van (hereafter referred to as the pressure coring system [PCS] van) contained the PCS degassing manifold, a vertical gamma ray attenuation (GRA) density logger, and an Agilent microgas chromatograph. The core technician shop container (hereafter referred to as the HYACINTH van) housed the HYACINTH transfer chamber and a *P*-wave velocity, GRA, and linear X-ray core logger.

At the end of the expedition, the cores were transferred from the ship into refrigerated containers and shipped to the IODP Gulf Coast Core Repository in College Station, Texas, USA. Gas hydrate samples (preserved in liquid nitrogen or pressure vessels) and HYACINTH pressure cores were transferred to the Pacific Geoscience Centre of the Geological Survey of Canada, Sidney, British Columbia, for inventory and shore-based analyses prior to distribution to approved investigators.

Lithostratigraphy

The techniques and procedures used to describe, analyze, and name the lithologies recovered during Expedition 311 are described below. These include VCDs, smear slide and thin section descriptions, XRD analyses, color spectrophotometry, and high-resolution digital color imaging. Any significant deviations from the procedures outlined in this section are discussed in the individual site chapters.

Sediment classification

The naming conventions adopted during Expedition 311 follow a slightly modified version of the ODP sediment classification scheme of Mazzullo et al. (1988). We do not distinguish mixed sediments but only siliciclastic and/or volcaniclastic (>50% components), biogenic (>50% components), and diagenetic (>50% components) sediments. Principal names were assigned to sediments based on composition, texture, and degree of lithification as determined primarily from visual description and smear slide analyses. Modifiers to the principal name were determined based on both the abundance and type of the nonprincipal component or components (e.g., siliciclastic or biogenic). Major modifiers, those components that compose >25% of the sediment, precede the principal name and are listed in order of increasing abundance. Genetic terms, such as pelagic, neritic, and debris flow, were not used in classifying the sediments and are used only in geologic interpreta-

tions of the sedimentary sequence. Minor modifiers, those components that compose 10%–25% of the sediment, follow the principal name; they are preceded by the term "with" and are listed in order of increasing abundance.

Siliciclastic sediments

For sediments and rocks composed of >50% siliciclastic components, the principal name was determined by the texture of the grains. Textural names were derived from the Udden-Wentworth grain-size scale (Wentworth, 1922) (Fig. F2). In this classification scheme, the term "clay" is independent of mineralogy and refers to all siliciclastic grains <3.9 µm in size, regardless of composition. The relative proportion of different grain sizes was determined by visual percentage estimation using the comparison chart of Terry and Chilingar (1955). Once the relative proportions were determined, a modified Shepard (1954) classification scheme was used to assign the principal name (Fig. F3). Clay, silt, and sand are the principal names in the Shepard diagram. If any component exceeds 25% of the total siliciclastic grains, it becomes a modifier to the principal name. For example, sediment composed of 10% clay and 90% silt is simply a silt, whereas sediment composed of 30% clay and 70% silt is a clayey silt.

The lithologic classification of sediments was refined by adding major and minor modifiers. The most common uses of major and minor modifiers are to describe the composition and textures of grain types that are present in major (>25%) and minor (10%–25%) proportions.

Biogenic sediments

Unlike siliciclastic sediments, biogenic sediments, defined as containing >50% biogenic components, are not described based on texture. Rather, the principal name for all biogenic sediments is ooze. Thus, a sediment with 65% sand-sized foraminifers and 35% siliciclastic clay is called clayey foraminifer ooze.

Authigenic carbonates

During Expedition 311, unlithified, partly lithified, and lithified authigenic carbonates (e.g., aragonite, calcite, dolomite, siderite, and rhodochrosite) were encountered as nodules or irregular precipitates. Different symbols were given for unlithified carbonate cements and for lithified/partly lithified carbonates (Fig. F4). These symbols appear in the Diagenesis column of the VCD forms ("barrel sheets") (Fig. F5). In cases where it was possible to clearly identify the carbonate mineralogy, it was given in the VCD form. Carbonates are mostly composed of tiny calcite and/or dolomite crystals (Fig. F6). They are classified according to their mineralogy, grain size (<4 µm: micritic; 4–63 µm: microcrystalline), and degree of lithification (unlithified, partly lithified, or lithified carbonate). The principal name is followed (preceded by "with") by any modifier (>10% component). For example, a lithified carbonate composed of crystals <4 µm long with 10% quartz would be named micritic lithified carbonate with quartz.

Firmness

Calcareous sediments and rocks are divided into three classes of firmness:

1. Unlithified = soft sediments that readily deform under the pressure of a fingernail or spatula.
2. Partly lithified = firm but friable sediments that can be scratched with a fingernail or the edge of a spatula.
3. Lithified = hard, nonfriable cemented rocks that are difficult or impossible to scratch with a fingernail or the edge of a spatula.

Visual core descriptions

Detailed sedimentologic observations and descriptions were recorded manually for each core section on VCD forms. A wide variety of features that characterize the sediments were recorded, including lithology, bioturbation, sedimentary structure, fossils, core disturbance, diagenetic precipitates, samples, and color. Compositional data were obtained from smear slides. The color (hue and chroma) of the sediments was determined by both color spectrophotometry and by visual comparison with the Munsell soil color chart (Munsell Color Company, 1975). This information was synthesized for each core in AppleCORE (v9.4a), which generates a one-page graphic description (barrel sheet) of each core (Fig. F5). Barrel sheet symbols used during Expedition 311 are described in Figure F4. For more detailed information on sedimentary features, VCD forms are available from IODP upon request.

Of particular interest during Expedition 311 were the visual indications of disruption to the sediment caused by the dissociation of gas hydrate in the recovered sediment noted in the Disturbance column. Massive forms of gas hydrate were removed on the catwalk prior to core description and sampled intervals were noted in the barrel sheets. The two primary textures identified as resulting from the dissociation of gas hydrate are soupy and mousselike. Soupy sediments are watery, homogeneous, and fluidized (Fig. F7). These sediments are often associated with centimeter-scale void spaces in the core because they are able to flow from their original position during core

recovery and therefore retain no original sedimentary structures. Sediments with mousselike texture contain small millimeter-scale voids and obscure primary sedimentary structures (Fig. F8). These sediments are often wet, soft, and deform plastically under slight pressure from one finger.

Mousselike and soupy textures related to the dissociation of gas hydrate not sampled prior to description were noted on the barrel sheets. Remarks made on barrel sheets for each core describe any additional potential indications of gas hydrate near the sampled intervals, including the presence of dry, flaky sediment that may have been dewatered by the formation of gas hydrate nearby.

Lithology and grain size

The lithology of the described sediments is represented in the Graphic Lithology column of the barrel sheets using the symbols shown in Figure F4. A maximum of three different lithologies (for interbedded sediments) or three different components (for mixed sediments) can be represented within the same core interval. Intervals >1 cm in thickness can be portrayed accurately in the lithology column. Percentages are rounded to the nearest 10%, and lithologies that constitute <10% of the core are generally not shown but are listed in the Description column.

Bioturbation

Visible bioturbation was classified into four intensity levels based on the degree of disturbance of the physical sedimentary structures:

1. Absent = no bioturbation; all sedimentary structures are preserved.
2. Rare = isolated trace fossils; up to 10% of sedimentary structures are disrupted.
3. Moderate = ~10%–40% disrupted sedimentary structures; burrows are generally isolated but may overlap locally.
4. Abundant = bedding completely disturbed; burrows are still intact in places.

These categories are based on the ichnofossil indexes of Droser and Bottjer (1986) and are illustrated with graphic symbols in the Bioturbation column on the barrel sheets. Visual recognition of bioturbation was often limited in homogeneous sediments, particularly in hemipelagic clay zones without sulfide material.

Sedimentary structures

Each type of sedimentary structure and its exact location is displayed in the Structure column of the barrel sheet. Symbols used to note the wide variety of sedimentary structures encountered throughout Expedition 311 are listed in the barrel sheet legend (Fig. F4). Some of the more common structures observed were parallel bedding, fining-upward sequences, and the mottled appearance of sulfide-rich layers.

Fossils

The presence of macroscopic fossils (including aggregates of sponge spicules, large foraminifers (~1 mm), bivalve shell fragments, preserved whole bivalve shells, and gastropods) is displayed in the Fossils column on the barrel sheets.

Sediment disturbance

Drilling-related sediment disturbance is recorded in the Disturbance column. Separate terms describe the degree of drilling disturbance in soft and firm sediments:

- Slightly disturbed = bedding contacts are slightly deformed.
- Moderately disturbed = bedding contacts have undergone extreme bowing.
- Highly disturbed = bedding is completely deformed as flow-in, coring/drilling slough, and other soft sediment stretching and/or compressional shearing structures attributed to coring/drilling.

Further coring/drilling-related sediment disturbance observed includes

- Drilling "biscuits" (drilling slurry surrounding an intact or slightly fractured dense mass of sediment) and
- Gas-expansion cracks (cracking and pushing apart of sediments resulting from the expansion of gases during core retrieval). This process produces many, mostly centimeter-scale voids.

Gas hydrate–related sediment disturbance is recorded in the Disturbance column. Separate terms describe the degree of gas hydrate–related sediment disturbance:

- Mousselike = texture is soft and deforms plastically under slight pressure. Some primary sedimentary structure is preserved.
- Soupy = intervals are water saturated and have lost all primary sedimentary structures.

Cores recovered from gas- and gas hydrate–bearing sediments are often disturbed by gas expansion and fracturing. In cases where it was possible to distinguish between disturbance of the core resulting from drilling and disturbance resulting from gas expansion, notes were made in the Comments column of the barrel sheets listing the depths at which gas fracturing was observed.

Diagenesis

The relative positions of features that are related to diagenesis are displayed in the Diagenesis column on the barrel sheets. These are mineral precipitates (e.g., iron sulfide and carbonates).

Samples

The position of whole-round samples, as well as smear slides and samples taken to support and verify the observations of the smear slide and thin section analyses, are indicated in the Sample column on the barrel sheets. The abbreviations are as follows:

SS = smear slide.
THS = thin section.
XRD = X-ray diffraction.
IW = interstitial water.
MB = microbiology.
HYD = gas hydrate.
HS = headspace gas (only used when complete whole-round sample was taken).
PAL = micropaleontology.
OG = organic geochemistry.
WRP = whole-round physical property.

Analysis of smear slides and thin sections

Smear slides were prepared from the archive halves of the cores. With a toothpick, a small amount of sediment was taken and put on a 25 mm × 75 mm glass slide, homogenized, and dispersed over the slide with a drop of deionized water. The sample was then dried on a hot plate at ~80°C. A drop of Norland optical adhesive and a 22 mm × 22 mm cover glass were added. The smear slide was fixed in an ultraviolet light box. With a transmitted light petrographic microscope, both the grain size and abundance of dominant components in a sample were determined. Abundance was estimated with the help of a comparison chart for visual percentage estimation (after Terry and Chilingar, 1955). Note that smear slide analyses tend to underestimate the amount of sand-sized and larger grains because these grains are difficult to incorporate into the slide. Table **T1** is an example of data obtained from smear slide analyses and was generated using a spreadsheet. This table includes information about the location of samples, their grain-size distribution, and whether the sample represents the dominant (D) or the minor (M) lithology in the core. Additionally, it provides estimates of the major mineralogical and biological components from the examination of each smear slide. The presence of authigenic minerals, such as iron sulfides or carbonates, as well as the presence of rare trace minerals, was noted in the Comments column. The mineralogy of the major smear slide components was also validated by XRD analyses, and the relative proportion of carbonate and noncarbonate material was validated by chemical analysis of the sediments (see **"Organic geochemistry"**).

Thin sections were taken from several authigenic carbonate precipitates. Tables summarizing thin section data, such as grain size and relative abundance of sedimentary components, were also generated using spreadsheets and are available in **"Core descriptions."** A Zeiss Axioplan microscope equipped with a digital camera was used to obtain images of the smear slides and thin sections on board. Digital photomicrographs were obtained and stored as TIFF files. Thin section results complement the VCDs.

X-ray diffraction analyses

XRD analyses supported and verified smear slide and thin section descriptions. Each sample was freeze-dried, ground, and mounted with a random orientation into an aluminum sample holder. These measurements were made on a Philips PW-1729 X-ray diffractometer with a CuK_α source (40 kV and 35 mA) and Ni filter. Peak intensities were converted to values appropriate for a fixed slit width. The goniometer scan was performed from 2° to 70°2θ at a scan rate of 1.2°/min (step = 0.01°, count time = 0.5 s). Diffractograms were peak-corrected to match the (100) quartz peak at 3.343 Å. Common minerals were identified based on their peak position and relative intensities in the diffractogram using MacDiff (v4.1.1) (R. Petschick; **www.geologie.uni-frankfurt.de/Staff/Homepages/Petschick/RainerE.html**).

Color reflectance spectrophotometry

In addition to visual estimates of color, reflectance of visible light from soft sediment cores was measured using a Minolta spectrophotometer (model CM-2002) mounted on the AMST. The AMST measures the archive half of each core section and provides a high-resolution record of downcore color variations for the visible wavelengths (400–700 nm). Freshly split cores were covered with clear plastic wrap and placed on the AMST. Measurements were taken at 5.0 cm spacing. The AMST skips empty intervals and intervals where the core surface is well below the level of the core liner but does not recognize relatively small cracks or disturbed areas of core. Thus, AMST data may contain spurious measurements that should, to the extent possible, be edited out of the data set before use. Each measurement recorded consists of 31 separate determinations of reflectance in 10 nm wide spectral bands from 400 to 700 nm. Additional detailed information about the measure-

ment and interpretation of spectral data with the Minolta spectrophotometer can be found in Balsam et al. (1997, 1998) and Balsam and Damuth (2000).

Digital color imaging

All core sections were imaged using the GeoTek X-Y DIS immediately after being split and scraped. We found it particularly useful to scrape the cores immediately prior to imaging to capture the ephemeral nature of some sedimentary features, particularly sulfide precipitates, which become oxidized within minutes of core splitting. The effect of oxidation can be seen in Figure **F16** in the "Site U1328" chapter. It is worth noting that this fresh scraping did not occur prior to the regular photo imaging, which can take place between 30 and 60 min after scraping. Consequently, some of the sedimentary details may be lost using the more conventional archive core–table photographs. For this reason, cores were scraped before close-up photographs were taken. Some problems were encountered with occasional system crashes, which were probably a result of automated network uploading of files during image transfer from the camera hardware to the local computer.

In the DIS core section dialogue box, we set the section subbottom depth at zero for Section 1 and let it automatically increment down the remaining sections for each core. All images were acquired at a crosscore and downcore resolution of 100 pixels/cm. At the beginning of Expedition 311 coring operations, the aperture was fixed at a value that would image most cores without the need for further adjustment. It was, therefore, set to f/6.7 for Sites U1327 and U1329, which maximized the dynamic range for most of the core sections. At the beginning of Hole U1325B, the aperture was changed to f/5.6. Care was taken to ensure that the system was correctly calibrated using the "white tile" procedure and that the camera position was correctly set up. Output from the DIS corresponds to an uncompressed TIFF file (available upon request) for each scanned section. Additional postprocessing of the color imagery was done to achieve a medium-resolution JPEG image of each section.

Biostratigraphy

During Expedition 311, diatoms were studied to assign preliminary ages to core catcher samples. Samples from within the cores were examined when a more refined age determination was necessary. The timescale of Berggren et al. (1995) was used. The biostratigraphic zones of diatoms are summarized in Figure **F9.**

We used the Neogene North Pacific diatom zones of Akiba (1986) and Yanagisawa and Akiba (1998). Ages for bioevents that define the zones or characterize certain horizons are based primarily on Yanagisawa and Akiba (1998). The biohorizon ages of Barron (1992), Barron and Gladenkov (1995), Koizumi (1992), and Koizumi and Tanimura (1985) were also used.

Unprocessed strewn slides (Akiba, 1986) were prepared for each sample using a 22 mm × 22 mm coverslip and Pleurax mounting medium. The slides were examined on a normal light microscope at a magnification of 400×. One hundred diatom valves were counted for each sample. After counting, the slides were scanned to record the presence of other diatom species missed in the original tally. More than 200 and usually ~1000 valves were observed for samples containing sufficient diatom remains. For those samples that contained <100 diatom valves per slide, all the diatom valves on each slide were counted. Resting spores of *Chaetoceros* were counted separately during the routine count of diatom valves. Approximate numbers of diatom valves per slide were calculated based on the length of scanning lines to get the 100 count. In the site report tables, the "+" symbol indicates the occurrence of <1% diatom valves and/or valve fragments.

Diatom abundance is indicated as

B = barren,
VR = very rare (<100 valves per slide),
R = rare (100–500 valves per slide),
C = common (501–1000 valves per slide),
A = abundant (1001–5000 valves per slide), and
VA = very abundant (>5000 valves per slide).

Based on the degree of breakage and dissolution of diatom valves, the state of diatom preservation is recorded as

VP = very poor,
P = poor,
M = moderate, and
G = good.

Most of the diatom species recognized were tabulated, but several species that occur only sporadically and are not important for biostratigraphic or paleoceanographic studies were included as "miscellaneous" in the tables for each site chapter.

Interstitial water geochemistry

The majority of shipboard IW samples were obtained on 5 to 30 cm long whole-round cores that were collected according to the following scheme. Generally, routine samples were collected from one of the holes

at a frequency of approximately four samples per core from the seafloor to the sulfate/methane interface (SMI), followed by a sampling resolution of three whole-round samples in the first core below the SMI, two whole-round samples per core to a depth of two cores below the bottom-simulating reflector (BSR), and one sample per core below that to the total depth of the hole. These whole-round samples were cut on the catwalk, capped, and taken to the laboratory for immediate processing. Samples were taken at higher resolution (three to four samples per section) in the upper 15 m of holes dedicated for microbiological sampling. During high-resolution sampling and when there were too many IW samples to process immediately, capped whole-round core sections were stored under a nitrogen atmosphere until they were squeezed, which occurred no later than 12 h after core retrieval. Gloves were used during sample processing.

After extrusion from the core liner, the surface of each whole-round core sample was carefully scraped with a clean spatula to remove potential contamination from seawater and sediment smearing in the borehole. In APC cores, 1 cm from the outer diameter, top, and bottom faces was removed. In XCB cores, where borehole contamination is higher, as much as 90% of the sediment was removed from each whole-round sample. In rare cases, the entire whole-round sample had to be discarded. The remaining sediment (~50–300 cm^3) was placed into a titanium squeezer, modified after the stainless steel squeezer of Manheim and Sayles (1974). In most cases, gauge pressures up to 20 MPa were applied using a laboratory hydraulic press to extract interstitial water. In a few very dry cores recovered from greater depths, gauge pressure up to a maximum of 30 MPa was applied. Interstitial water was passed through a prewashed Whatman number 1 filter fitted above a titanium screen, filtered through a 0.2 µM polysulfone disposable filter, and subsequently extruded into a prewashed (10% HCl) plastic syringe attached to the bottom of the squeezer assembly. In most cases, 15–40 cm^3 of pore water was collected from each sample, which required squeezing the sediment for 20–40 min.

IW subsamples were first collected in a 10 mL syringe and immediately analyzed for salinity, pH, sulfate, and alkalinity. Using the 10 mL syringe avoided air bubbles, minimized contamination of this fraction of the interstitial water by dissolved oxygen, and allowed for efficient and rapid subsampling during sediment squeezing. After collection of the first 10 mL, a 50 mL syringe was used to collect the remaining interstitial water.

Collection of subsamples for shore-based analyses

Subsamples were collected in glass vials and ampules for shore-based isotopic characterization of the interstitial water (oxygen and deuterium) and dissolved metabolites (e.g., dissolved inorganic and organic carbon, sulfate, and sulfide). In addition, subsamples were collected for analyses of dissolved volatile fatty acids (in glass vials and frozen), halogens, minor and trace metal constituents, and their isotopes (in acid-cleaned plastic containers).

Shipboard interstitial water analyses

IW samples were analyzed for routine shipboard measurements according to standard procedures (Gieskes et al., 1991). Salinity was measured as total dissolved solids using a Goldberg optical handheld refractometer. The pH was determined by ion-selective electrode. Alkalinity was determined by Gran titration with a Metrohm autotitrator. Sulfate (SO_4) concentration was measured by manual dilution and manual injection into a Dionex DX-120 ion chromatograph immediately after IW collection. A subsample was treated with $CdNO_3$ solution, which precipitated the sulfide as CdS for subsequent shore-based concentration and S isotope analyses; this treatment prevented the sulfide from oxidizing to sulfate.

High-precision chloride concentrations were determined by Mohr titration using silver nitrate ($AgNO_3$). Quantification was based on comparison with International Association of the Physical Sciences of the Ocean (IAPSO) standard seawater. The values were corrected for the presence of other halogens assuming seawater ratios, as detailed by Gieskes et al. (1991). Dissolved calcium was either measured by titration with ethylene-bis-(oxyethylenenitrilo)-tetra-acetic acid and corrected for interference by magnesium or by inductively coupled plasma–atomic emission spectroscopy (ICP-AES). Similarly, dissolved magnesium was obtained by titration with disodium ethylenediamine-tetra-acetate and corrected for Ca or measured by ICP-AES. The analytical procedures and calculations involved in the alkaline earth analyses are detailed in Gieskes et al. (1991).

Dissolved phosphate (PO_4) and ammonium (NH_4) concentrations were determined by spectrophotometric methods using a Milton Roy Spectronic 301 spectrophotometer using cuvettes or a Milton Roy sample introduction system (Gieskes et al., 1991).

Major and selected minor element concentrations were obtained by ICP-AES with a Jobin Yvon JY2000 spectrometer using dilutions of IAPSO standard sea-

water as calibration standards. For calcium, magnesium, sodium, and potassium analyses, samples and standards were diluted 1:5 with nanopure water followed by a 1:10 dilution with a 2.5% HNO_3 (by volume) matrix solution with 10 ppm yttrium as an internal standard. The two analytical methods for Ca and Mg (titration versus ICP-AES) were compared before coring began. Six water samples were prepared by dilution of IAPSO seawater and analyzed by both the titration and ICP-AES methods for Ca and Mg concentrations. The average percent deviation for Mg concentration between 15 and 54 mM was 1.1% (0.35 mM) and much higher at lower concentrations. For Ca, the average percent deviation between 1 and 10.5 mM was 2.9% (0.1 mM). In addition, at Site U1329 all IW samples were analyzed for Ca and Mg concentrations by both methods. The average deviation for Ca was 15% (0.5 mM) and for Mg it was 4% (1.6 mM). The Ca and Mg concentration data reported in **"Interstitial water geochemistry"** in the "Site U1329" chapter were obtained by the titration method. At all other sites the reported Ca and Mg data were obtained by ICP-AES.

ICP-AES techniques for the minor elements H_4SiO_4, B, Ba, and Li were modified from those described by Murray et al. (2000) by preparing calibration standards in an acidified (2.5% HNO_3 by volume) sodium chloride matrix (35 g NaCl/L). In addition, a 2.5% HNO_3 matrix solution with 10 ppm yttrium (1:10) served as an internal standard to dilute standards and acidified IW samples (Mix, Tiedemann, Blum, et al., 2003).

The reproducibility of techniques (Table **T2**), expressed as 1σ relative standard deviations of the means, was evaluated by replicate analyses of solutions, IAPSO seawater, and/or samples both within a given analytical run and in different analytical runs. The IW data are reported in molar concentration units in the tables of this volume.

Organic geochemistry

The primary focus of the shipboard organic geochemistry program for Expedition 311 was the analysis of volatile hydrocarbon (C_1–C_5) and nonhydrocarbon (i.e., O_2 and N_2) gases from headspace (HS) gas samples, void gas samples, gas samples recovered during PCS degassing experiments, and dissociated gas hydrates. We also measured the inorganic carbon (IC), total carbon (TC), and total nitrogen (TN) content of the sediments. Procedures and instruments used during Expedition 311 are described by Pimmel and Claypool (2001) and are generally the same as those used during most recent ODP legs and IODP expeditions. Brief comments on routine sampling and deviations from standard practice are noted below.

Gas sampling

The IODP gas sampling protocol for pollution prevention and safety as required by IODP safety regulations was modified to better constrain the concentrations of dissolved gases. We followed the approaches that were employed during previous expeditions with a strong biogeochemical focus, in particular ODP Legs 164 (Hoehler et al., 2000) and 201 (Shipboard Scientific Party, 2003a) and IODP Expeditions 301 (Expedition 301 Scientists, 2005) and 307 (Expedition 307 Scientists, 2006). Samples for HS analysis were collected on the opposite core end facing the IW sample to integrate the IW and gas data sets. The sampling frequency was adjusted to the geochemical redox zonation known from previous studies at the northern Cascadia margin to achieve a high depth resolution at the SMI. The overall IW sampling strategy is explained in **"Interstitial water geochemistry."** In general, the HS gas sampling protocol only deviated from the IW sampling strategy at depths greater than two cores below the BSR, where one additional HS sample was taken in between the IW samples.

Upon core retrieval, a 3 mL sediment sample was collected with a 5 mL cut-off plastic syringe from a freshly exposed end of a core section and was extruded into a 20 mL glass serum vial. For this purpose, the plunger was held at the sediment surface while inserting the barrel to avoid trapping air. After withdrawing the syringe, the plunger was advanced slightly to extrude a small amount of sediment. This excess was removed from the end of the syringe barrel to provide an accurate determination of the sediment volume within the syringe. The samples were immediately sealed with a 10 mm thick septum and metal crimp cap. In the laboratory, 1 mL of saturated NaCl was added to the vials and they were shaken vigorously until the sediment plug disintegrated. Prior to gas chromatograph (GC) analysis, the samples were heated to 60°C for at least 20 min. Air blanks incubated with septum fragments confirmed that no hydrocarbons (C_1–C_7) were released from the septum.

Gas samples from voids caused by gas expansion in the core were collected by piercing the core liner and allowing gas to expand into a 60 mL syringe connected to the penetration tool. Gas hydrate gas samples were collected by placing a small (~5 mL) piece of solid gas hydrate into 60 mL syringes, expelling the air, and allowing the gas hydrate to dissociate.

The residual water was preserved for analysis of dissolved constituents (see **"Interstitial water geochemistry"**).

PCS samples were collected in a 60 mL syringe during the degassing experiments (see **"Pressure coring"**). The gas was transferred into serum vials filled with a saturated NaCl solution by displacing the brine with the gas sample. A few gas samples were analyzed to observe changes in the gas composition during core degassing. In cases where numerous samples from a degassing experiment were analyzed, the average value of samples not contaminated with air or helium is reported.

Gas analysis

For HS analysis, 1 to 2 mL of gas was extracted from the vial using a 5 mL plastic syringe. The standard 5 mL gas-tight syringe typically used for IODP GC injections was determined to leak under certain conditions (i.e., blockage of needle with septum), whereas the 5 mL plastic syringe did not. The 1 to 2 mL sample volumes were selected to preserve HS gas for postcruise analyses. Previous ODP legs and IODP expeditions utilized 5 mL injection volumes for the HS analysis. We compared the results from 1 mL and 5 mL injections with the "B" standard and found no significant difference in the detector response for the 1 and 5 mL injection volumes. The HS samples were removed from the 60°C oven immediately before analysis to maintain a constant gas temperature of 60°C during sample injection. A volume of water equivalent to the volume of gas sampled was added to the vials to maintain atmospheric pressure. The vials were then frozen upside down to provide an additional seal during sample storage. For the large-volume void and gas hydrate gas samples, 5 mL of gas was injected directly from the 60 mL syringe through a luer-lock fitting.

Constituents of the HS were analyzed using a Hewlett Packard 6890 Plus (GC3) gas chromatograph equipped with an 8 ft × ⅛ inch stainless steel column packed with HayeSep S (100–120 mesh) and equipped with a flame ionization detector (FID). Concentrations of methane, ethane, ethene, and propane were obtained. We attempted to modify the GC program to quantify *i*-butane and *n*-butane but later determined that it was not possible to accurately quantify these compounds in the concentration range encountered during the expedition. The GC oven was programmed from 100°C (5.5 min hold) to 140°C (4.5 min hold) at a rate of 100°C/min. The carrier gas (helium) was programmed from 30 mL/min (2.2 min hold) to 60 mL/min (0.3 min hold) to 30 mL/min (6.0 min hold) at a rate of 100 mL/min. Data were collected using the Hewlett Packard 3365 Chemstation data processing program. The precision of analysis for the "B" standard with the GC3 was ≤1% for all gases analyzed.

Gas hydrate, void gas samples, and selected HS samples were analyzed on the natural gas analyzer (NGA). The NGA system consists of a Hewlett Packard 6890 Plus GC equipped with four different columns and two detectors. Hydrocarbons from methane to hexane were separated using a 60 m × 0.32 mm DB-1 capillary column and analyzed with a FID. The GC oven was heated isothermally at 50°C for 15 min. The hydrocarbons, as well as oxygen, nitrogen, and CO_2, were also analyzed with a thermal conductivity detector (TCD). Separation of the compounds was achieved with a multivalve, multicolumn system that includes a 6 inch stainless steel column packed with Poropak T (50/80 mesh), a 3 ft column packed with a 13× molecular sieve, and a 6 ft stainless steel column packed with HayeSep R (acid washed). The precision of analysis for the "B" standard with the NGA was ≤1% for all gases analyzed.

The HS, void, gas hydrate, and PCS gas concentrations are expressed as component parts per million by volume (ppmv) relative to the analyzed gas. To the extent that sampling procedures are uniform, the differences in the HS results reflect differences in the amount of gas remaining in the cores. Major variation in concentrations between the void gas and gas hydrate gas results reflects dilution of the void gas samples with air. The volumetric units of the void gas samples were converted to concentration units (mM) to facilitate comparisons with dissolved IW constituents using

$$CH_4 = (\chi_M \times P_{atm} \times V_H)/(R \times T \times \phi \times V_S), \quad (1)$$

where

- V_H = volume of the sample vial headspace,
- V_S = volume of the whole sediment sample,
- χ_M = molar fraction of methane in the HS gas (obtained from GC analysis),
- P_{atm} = pressure in the vial HS (obtained from the bridge),
- R = the universal gas constant,
- T = temperature of the vial headspace in Kelvin, and
- ϕ = sediment porosity determined either from moisture and density (MAD) measurements on adjacent samples (see **"Physical properties"**) or porosity estimates derived from the EcoScope tool (see **"Downhole logging"**).

Quantities of methane that remained in solution are minimal (e.g., Duan et al., 1992) and are not accounted for. The internal volumes of 15 representative HS vials were carefully measured beforehand and were determined to average 25.41 ± 0.18 mL.

This volume was taken as a constant in calculations of gas concentrations.

Sediments

IC concentrations were determined using a Coulometrics 5011 CO_2 coulometer. About 10–15 mg of freeze-dried, ground sediment was weighed and reacted with 2N HCl. The liberated CO_2 was titrated, and the end-point was determined by a photodetector. Calcium carbonate, expressed as weight percent, was calculated from the IC content, assuming that all evolved CO_2 was derived from dissolution of $CaCO_3$, by the following equation:

$$CaCO_3\ (wt\%) = 8.33 \times IC\ (wt\%). \quad (2)$$

No correction was made for the presence of other carbonate minerals.

TC and TN concentrations were determined using a Carlo Erba 1500 CNS elemental analyzer. About 10 mg of freeze-dried, ground sediment was weighed and combusted at 1000°C in a stream of oxygen. Nitrogen oxides were reduced to nitrogen and the mixture of CO_2, nitrogen, and SO_2 was separated by GC and detected with a TCD. Total organic carbon concentrations were calculated as the difference between TC and IC concentrations.

Microbiology

Microorganisms are the kinetic controls on both methane production and consumption. Their distribution, identities, and activity must, therefore, be estimated to model the dynamics of the gas hydrate system. Target zones of interest include

- The top of the sediment column, where microbial sulfate reduction and microbial methane oxidation are coupled;
- The base of the gas hydrate stability zone (GHSZ), which was a region of increased microbial numbers at Blake Ridge (Wellsbury et al., 2000); and
- Sediments hosting massive and disseminated gas hydrate, which may also host distinct microbial communities.

In addition to investigating the methanogens, the deep cores provide an opportunity to explore extremophiles, particularly piezophiles. These organisms live optimally at high hydrostatic pressure (e.g., Yayanos, 1995). We are interested in cultivating novel piezophilic microorganisms originating from the top 10 cm and bottom of cored holes at high pressure.

Because good microbiology samples can only be taken when the cores are fresh, the shipboard microbiologists focused on obtaining the best samples possible for future investigations. Cores were sampled for microbiology studies at all sites.

Core handling and sampling

Core collection and retrieval

Because of the need to monitor contamination and control core temperature, cores for microbiological sampling were specified prior to core collection. Two types of tracers monitored drilling fluid (seawater) infiltration into the cores, soluble perfluorocarbons and fluorescent microparticles (microspheres). The perfluoro(methylcyclohexane) tracer was pumped into the drilling fluid (surface seawater) by a variable-speed, high-pressure liquid chromatography pump connected to the mud pump system. The tracer pump operated at a fixed rate relative to the mud pump speed so that the concentration of tracer was always 1 ppmv. The tracer pump was run continuously in the continuously cored hole at each site. The fluorescent microspheres were delivered in a plastic bag designed to rupture on contact with the sediment and attached to the core catcher (see **"Contamination tests"**).

Core temperature is an important consideration when taking microbiological samples. Ideally, cores should be maintained as close to in situ temperatures as possible; in practice, cooling cores below in situ temperatures is acceptable, whereas warming cores above in situ temperatures is not. Whereas our goal was to maintain core temperature at or below in situ temperatures at all times, as a practical matter it is difficult to avoid some warming above in situ temperatures. Shallow cores at the northern Cascadia accretionary prism have in situ temperatures below the temperature of surface seawater in this region (12°–14°C), which was used as drilling fluid and through which the cores traveled to reach the rig floor. To keep warming to a minimum, microbiology cores were retrieved and sent to the catwalk using the expedited core-retrieval protocol implemented during Leg 201 (see "Microbiology" in Shipboard Scientific Party, 2003a), except at Site U1329 (see **"Microbiological sampling"** in the "Site U1329" chapter). When a core barrel was retrieved, the core was immediately removed from the barrel and sent to the catwalk. Once the core was in the hands of the core technicians, the drilling crew sent the next core barrel down the wireline. This core-handling protocol increased the coring time but was necessary to minimize core warming. Temperatures were monitored using the IR camera on freshly cut core ends of each section identified for microbiology (see **"Physical properties"**). These images provide a temperature profile of the section immediately prior to moving it to the microbiology sampling area in the hold reefer

and are available for postcruise assessment of microbiology sample quality. Examples of core-end temperature profiles at different times are provided in Figures F36 and F37 in the "Site U1327" chapter. For these particular examples, the temperature of the center of the core was ~9° and ~10°C, respectively, at times when microbiology samples were typically taken to the hold deck reefer.

Core section subsampling

Core sections were cut on the catwalk following ODP/IODP standards as described in ODP *Technical Note 36* (ODP Science Services, 2006), but acetone was not used to seal the end caps of sections dedicated for microbiological sampling. Most sections that were sampled for microbiology had IW whole-round (WR) samples removed from the bottom end. The hold deck reefer on the *JOIDES Resolution* was maintained at 4°C and served as microbiological laboratory space. All sections used for microbiological study were transported directly from the catwalk to the reefer, where they were subsampled and packaged.

Core sections sampled for microbiology were generally intact and undisturbed. WR samples were removed from these sections in the refrigerated reefer by first cutting the liner with the rotary knife cutter and then fracturing, rather than cutting, the sediment. If the sediment was slurrylike in texture and would not fracture easily, an ethanol-rinsed wide spatula was used to cut through the sediment and contain it in the liner. The WR samples were dropped into sterile plastic bags (Nasco or Fisher) and either frozen, refrigerated, or further subsampled. Although this method leaves most samples in contact with contaminated material near the core liner, a decision was made that, in view of the very slow nature of the diffusion process and the low storage temperatures involved, such treatment was preferable to additional processing under adverse shipboard conditions.

WR samples were subsampled with sterile, truncated 5 mL syringes or alcohol-rinsed spatulas. Subsamples were placed in preservative solutions for direct microscopic counts, fluorescence in situ hybridization (FISH), or microsphere enumeration. WR samples that were stored unpreserved at 4°C were sealed in nitrogen-flushed aluminized polyester heat-seal bags (Kapak Corp.) to maintain an anoxic environment. Samples to be frozen were stored at –80°C.

A glove bag (Coy) containing a nitrogen atmosphere with 5% CO_2 and 5% H_2 was used for anaerobic handling of core samples to inoculate growth media selective for sulfate-reducing microorganisms to be cultured under high pressure. Subsamples were brought into the glove bag in nitrogen-filled bags, kept cold in an ice box with lid, and quickly processed to minimize warming. All media and sterile tools were also precooled and kept on ice during processing. Hydrogen was present to combine with residual oxygen in a reaction to make water, which was catalyzed by palladium pellets maintained within the bag. The water was absorbed by a desiccant, and, thus, the glove bag's atmosphere was scrubbed of any oxygen. The bag was maintained regularly, and several hours before each use it was flushed with a gas mixture and provided with freshly baked (140°C) catalyst. As an additional precaution to minimize oxygen contamination, tools and glassware to be used for manipulation and storage of samples for strict anaerobic work were stored within the glove bag.

Although cores were processed as quickly and carefully as possible, shipboard handling should not be simply accepted as aseptic. We recommend that investigators receiving samples treat them as potentially contaminated and subsample accordingly whenever possible. Microsphere enumerations, summarized in the relevant site chapters, and additional microsphere evaluations performed postcruise at individual laboratories should be used to evaluate the quality of individual samples.

Contamination and sampling of extended core barrel cores

The XCB coring system is typically used when the APC coring system reaches resistance in the sediment below the seafloor. Although this coring method captures deeper sediment, the quality of the cored sediment is compromised by increased mixing of drill fluid and extraneous sediment (drill slurry). Thus, the WR samples may contain sediment, drilling slurry, or biscuits, sometimes regularly spaced, embedded in lower density drilling slurry. Drilling slurry is soft, moldable, and wet and cracks with a "fluffy" texture, whereas the biscuit is firm and drier and cracks with distinct edges. Figure F10A is an example of an XCB core section where it is difficult to distinguish between sediment and drilling slurry. Figure F10B represents an XCB core section that appears to be mostly sediment in the upper part and mostly slurry surrounding small biscuits in the lower part. Figure F10C shows a typical alternating pattern of biscuits and drill slurry.

Biscuits are coherent pieces of sediment and they are typically less contaminated than the surrounding drilling slurry. Five biscuit/slurry microsphere comparisons (Tables T8 in the "Site U1325" chapter, T9 in the "Site U1326" chapter, and T12 in the "Site U1328" chapter) showed the biscuits remained un-

contaminated even if the slurry contained microspheres. Unfortunately, biscuits and slurry were not distinguished during subsampling of XCB cores during the early part of Expedition 311. Samples contaminated with drilling slurry may still be suitable for some purposes (e.g., enrichment cultures) but are inappropriate for others (e.g., biomarker analysis for microbial community structure).

Sampling biscuits within XCB cores is not trivial. In the past, microbiologists have split the core liner while keeping the sediment intact and cleaned off biscuits by hand, in a manner similar to that used by the geochemists when preparing IW samples. This method is not completely satisfactory, as it is time-consuming, has the potential for contamination and warming, and allows oxygen to contact the core unless performed inside the glove bag. Nondestructive testing of XCB sections to reveal biscuits would allow quicker, cleaner processing of core material for microbiology. Gamma density, electrical resistivity, and X-ray density all show potential for distinguishing biscuits from slurry without removing the core from the liner; however, some of these measurements may adversely affect sediment microorganisms.

We experimented with a modification of the geochemical paring method with an XCB WR sample (311-U1328C-27X-3, 55–70 cm; 297.0 mbsf) that had already been sampled for shipboard high-pressure culturing experiments. The anaerobic chamber was turned into a temporary cold box by filling it with blue ice packets to keep the sediment cool. The WR sample was extruded onto a sheet of ethanol-sterilized aluminum foil in the glove bag and inspected for the biscuit. Once the biscuit was identified and isolated from the surrounding slurry, biscuit fragments were immediately placed into sterile, anoxic, 50 mL screw-cap tubes and temporarily placed in ice buckets until they could be frozen at –80°C. When the frozen biscuit fragments were ready for sampling deoxyribonucleic acid (DNA) for analysis, the fragment was cracked open and subsampled from the center to obtain an undisturbed sample for microbial DNA. This method is the most reliable way to find the appropriate sediment for phylogenetic studies. Reexamination of XCB gas hydrate WR samples from previous sites should ideally have been done immediately but will be done on shore because of the uncertain condition of the ship's anaerobic glove bag and the difficulty in chilling all the exposed sediment in this glove bag while searching for biscuits.

In XCB cores, it is best to obtain at least 10–15 cm of a WR sample, instead of 5 cm, to increase the chances of obtaining intact biscuits. These WR samples are better suited for "spiraling," a slightly less invasive, quick, and simple technique that can be performed immediately as core sections arrive in the cold room. The 10–15 cm XCB WR sample was secured to the liner clamp in the hold deck reefer and the cutting end was uncapped. Using a small ethanol-sterilized spatula, the sediment at the end was inspected by observation and tactilely (cracking, texture, scrapings, etc.) as it remained in the liner. If it appeared to be drill slurry, then a ~1–2 cm ring of the core liner (containing the slurry) was removed with the core liner cutter. Usually when cutting a relatively thin section of core liner, 1–2 cm will be nicked but cannot be completely removed as a ring. This is because the physical interference between the liner clamp and core liner cutter restricts blade contact. However, slowly unwinding the nicked liner in a spiral motion until the liner breaks off works well. The sediment at the exposed end was inspected again and if the sediment appeared relatively dry, firm, and dense, the WR sample was immediately subsampled for DNA analysis, frozen at –80°C, capped, sealed in a nitrogen-flushed bag, heat-sealed, and stored at 4°C. An XCB WR sample that did not contain any dense, firm, dry sediment at either end was either rejected or saved at the discretion of the microbiologist. Spiraling may help minimize the error of subsampling slurry for DNA analysis and help eliminate WR subsamples of pure slurry. It can result in the loss of culturable sediment unless the removed slurry is captured in a sterile bag flushed with nitrogen. The chance of capturing quality "live" sediment samples can increase under the strict conditions of a chilled, sterilized, anoxic chamber. However, during this expedition, the available hold deck reefer was equipped for spiraling and an intact chilled anaerobic glove bag was equipped for completely dissecting the WR samples.

Shipboard microbiological procedures and protocols

Contamination tests

The greatest challenge for subsurface microbiological investigations is verification that observed populations and activities are in situ and not the result of the drilling and sampling process itself, including introduced microbial contaminants. Chemical (perfluorocarbon) and particulate (latex microsphere) tracers were used during coring to test for the potential intrusion of drilling fluid and assess the suitability of the core material for microbiological research. The presence or absence of these two tracers also acts as a quality assurance check on core-handling methods. These tracer techniques were used during Leg 201

and are described in ODP *Technical Note 28* (Smith et al., 2000b).

Perfluorocarbon tracer

Perfluorocarbon tracer (PFT) was continuously fed into the drilling fluid at a concentration close to the limit of solubility (1 µg/g) and well above the detection limit for GC analysis of that material (1 pg/g). Samples for PFT analysis were taken from all cores intended for microbiological studies. Syringe subcores were taken from the interior (to monitor intrusion) and exterior (to verify delivery) of a freshly broken core or biscuit surface, extruded into HS vials, and sealed with polytetrafluoroethylene (PTFE) septa. Air samples were occasionally taken to monitor the background level of PFT in the hold deck reefer or on the catwalk. Samples were kept at –80°C until ready for GC analysis. The method described in Smith et al. (2000b) was used for PFT analysis, with minor modifications. The same GC setup was used, but the instrument was modified by installation of a 1 cm^3 sample loop and injector valve to standardize injection volumes.

Fluorescent microparticle tracer

Latex fluorescent microspheres (Poly Sciences, Inc.) (YG; 0.5 µm diameter) were used as a particulate tracer complementary to the volatile PFT. A 2 mL aliquot of microsphere stock (2.69% solids) was diluted with 40 mL of distilled water, sonicated for 2 min, and heat-sealed into a 0.12 L (4 oz) sterile plastic bag (Nasco). The bag was then attached as described in Smith et al. (2000a, 2000b) to the inside of the core catcher and positioned to rupture upon impact of the core tube with bottom sediments, where the microspheres mix with seawater and coat the outside of the core as it is pushed into the liner. During core processing, subsamples of sediments were collected from outer and inner layers for microscopic examination. Weighed samples were mixed thoroughly with saturated sodium chloride solution to extract microspheres. The slurry was then centrifuged to separate the liquid phase (Marathon 21K; 5 min; 1000 relative centrifugal force), the supernatant was filtered onto a black polycarbonate filter (Millipore; 0.2 µm pore size), and the filter was mounted on a clean slide for microscopic examination. Microspheres in slide preparations were counted using a Zeiss Axioplan fluorescence microscope equipped with the Zeiss Number 9 filter set (BP 450–490; LP 520), and the number of spheres observed was used to quantify contamination in spheres per gram of sample. Comparison of microsphere numbers between paired samples from inner and outer core layers provides a relative measure of fluid intrusion. A sample with many spheres in outer layers and few or none within may be considered of "higher quality" than one with very few spheres in the outer layers and few or none within.

Enrichment cultures

Liquid culture enrichments were started for anaerobic and aerobic piezophiles. Samples for anaerobic enrichments were taken as quickly as possible from cores that had been maintained at low temperatures and oxygen-free conditions. Subsamples for enrichment of aerobic microorganisms were separately kept cold in 15 mL sterile tubes. For sediment transfers, subcores were brought into the glove bag in nitrogen-filled sealed bags and insulated on ice; work was performed quickly to minimize warming. All media and sterile tools were also precooled during processing. In the glove bag, anaerobic sulfate-reducing bacteria (SRB) presumed to be in 1 g of sediment were vigorously mixed, serially diluted 10-fold three times, and inoculated in cold Widdel's medium (R.J. Parkes, pers. comm., 2005) amended with acetate, lactate, or formate as an energy source. Aerobic heterotrophic microorganisms were enriched in Zobell/10 medium lacking yeast extract (F. Malfatti, pers. comm., 2005) outside the glove bag. Aerobic Actinomycetes (e.g., *Salinospora* spp.) was also selected and enriched in A/10 medium (Mincer et al., 2002; P. Jensen, pers. comm., 2005). These cultures (SRBs, heterotrophs, and Actinomycetes) were maintained at 55.1 MPa of pressurized water in an attempt to discover novel piezophiles. The pressure vessels were incubated at 4°C until shipment at the end of the voyage to Scripps Institution of Oceanography (La Jolla, California) for enrichment and isolation study.

Enrichment culturing for methanogens began in the anaerobic chamber. Samples for methanogen enrichments were taken from cores that had been maintained at low temperature and placed in oxygen-free conditions as quickly as possible. For sediment transfers, subcores were brought into the glove bag in nitrogen-filled bags and insulated on blue ice. Approximately 1 g from the final inner pared core sample was placed in a serum vial containing 9 mL of MSH medium (Ni and Boone, 1991) without KCl. The vial was stoppered and shaken vigorously for 10 s. H_2 was added (2 atm), and cultures were incubated statically at 20°C (Mikucki et al., 2003).

Summary of sampling for shore-based studies

The bulk of the samples taken were for shore-based investigations. WR samples taken for lipid analysis, DNA extraction, and organic matter analysis were stored in sterile plastic bags at –80°C. Subsamples preserved for direct counts were fixed in a final con-

centration of 1% glutaraldehyde, sonicated, filtered onto 0.2 µm black polycarbonate filters (Lunau et al., 2005), or preserved in 1:1 ethanol and phosphate-buffered saline (PBS). Subsamples for FISH were fixed in 2% formalin and stored in a 1:1 solution of ethanol-PBS (Boetius et al., 2000); all of these samples were stored at –20°C. Cores to be used for culture-based analyses and for methods that require living cells as starting material (e.g., rate measurements) were stored at 4°C under nitrogen either in triple-ply aluminized polyester heat-sealed bags or in sterile plastic bags inside canning jars that were flushed with nitrogen before sealing.

Physical properties

A suite of physical property measurements was made to complement other data sets taken on board and to support the scientific objectives of Expedition 311. Physical characteristics of the subsurface environment play an important role in determining the nature of fluid and gas migration, which, in turn, affects the nature of gas hydrate formation and microbial communities.

As soon as cores arrived on the catwalk, they were wiped to remove excess water or sediment film and then scanned using a track-mounted IR camera system. These scans provided the temperature of the outer surface of the butyrate liner for virtually all cores recovered. After sectioning, section-end IR images were taken of selected cores, primarily of cores dedicated to microbiological studies. Cold spots in the IR images, interpreted to represent partially or completely dissociated gas hydrate, were used to select a subset of the samples collected on the catwalk, mainly IW, HS, and gas hydrate samples. The IR images were also processed to provide downcore temperature images and plots as described below. The core sections were then moved into the laboratory to equilibrate to room temperature. Thermal equilibration, which was monitored with temperature probes in a subset of the cores, took ~4 h. Magnetic susceptibility, GRA density, noncontact electrical resistivity, and seismic *P*-wave velocity (V_P) were measured on whole-round cores using the MST. Thermal conductivity was also measured on whole-round cores. The core sections were then split for measurements of contact resistivity, shear strength (handheld Torvane device or Giesa automated shear vane [AVS]), and V_P with a Hamilton Frame velocimeter. Discrete samples were taken for measuring MAD properties (e.g., bulk density, porosity, and grain density). Selected cores were taken directly from the catwalk for special gas hydrate dissociation experiments and imaging using the MST and IR camera. This volume also presents methods used to determine in situ temperature and to monitor the temperature of cores during acquisition and recovery, including tests of a prototype next-generation downhole temperature tool.

Core temperature measurement and infrared thermal imaging

The temperature history of a core sample from in situ conditions beneath the seafloor to thermal equilibrium on the ship is complicated but needs to be known to understand the impact of this history on microbiology and gas hydrate studies. During the coring process, frictional heat is generated, warming the cores by a poorly known, variable amount. Frictional heat is also generated by rotary drilling, even though the bit is being cooled by seawater that is pumped downhole at near-bottom water temperatures (<6°C). During core recovery, the sediments are first exposed to cooler temperatures, with the minimum occurring at the seafloor. Significant warming does not start until the cores pass through the ocean's thermocline on the way to the surface, and continued warming occurs once a core arrives on deck. During Expedition 311, surface seawater and ambient air temperatures were ~14° and 15° ± 3°C, respectively. Because of these complications and others discussed below, temperatures of marine cores are not commonly measured. However, since the process of core retrieval is fairly uniform, the temperatures at which neighboring cores arrive on the catwalk should be relatively consistent unless there are additional heat sources or sinks. Dissociation of gas hydrate, which is an endothermic process, represents one such heat sink, resulting in anomalous cold spots in the core. Other processes that can lead to cold spots in cores include gas exsolution from pore water and adiabatic expansion of gas (Ussler et al., 2002).

A variety of approaches have been used to measure core temperatures to take advantage of the thermal impact of gas hydrate dissociation. One of the early systematic approaches, applied during ODP Leg 164, used an array of digitally recorded thermocouple probes (Paull, Matsumoto, Wallace, et al., 1996). Since those early efforts, two developments have markedly changed our ability to obtain useful information about gas hydrates from core temperature measurements. First, commercially available digital IR imaging cameras permit quantitative temperature estimates for each pixel in a recorded scene, and second, the advanced piston corer methane (APCM) tool, initially deployed during Leg 201, is now deployed on a routine basis, providing temperature, pressure, and conductivity information at the top of APC cores at 1 s intervals (Ussler et al., 2006). By

combining these two developments, it is theoretically possible to forward-model the thermal behavior of individual cores, including the impact of gas hydrate dissociation, thus constraining gas hydrate concentrations in a manner not previously possible. Initial development of the IR imaging technique was accomplished during Leg 201, where thermal anomalies in IR images were associated with gas hydrate and voids (Ford et al., 2003). Systematic IR thermal imaging of the surface of the core liner was first fully implemented during ODP Leg 204 (Tréhu, Bohrmann, Rack, Torres, et al., 2003; Tréhu et al., 2004). For Expedition 311, an improved IR track system was used in which the IR camera traveled along the core on a skate guided by a rail/belt system. This system automatically stitches images and produces a single IR image and temperature array for each core.

The primary benefits of using IR cameras include

- Rapid identification of gas hydrate for sampling from temperature anomalies on the surface of the core liner,
- Quantification of the relative proportions of different gas hydrate textures,
- Assessment of the thermal structure of entire cores and the differences in thermal structure between APC and XCB cores,
- Estimation of the cross-sectional temperature gradient in cores prior to sampling for microbiology and to support postcruise thermal modeling of gas hydrate abundance and dissociation kinetics, and
- Estimation of gas hydrate volumes from processed images.

The IR camera is also quicker and simpler to use and has a much higher spatial resolution than an array of thermocouples. The resolution of thermal anomalies observed indicates that the camera can detect small volumes of gas hydrate if they are adjacent to the core liner. Determining quantitative estimates of gas hydrate in cores was an objective during Leg 204 that was accomplished only after extensive postcruise analysis of collected data (e.g., Tréhu et al., 2004). For Expedition 311, many of the analyses of the IR data were completed shipboard and concatenated images of each core were made available as prime data for the cruise. Substantial postcruise analysis will also be required to fully exploit the IR data.

Methodology

During Expedition 311, two ThermaCam SC 2000 cameras and a ThermaCam SC 500 camera (all FLIR Systems) were used to map temperature variations along cores. The FLIR Systems cameras provide temperature-calibrated images over a temperature range from –40° to ≥1500°C. For shipboard measurements, the cameras were set to record a more limited range of temperatures from –40° to ≥120°C (Range 1). To perform the critical task of rapid identification of gas hydrate within the core on the catwalk, one of the IR cameras was mounted on a track above the catwalk and driven automatically by a stepper motor controlled by custom software. The camera track and software were provided by GeoTek, Ltd. The camera was mounted with the lens 33 cm above the core liner, providing a 15.5 cm field of view along the core. To minimize the effect of external IR radiation reflecting off the core-liner surface, the camera was enclosed by black felt (Fig. **F11A, F11B**). The catwalk was also shaded with 17 mm thick plywood. Images and data for each core were acquired immediately after the core liner was wiped nearly dry and positioned with the top of the core at a fixed zero point. The camera moved along the track in 13 cm increments, starting 6.5 cm from the top of the core. During the scan, images were saved in FLIR Systems proprietary format, as bitmap images, and as temperature arrays. Bitmap images and temperature arrays were automatically concatenated and output as single files for analysis. A physical property scientist, a Co-Chief Scientist, and other personnel on the catwalk observed the scan results by looking at one of four monitors connected to the computer controlling the scan. The locations of thermal anomalies were identified from the concatenated images on the catwalk monitors and whole-round samples (e.g., gas hydrate, IW, and microbiology samples) were collected as defined by the core-sampling plan for the hole.

The core liner–mounted IR camera was supplemented on most cores by discrete imaging using a second, handheld SC 2000 camera (Fig. **F11C, F11D**) to obtain section-end IR images as quickly as possible after sections were cut. These images were collected using a device to mate the camera lens and the core liner, providing a fixed focal length while minimizing stray IR radiation from the catwalk environment. The top and bottom of each core section selected for microbiological sampling was imaged and systematically recorded and uploaded to a shipboard data server. Additional images were acquired for further analysis of the thermal history of cores.

The IR images were internally calibrated to a thermocouple/temperature logger (Thermistor model 6001-075, Barnant Company, Barrington, IL, and YSI 709B, Yellow Springs Instrument Co.; temperature accuracy = ±0.15°C; time constant = 1.1 s) in the field of view of each IR image. A set of external, known emissivity standards was imaged at the "home" position for the IR camera just prior to each scan. The standards included imbedded temperature

logger (HOBO Pendant, Onset Computer Corporation; see **"Monitoring the catwalk environment"** for specifications) and light intensity measurements once per minute. An additional HOBO Pendant logger was also deployed on the opposite side of the IR camera field of view from the YSI temperature probe.

Monitoring the catwalk environment

A total of eight temperature measurement devices were deployed on the catwalk, including the three discussed above. Catwalk data were collected during Expedition 311 to ensure that any temperature gradient along the catwalk could be corrected for if necessary. HOBO Pendant temperature loggers were deployed at five locations along the core rack and provided a record of temperature and light intensity as a function of time and position on the catwalk (temperature accuracy = ±0.47°C; temperature resolution = 0.1°C; light intensity = 0–320,000 lux, with an equivalent response >40% of the human eye from 400 to 1130 nm wavelength). The HOBO Pendant loggers were positioned at –0.3, 2.35, 3.9, 6.2, and 7.7 m along the catwalk relative to the top of the core rack and at ~5 cm below the lower edge of the core liner. In addition, a single point midway on the catwalk was monitored for both temperature and humidity (HOBO Pro RH/Temp H08-32-08; temperature accuracy = approximately ±0.2°C; temperature resolution = approximately ±0.05°C; relative humidity range = 0%–100%; drift = <3%/y, except for when humidity is >70%, in which case drift can be >3%/y). This device was attached to the plywood sun shield, 5 m horizontally from the top of the core rack and ~75 cm above the core. Prior to processing the first cores and again near the end of Expedition 311, an ice bath calibration check was performed on most temperature loggers used on the catwalk or for core temperature measurements. All tested devices returned values that were within manufacturer's specifications.

Monitoring core equilibration by direct contact measurement of core temperature

Direct measurement of core temperature was made on a routine basis using weatherproof temperature loggers (HOBO H08-008-4) and stainless steel-sheathed thermocouples (TMC6-HC; temperature accuracy = ±0.5°C; temperature precision = ±0.41°C; response time = 3 min in air, 15 s in stirred water). The probes were inserted ~3 cm into the center of the bottom of three to four sections per core. Temperature measurement was started after sections were brought into the core laboratory for thermal equilibration. Thermocouples were checked for accuracy in ice-water baths prior to the beginning of coring and once again during the last week of the expedition. Full thermal equilibration of cores typically took as much as 4 h, and temperature probes were left in the cores until the temperature was greater than ~17°C. It was not possible to collect probe temperatures on all cores because of the degree of induration of accretionary wedge sediments and because of limitations in the number of available temperature probes. Direct-contact temperature measurements were not routinely done on the catwalk because of the difficulty of handling temperature probes in the catwalk environment and because of the quality of the IR images. However, as a cross check, selected cores were monitored with direct-contact temperature probes inserted 10 cm into the bottom of cores immediately after the first IR scan. These probes were left in place as long as possible, usually ~10 min, while the core was being sampled and cut into sections. The typical temperature probe arrangement was one probe in the center, two probes directly beneath the liner on opposites sides of the core, and one probe between the center and liner probes.

Infrared image processing and extraction of thermal anomaly data

Following initial image concatenation and creation of temperature arrays, temperature images for each core were combined to make montages of downhole temperature anomalies. Temperature arrays for each core were processed in a spreadsheet by averaging cross-core temperatures at a given pixel depth after removing the outer edges and central portion of the array to eliminate thermal artifacts along the sides of the core and a central reflection from the IR camera. The resulting averaged temperatures at each depth were then concatenated into a downcore array and plotted. Thermal anomalies were identified from the downcore temperature profiles. An analysis of thermal data on board showed that T values indicative of gas hydrate were relatively insensitive to ambient catwalk temperature and illumination conditions. The T values provide an approximate measure of gas hydrate abundance, albeit influenced by the proximity of gas hydrate to the core liner. Gas hydrate undergoing dissociation and directly in contact with the core liner produces a larger T than gas hydrate insulated from the liner by sediment. It is important to note that depth measurements from the IR scans are relative to uncut core liners, prior to sectioning and removal of gas voids. Depth assignments of IR temperature anomalies must be adjusted to precisely match the curated depths of core sections.

Correlation of infrared thermal anomalies with interstitial water chlorinity anomalies and headspace gas composition

Selection of catwalk samples for IW chemical analyses was, in part, based on IR anomalies. For selected samples with varying *T* values, IR images and visible digital images were taken to identify internal parts of the sample that were still cold. Subsampling could then be more selective for parts of the sample formerly containing gas hydrate. For most of the samples, gas hydrate had already dissociated, but the thermal signal was almost always obvious, allowing designation of the sediment type (sand, silt, or clay) hosting the gas hydrate in situ.

Special experiments

Selected sections with and without gas hydrate were removed from the catwalk immediately after sectioning and taken to the core laboratory. Sections were immediately run through the MST and then instrumented with temperature probes similar to those used for direct measurement of core temperatures (see above). Time-lapse IR images were obtained using a FLIR SC-500 IR camera. After ~15 min, the section was returned to the MST, and the process was repeated until thermal equilibrium was achieved (~2–4 h).

Multisensor track

The MST has five physical property sensors mounted on an automated track that sequentially measure magnetic susceptibility (MS), GRA density, V_P, natural gamma ray emissions, and noncontact electrical resistivity (NCR). During Expedition 311, we recorded MS, GRA, V_P, and NCR data. Whole-core MST measurements are nondestructive to sediment fabric and can be used as proxies for other data as well as for facilitating core-to-core correlation between adjacent holes at the same site or among different sites. Data quality is a function of both core quality and sensor precision. Optimal MST measurements require a completely filled core liner with minimal drilling disturbance. Precision is a function of measurement time for MS and GRA density but not for V_P. The spatial interval used for all sensors was 2.5 cm.

Magnetic susceptibility

Magnetic susceptibility was measured using a Bartington MS2 meter with a 88 mm diameter sensor coil at a 565 Hz frequency and an alternating field of 80 A/m (0.1 mT) with the sensitivity range set to 1.0 Hz. Data were archived as raw instrument units (SI) and not corrected for changes in sediment volume or drift during the course of a run. The data are reported as "uncorrected volume susceptibility."

Gamma ray attenuation density

GRA density was determined using the GRA densitometer. This sensor system measures the attenuation (mainly by Compton scattering) of a gamma beam caused by the average electron density in the gamma path. A well-collimated gamma beam (primary photon energy = 662 keV) is produced from a small (370 MBq; ~1994) ^{137}Cs source (half life = 30.2 y) and passes through an assumed known thickness of sediment (internal diameter of core liner).

The measurements are empirically related to the bulk density of the material, and hence, the data are often referred to as "wet bulk density." However, we believe this to be confusing and prefer to refer to this data set as "gamma density," or GRA density, which we then compare to wet bulk density measured by MAD gravimetric techniques. Although the empirical calibration procedure for GRA is based on bulk density measurements (i.e., of a known graduated aluminum and water standard), the measurements will vary from true gravimetric bulk density because of variations in mineralogy. Gamma attenuation coefficients for different materials vary as a function of atomic number. Fortunately, most earth-forming minerals have similar and low atomic numbers (similar to aluminum). Consequently, the correlation of GRA density and bulk density is usually very good. In summary, GRA density should be considered to be the density of sediment and rocks as determined from GRA measurements using aluminum and water as reference materials.

The gamma source collimator is 5 mm, which produces an effective downcore spatial resolution of ~1 cm. Following our detailed setup and calibration procedure, we logged the graduated aluminum and water standard as a check to confirm accurate calibration. These data indicate an excellent calibration and illustrate the downcore spatial resolution (Fig. F12). The minimum integration time for a statistically significant GRA density measurement is 1 s. During many ODP legs, a count time of 2 s was used; however, we considered this count period to be too short and used a 5 s count time throughout Expedition 311 to improve precision. A freshwater control was run with each section to measure instrument drift. GRA data are of highest quality when measured on nongassy APC cores because the liner is generally completely filled with sediment. In XCB cores, GRA measurements can often be unreliable (unless the sample points are very carefully chosen) because of the disturbance caused by the mixing of drilling slurry and core biscuits.

Noncontact resistivity

The NCR system installed during Leg 204 rapidly measures sediment resistivity on a whole core in the plastic liner. The NCR technique operates by inducing a high-frequency magnetic field in the core from a transmitter coil, which in turn induces electrical currents in the core that are inversely proportional to the resistivity. A receiver coil measures very small magnetic fields that are regenerated by the electrical current. To measure these very small magnetic fields accurately, a difference technique has been developed that compares the readings generated from the measuring coils to the readings from an identical set of coils operating in air. As with other parameters, the measurements are sensitive to core temperature and should be obtained in a stable temperature environment for best results. The NCR calibration is shown in Figure **F13.**

Compressional wave velocity

Transverse V_P was measured on the MST with the *P*-wave logger (PWL). The PWL transmits a 500 kHz *P*-wave pulse through the core at a specified repetition rate (50 pulses/s). The transmitting and receiving ultrasonic transducers are aligned so that wave propagation is perpendicular to the core axis. Core diameter is measured using two displacement transducers that are mechanically linked to the ultrasonic transducers. The recorded velocity is the average of the user-defined number of acquisitions per location (10 during Expedition 311). Calibrations of the displacement transducers and measurement of electronic delay within the PWL circuitry were conducted using a series of acrylic blocks of known thickness and *P*-wave traveltime. Repeated measurements of V_P through a core liner filled with distilled water at a known temperature were used to check calibration validity. The PWL was generally not used when cores were full of gas expansion cracks or when they were taken with the XCB, as the poor core quality precluded reliable velocity measurements.

Moisture and density analysis

MAD analyses measure wet mass, dry mass, and dry volume to determine moisture content, grain density, bulk density, porosity, and void ratio, as described in Blum (1997). Push-core samples of ~10 cm^3 were placed in 10 mL beakers. Care was taken to sample undisturbed parts of the core and to avoid drilling slurry. Immediately after the samples were collected, wet sediment mass was measured. Dry mass and volume were measured after samples were heated in an oven at 105° ± 5°C for 24 h and allowed to cool in a desiccator. Sample mass was determined to a precision of 0.01 g using two Scientech 202 electronic balances and a computer averaging system to compensate for the ship's motion. Sample volume was determined using a helium-displacement pentapycnometer with a precision of 0.02 cm^3. Volume measurements were repeated five times, until the last two measurements exhibited <0.01% standard deviation. A reference volume was included within each sample set and rotated sequentially among the cells to check for instrument drift and systematic error. Sampling frequency was one or two per section. The mass and volume of the evaporated pore water salts were calculated for standard seawater salinity and density at laboratory conditions (1.024 g/cm^3), and an average seawater salt density of 2.20 g/cm^3.

Thermal conductivity

Thermal conductivity measurements on whole-core samples were made using the TK04 (Teka Bolin) system described by Blum (1997). Measurements were generally made on every second core. The measurement system employs a single-needle probe (Von Herzen and Maxwell, 1959) heated continuously in "full-space configuration." At the beginning of each measurement, temperature in the sample was monitored automatically, without applying a heater current, until the background thermal drift was <0.04°C/min. Once the sample equilibrated, the heater circuit was closed and the temperature rise in the probe was recorded. The needle probe contains a heater wire and calibrated thermistor. The probe is assumed to be a perfect conductor because of its high conductance relative to the core sediments. With this assumption, the temperature of the probe has a linear relationship with the natural logarithm of the time after the initiation of heating:

$$T(t) = (q/4k)\ln(t) + C, \quad (3)$$

where

- T = temperature,
- q = heat input per unit length per unit time,
- k = thermal conductivity,
- t = time after the initiation of the heat, and
- C = constant.

The thermal conductivity was determined using Equation 3 by fitting the temperatures measured during the first 150 s of each heating experiment (for details see Kristiansen, 1982; Blum, 1997).

The reported thermal conductivity value for each sample is the average of three repeated measurements. Data are reported in watts per meter degree Kelvin (W/[m·K]), with measurement errors of 5%–10% in high-quality cores. Unless otherwise specified, no corrections for in situ temperature or pressure conditions were made to thermal conductivity values reported in tables and figures (Pribnow et al.,

2000). Throughout Expedition 311, we compared the thermal conductivity data to regional trends defined by Davis et al. (1990), who reported the relation

$$T(d) = 1.07 + 0.000586 \times d - 0.000000317 \times d^2, \quad (4)$$

where the depth (d) is in meters.

Contact electrical resistivity measurements

Within the physical properties laboratory, electrical resistivity was the first of the contact measurements to be made on the working half of split cores to reduce evaporation of pore water, which affects the measurements. The split cores were wrapped in cellophane after cutting to further decrease water loss if they could not be processed within an hour or two after being split. The instrument used during Expedition 311 was constructed by Randolph Enkin (Geological Survey of Canada). The experimental apparatus uses a four-pin Wenner electrode array. Each electrode is 3 mm in length and spacing between electrodes is 2.5 mm (Fig. **F14**). Gold-plated electrodes minimize corrosion. The probe was pushed into the sediment and a 90 Hz square wave of 18 V amplitude and 10 kΩ resistance (i.e., 1.8 mA current) was sent between the outer two electrodes. Because the resistance of the sediment (<2 Ω) is negligible compared to the resistance of the circuit generating the current, the voltage between the inner two electrodes should be proportional to the sediment resistivity. The sediment resistivity was derived by measuring the voltage between the two inner electrodes. Alternating current was used rather than direct current (DC) to prevent charge buildup around the electrodes and unwanted electrochemical effects. The temperature of the sediment was also recorded, and the resistivity of the sediment was corrected to the resistivity at 20°C.

Electrical resistivity was measured along the split core every 10 cm in the uppermost ~10 m and at 20 to 30 cm intervals below this depth, avoiding drilling mud and cracks in the sediment fabric. The probe was set up so that it was perpendicular to the bedding (i.e., parallel to the core). In selected places, the probe was rotated 90° to be parallel to the bedding, and measurements were repeated with the probe in this position to allow detection of possible anisotropy.

The probe was cleaned regularly to prevent buildup of sediment residue on the electrodes, which can lead to inaccurate results. When results became erratic, the electrodes were replaced. The probe electrodes were also washed in distilled water and dried before calibrating. The probe was calibrated every two cores while in use, using standard mean ocean water.

Directional *P*-wave measurement

P-wave velocities were measured in three orthogonal directions on the split core (Fig. **F15**): PWS1 is the velocity along the axis of the core, PWS2 is perpendicular to the core in the plane along which it was split, and PWS3 is perpendicular to the core and to PWS2. PWS1 and PWS2 transducers were mounted onto a set of stainless steel blades that were sunk into the sediment. The PWS1 transducers were separated by 69.65 mm, and the PWS2 transducers were separated by 34.85 mm. The PWS3 transducer separation is determined by the size of the core. One transducer in each pair emits a 500 kHz, 100 V, peak-to-peak square wave. The traveltime between the transducers can either be picked by hand or picked automatically. Velocity was calculated by dividing the transducer separation distance by the traveltime. Temperature affects the results and was therefore measured and recorded as the velocity measurements were being made. During Expedition 311, temperature in the laboratory was reasonably constant at ~22°C, and cores had equibrated to room temperature when V_p measurements were made.

The PWS1 and PWS2 transducers were calibrated using distilled water with a known velocity, which was corrected for temperature. PWS3 transducers were calibrated using a variety of different standards followed by a series of velocity measurements through distilled water. The transducers were calibrated for every core.

P-wave measurements can be made as frequently as needed whenever cores are undisturbed enough to yield a meaningful result. The measurement should be made in an undisturbed part of the core. *P*-wave velocities are generally more reliable in shallow core sections. Cores from deeper in the subsurface often contain many cracks and voids caused by gas expansion, causing the instruments to give unreliable results. During Expedition 311, velocity measurements were generally made every 20 cm in the upper 5–10 m of each hole.

Shear strength

Shear strength measurements were made on the split sections of cores after the contact electrical resistivity and *P*-wave velocity measurements. There are two devices that can measure shear strength: an AVS and a handheld Torvane. When using the AVS, a vane with four blades is inserted into the sediment. The vane is generally rotated 90°/min. The torque applied to the vane is recorded before, during, and after sediment failure. The maximum torque recorded is the shear strength of the sediment. The Torvane comes in three sizes (19, 25, and 48 mm), which

measures a maximum shear stress up to 20, 100, and 250 kPa, respectively. Each size records on a continuous scale of 0–10 units, and measurements are multiplied by 2, 10, and 25, respectively, to obtain shear stress in kilopascals.

One to three shear strength measurements were made per core section. Unfractured segments of the split core that were generally at least 5 cm away from places that had been disturbed by the *P*-wave measurements were chosen to make shear strength measurements. Measurements were made regularly throughout all holes at each site. Lower in the cored interval, gas expansion during recovery had usually strongly modified the sediment fabric. When making measurements on deeper cores, an effort was made to identify those sections of the core that were least disturbed.

In situ temperature

Four different downhole temperature tools were used during Expedition 311. The advanced piston corer temperature (APCT) tool fits into the cutting shoe of the APC and measures temperature during regular piston coring. We also tested a prototype for a new generation of this tool (see **"Third-generation advanced piston corer tool"**) that is being developed by A. Fisher and H. Villinger (see **Heesemann et al.,** this volume). In more indurated sediments where piston coring is not possible, we used the Davis-Villinger Temperature Probe (DVTP) or the Davis-Villinger Temperature-Pressure Probe (DVTPP). When deploying the DVTPP, we only attempted to acquire temperature measurements because the ship's heave was generally too large for pressure measurements.

Advanced piston corer temperature tool

The APCT tool consists of electronic components, including battery packs, a data logger, and a platinum resistance-temperature device calibrated over a temperature range of 0°–30°C. Descriptions of the tool and data analysis principles can be found in Pribnow et al. (2000) and Graber et al. (2002) and references therein. The thermal time constant of the cutting shoe assembly where the APCT tool is inserted is ~2–3 min. The only modification to normal APC procedures required to obtain temperature measurements is to hold the corer in place 5–10 min near the seafloor to record bottom water temperatures and to hold it for ~10 min in the hole after cutting the core. During this time, the APCT tool logs temperature data on a microprocessor contained within the instrument as it approaches equilibrium with the in situ temperature of the sediments. The tool can be preprogrammed to record temperatures at a range of sampling rates. A sampling rate of 10 s was used during Expedition 311.

A typical temperature history recorded by the APCT tool is shown in Figure **F16A.** It consists of a mudline temperature record lasting 5 min. This is followed by a pulse of frictional heating when the piston is fired, a period of thermal decay that is monitored for 10 min or more, a frictional pulse upon removal of the corer, and a second mudline temperature measurement for 5 min. The in situ temperature is determined by extrapolating from the thermal decay that follows the frictional pulse when the piston is fired. Details of this process and the associated uncertainties are discussed in the individual site chapters.

During the LWD phase of Expedition 311, we undertook a series of bench and tank tests to calibrate the APCT tool relative to the third-generation advanced piston corer temperature (APCT-3) tool prototype temperature tool, which had been calibrated to an accuracy of better than 0.01°C three days before the start of Expedition 311 (see **"Third-generation advanced piston corer temperature tool"**). For these tests, we transferred the tools rapidly from a cold-water bath that had reached a stable temperature in the reefer to a room-temperature bath located just outside the reefer. As a result of these tests, we selected APCT16, which had a response time that was similar to the APCT-3 tool and an offset relative to the APCT-3 tool that was large (~0.97°C) but relatively stable over a large range of temperatures. This offset was confirmed by observations of bottom water temperatures made with both tools.

Third-generation advanced piston corer temperature tool

The APCT-3 tool was designed to replace the APCT tool, which is no longer supported by the manufacturer. Like the APCT tool, the APCT-3 tool fits into the cutting shoe of the APC. Data are recorded in solid-state memory. The larger memory capacity, compared to the APCT tool, allows for a finer sampling rate (up to 1 Hz). Expedition 311 was the first field test for this new tool. For additional tool information, see **Heesemann et al.** (this volume).

Davis-Villinger Temperature Probe

The DVTP is described in detail by Davis et al. (1997) and summarized by Pribnow et al. (2000) and Graber et al. (2002). The probe is conical and has two thermistors. The first is located 1 cm from the tip of the probe and the second is 12 cm above the tip. A third thermistor is in the electronics package. Thermistor sensitivity is 1 mK in an operating range from –5° to 20°C. In addition to the thermistors, the probe con-

tains an accelerometer sensitive to 0.98 m/s². The accelerometer data are used to track disturbances to the instrument package during the equilibration interval. Data were recorded at a sampling rate of 3 s. A typical deployment of the DVTP showing the two temperature records from the probe is shown in Figure **F16.**

Unlike the APCT and APCT-3 tools, the DVTP requires a dedicated tool run, which consists of lowering the tool by wireline to the mudline, where there is a 5–10 min pause to collect temperature data within the drill pipe. Subsequently, it is lowered to the base of the hole and latched in at the bottom of the drill string with the end of the tool extending 1.1 m below the drill bit. The extended probe is pushed into the sediment below the bottom of the hole and temperature is recorded for 10–20 min. Upon retrieval, a second stop of 5–10 min is made at the mudline. For discussion of ad hoc calibration of the DVTP relative to the APCT-3 and APCT tools, see **"Physical properties"** in the "Site U1329" chapter.

Davis-Villinger Temperature-Pressure Probe

Simultaneous measurement of formation temperature and pressure can be achieved using a modified DVTPP. The probe has a tip that incorporates both a single thermistor in an oil-filled needle and ports to allow hydraulic transmission of formation fluid pressures to a precision Paroscientific pressure gauge inside. A standard data logger was modified to accept the pressure signal instead of the second thermistor signal in the normal DVTP described above. Thermistor sensitivity of the modified tool is reduced to 0.02 K in an operating range from –5° to 20°C. A typical deployment of the tool consists of lowering the tool by wireline to the mudline, where there is a 10 min pause to collect data. Subsequently, it is lowered to the base of the hole and latched in at the bottom of the drill string with the end of the tool extending 1.1 m below the drill bit. The extended probe is pushed into the sediment below the bottom of the hole and pressure is recorded for ~40 min. If smooth pressure decay curves are recorded after penetration, then theoretical extrapolations to in situ pore pressures are possible. Unfortunately, excessive ship heave and time limitations did not allow for optimum deployment of this tool for obtaining in situ pressure. For temperature measurements only, the tool is operationally similar to the DVTP.

Thermal data reduction

Similar data reduction procedures were used for all temperature tools. Because equilibration to in situ temperatures takes much longer than the 10 min during which the instrument records subseafloor temperature, extrapolation based on the theoretical impulse response of the tools is required. The transient thermal decay curves for sediment thermal probes are known to be a function of the geometry of the probes and the thermal properties of the probe and the sediments (Bullard, 1954; Horai and Von Herzen, 1985). Analysis of data requires fitting the measurements to model decay curves calculated based on tool geometry, sampling interval, and tool and sediment thermal properties. For the APCT and APCT-3 tools, decay curves based on the model of Horai and Von Herzen (1985) were used, as implemented in TFIT. A new, more accurate numerical model for the impulse response of the APCT-3 tool is currently under development by M. Heesemann. For the DVTP and DVTPP, the impulse response of Davis et al. (1997), as implemented in CONEFIT, was used.

It is generally not possible to obtain a perfect match between the model temperature decay curves and the data because

- The probe does not reach thermal equilibrium during the penetration period;
- Contrary to ideal theory, the frictional pulse upon insertion is not instantaneous; and
- Temperature data are sampled at discrete intervals so that the exact time of penetration is uncertain.

Additional uncertainty in the in situ temperature occurs because of tradeoffs between sediment thermal conductivity, penetration time, and temperature and because of poorly understood effects related to the presence of gas hydrate (Hartman and Villinger, 2002; Tréhu, 2006). During Expedition 311, both the effective penetration time and equilibrium temperature were estimated by applying a least-squares fitting procedure, which involves shifting the synthetic curves in time to obtain a match with the recorded data. Generally, data within ~704 s after the apparent penetration time were not used. Laboratory thermal conductivity measurements were not corrected for in situ conditions because the correction would be small at the shallow depths drilled during Expedition 311. Postcruise processing will be necessary to better quantify and understand the uncertainties in the data and the effects of gas hydrate.

Advanced piston corer methane tool and pressure core sampler methane tool

The APCM tool and the pressure core sampler methane (PCSM) tool continuously record temperature, pressure, and electrical conductivity changes in the core headspace from the time the core is cut through its ascent to the rig floor. Both are derivatives of Monterey Bay Aquarium Research Institution's (MBARI's) Temperature-Pressure-Conductivity tool.

The APCM sensors are mounted in a special piston head on the standard APC piston, and the data acquisition electronics are embedded within the piston. The PCSM tool is a slimmed-down version of the APCM tool and is mounted on the top of the PCS manifold mandrel. Both tools operate passively and require little shipboard attention. Variations in the relative amounts of in situ gas and gas hydrate can be determined from the pressure and temperature behavior during core recovery (Ussler et al., 2006).

Both tools are very similar in construction, the only difference being that the APCM tool replaces the piston-rod snubber in the APC coring system and therefore has a seal package on its exterior. The tools consist of an instrumented sensor head with the electronics and battery pack housed in a sealed case. The three sensors (temperature, pressure, and conductivity) and a data port are packaged in the face of the 2 inch diameter (5.08 cm) sensor head. The temperature sensor has an accuracy of ±0.05°C. The pressure sensor is a 0 to 10,000 psi (0–68.95 MPa) "Downhole Series" transducer with a ±0.15% full-scale accuracy that is especially designed for temperature stability. The electrical conductivity sensor is a three-pin bulkhead connector with an inconel body and gold-plated 0.04 in (10 mm) diameter Kovar pins. The data port is a three-pin keyed bulkhead connector for RS-232 serial communication. The electronics consists of two boards, an analog to digital (A/D) board and a commercial microcontroller board. The microcontroller board plugs directly into the A/D board, and the A/D board is mounted on an aluminum backbone. The microcontroller includes a Motorola 68338 processor, a DOS-like operating system, and 48 MB of flash memory. The A/D board is an ODP/MBARI-designed board with one A/D device for the pressure transducer and one for the thermistor and conductivity sensors. The battery pack consists of an assembly of two double-C lithium/thionyl chloride batteries in series and an integral hard-mounted nine-pin connector. The battery pack provides 7.3 V, with a 100 mA rating. The APCM tool is installed on the APC piston after the APC piston-rod snubber and piston head body are removed from the lower piston rod. The connection at the lower piston rod consists of a threaded connection with a transverse spring pin running through the thread relief. The spring pin prevents the connection from unscrewing as a result of vibration. After the spring pin is punched out, the piston-rod snubber is removed and replaced with the APCM tool. This swap-out operation takes <3 min. The PCSM tool replaces the accumulator on the PCS and threads onto the top of the PCS manifold mandrel.

The APCM tool was deployed successfully once and the PCSM tool was deployed successfully several times during Expedition 311 (see Table **T3** in the "Expedition 311 summary" chapter and the "Operations," "Physical properties," and "Pressure coring" sections in each site chapter). Examples of data are shown in the **"Site U1328"** chapter, but data interpretation was deferred until postcruise.

Paleomagnetism

Note: This section was contributed by Jennifer Henderson and Katerina Petronotis (Integrated Ocean Drilling Program, Texas A&M University, 1000 Discovery Drive, College Station TX 77845, USA).

No scientist sailed as a paleomagnetist for Expedition 311 because of limited space. However, routine measurements of the remanent magnetization of archive-half sections before and after alternating-field (AF) demagnetization were made on cores.

Instrumentation and measurement procedures

Nonmagnetic core barrels were used, but the Tensor tool was not deployed.

Paleomagnetic analysis involved routine measurements of remanent magnetization using a pass-through cryogenic magnetometer equipped with a DC-superconducting quantum interference device (DC-SQUID; 2G Enterprises model 760-R). An AF demagnetizer aligned along axis with the magnetometer and set within the magnetometer's mu-metal shielding allowed uniform demagnetization of the cores so that the remanent magnetization could be measured before and after demagnetization. An automated sample-handling system moved the core sections through the AF coils and magnetometer sensor region. The standard IODP magnetic coordinate system was followed, in which +x is vertical upward from the split surface of archive halves, +y is the left split surface when looking upcore, and +z is downcore.

The remanent magnetization was measured in 10 cm increments along each archive-half section before and after AF demagnetization. AF demagnetization was applied at 10 and 20 mT to remove the drill string magnetic overprint. Disturbed intervals and voids were manually noted on the "cryomag log sheets" and entered in LongCore. At the beginning of each shift, a measurement of the background tray magnetization was taken and subtracted from all measurements. The tray was demagnetized between cores. All data were stored using the standard IODP file format.

Discrete samples for magnetic analyses

Discrete samples were collected from working halves of core sections in round plastic tubes marked with arrows pointing upcore on the face that represents the split surface of the core. Sampling intervals were every 50 cm, but areas of deformation were avoided. The samples were stored in sample bags and flushed with nitrogen before being sealed and stored at 4°C. Discrete samples will be analyzed postcruise by Randolph Enkin (Geological Survey of Canada).

Pressure coring

Expedition 311 had the most ambitious pressure coring and onboard pressure core analysis program ever attempted in the history of ocean drilling. Pressure cores retrieved at in situ pressures were used to determine gas hydrate quantity, using degassing techniques and mass balance calculations, and gas hydrate distribution, using nondestructive measurement of the physical properties of the cores at in situ pressures. Large improvements in temperature control over previous expeditions (e.g., Leg 204; Tréhu, Bohrmann, Rack, Torres, et al., 2003) made the recovery and analysis of pressure cores more practical.

Pressure cores were collected using the IODP PCS, the HYACINTH Fugro Pressure Corer (FPC), and the HYACE Rotary Corer (HRC) (see **"Description and operation of pressure coring systems"**). After a pressure core was retrieved, initial nondestructive measurements were made to characterize the core, determine the core length, and identify massive gas hydrate (see **"Nondestructive measurements on pressure cores"**). Following X-ray imaging, PCS cores were degassed on board (see **"Degassing experiments"**) to determine total gas composition and quantity in sediments (see **"Estimating the abundance of gas hydrate and free gas"**). The FPC cores were subsampled and degassed on shore at the Pacific Geoscience Centre of the Geological Survey of Canada immediately following Expedition 311. All cores had gamma ray density measurements made on them while undergoing degassing to document gas evolution, gas hydrate dissociation, or other changes in the core (see **"Measurements on pressure coring system cores"**). Following degassing, all pressure cores were X-rayed a final time and the released gas volume, X-ray images, and density scans guided subsampling for IW, physical properties, and other related analyses.

Why pressure core?

Pressure coring is crucial for understanding the concentrations of gas hydrate and free methane gas in marine sediments, their nature and distribution, and their effect on the intrinsic properties of the sediment. Methane and other components of natural gas in deep sediment may be present in three phases:

1. If the concentration of methane in pore water is less than its solubility, the methane is dissolved.
2. If the concentration of methane is greater than its solubility and the sediment is within the GHSZ, excess methane oversaturation is present as solid methane hydrate.
3. If the concentration of methane is greater than its solubility and the sediment is outside the GHSZ, excess methane oversaturation is present as a free phase (methane gas bubbles).

However, reliable data on methane concentrations are impossible to obtain from conventional coring techniques because conventional cores recovered from ocean depth often release large volumes of gas during recovery (Wallace et al., 2000; Paull and Ussler, 2000). Natural gas solubility decreases significantly as pressure decreases during the recovery of cores to the surface, and any gas volume measurements made on conventional cores will lead to gross underestimates of the in situ natural gas concentrations.

The only way to directly determine the in situ concentrations of natural gas in the subseafloor is to retrieve cores that are sealed immediately after the coring process and recovered to the surface without any loss of the constituents. To achieve this objective, the core must be sealed in an autoclave that is able to maintain the hydrostatic pressure at the coring depth when brought to the surface. This was the concept behind the original PCS, and it has proven to be an essential tool for estimating in situ gas concentrations (Dickens et al., 1997, 2000a, 2000b; Milkov et al., 2004).

Although the PCS is very effective at obtaining samples that are suitable for overall gas concentration analysis, it was not designed to be used for other types of analyses that might reveal the physical structure of gas or gas hydrate in the core. It is also not possible to transfer or sample the PCS core without releasing the pressure. To enable a more comprehensive investigation of gas hydrate–bearing sediments, a more recent program, HYACINTH, has developed not only the next generation of pressure coring tools but has initiated the development of techniques to nondestructively analyze the cores and to take subsamples for microbiological, chemical, and physical property analyses at in situ pressures.

Description and operation of pressure coring systems

Pressure coring system operations and core flow

The PCS is a downhole tool designed to recover a 1 m long sediment core with a diameter of 4.32 cm at in situ pressure up to a maximum of 69 MPa (Pettigrew, 1992; Graber et al., 2002). The pressure autoclave consists of an inner core barrel, which ideally collects a 1465 cm^3 sediment core, and an outer chamber, which holds 2964 cm^3 of seawater/drilling fluids (Fig. **F17**). Prior to Expedition 311, the PCS was successfully used to study in situ gases in gas-rich and gas hydrate–bearing sediments during Legs 164 on the Blake Ridge (Paull, Matsumoto, Wallace, et al., 1996; Dickens et al., 1997), 201 on the Peru margin (Dickens et al., 2003), and 204 on Hydrate Ridge (Tréhu, Bohrmann, Rack, Torres, et al., 2003; Milkov et al., 2004). In the course of these ODP legs, degassing technology has improved continuously and further modifications were made for Expedition 311 to optimize the control and monitoring of the PCS degassing experiments. Most importantly, we replaced the steel outer and inner barrels of the PCS with aluminum with a maximum working pressure of 250 bar so that recovered sediment could be investigated by the GeoTek pressure multisensor core logger (MSCL-P) X-ray system before and after depressurization (see **"Measurements on pressure coring system cores"**). We used a one-dimensional vertical gamma ray density scanner to evaluate the distribution of sediment, gas hydrate, and gas voids in the recovered PCS core and to monitor changes in the course of the degassing experiment (see **"Nondestructive measurements on pressure cores"**). In addition, the manifold was equipped with an additional valve for the collection and analysis of fluids, and the volume of fluid expelled from the PCS was monitored during degassing.

PCS operations and core flow included the following steps. The PCS tool was assembled in and on top of the core technician shop and deployed as during Leg 204 (Tréhu, Bohrmann, Rack, Torres, et al., 2003). When a core was retrieved during Expedition 311, it was immediately inserted into an ice shuck in the moonpool for 20–30 min (see **"Improvement of temperature control"**) to counteract any warming during the wireline trip. The cooled PCS autoclave was separated from the rest of the tool on the rig floor and delivered to a refrigerated van dedicated to HYACINTH logging located on top of the core technician shop. After X-ray imaging, the PCS autoclave was moved to another refrigerated van situated on top of the lab stack for PCS degassing experiments, either using a winch rigged on the porch outside the downhole tools laboratory or simply hand-carried up the stairs.

When degassing experiments were completed, the PCS autoclave was moved back to the core technician shop for core removal. Most of the PCS autoclaves were X-ray imaged again in the HYACINTH van before the inner core barrel was removed from the autoclave. Before removing the core, the water in the autoclave was carefully collected by opening the top valves all the way and the ball valve very slightly to allow water in the inner and outer barrel to flow out of the ball valve. This volume of water was measured for consideration in mass balance calculations from the depressurization experiments. The inner barrel was removed from the rest of the PCS autoclave and taken back to the HYACINTH van for X-ray analysis. This second X-ray analysis was necessary to obtain X-ray images of the entire core because steel components inside the outer core barrel obstruct X-ray imaging of the PCS autoclave below a core depth of 51 cm (Fig. **F17**). Final extrusion of the core into a half-liner took place in the core tech shop using a metal plug and broom handle or hydraulic pump (as dictated by the sediment stiffness). The core was given to the IODP curator and, with the aid of the X-ray images and gamma ray density profiles (see **"Measurements on pressure coring system cores"**), samples were taken for analysis of IW, physical properties, and dissolved gases.

HYACINTH coring systems and operations

Two types of wireline pressure coring tools were developed in the HYACE/HYACINTH programs: a percussion corer and a rotary corer, which were designed to cut and recover core in a wide range of lithologies where gas hydrate–bearing formations might exist (Schultheiss et al., 2005). Both tools have been designed for use with the same IODP bottomhole assembly (BHA) as the PCS (i.e., the APC/XCB BHA). The HYACINTH pressure coring system was used successfully during Leg 204 to recover gas hydrate and surrounding sediments (Tréhu, Bohrmann, Rack, Torres, et al., 2003).

The design and operation of the HYACINTH tools differs in four significant respects from that of the PCS:

1. The HYACINTH tools penetrate the sediment using downhole driving mechanisms powered by fluid circulation rather than by top-driven rotation with the drill string. This allows the drill string to remain stationary in the hole while core is being cut, which improves core quality.
2. The coring portion of the HYACINTH tools moves relative to the main bit during the coring process, which also improves core quality. However, the

extension of the core barrel up to 1 m past the drill bit makes these tools far more susceptible to ship heave than other coring tools, and it is essential that the bit remains stationary on the bottom of the hole during coring.
3. Both HYACINTH tools use flapper valve sealing mechanisms at the bottom end above the cutting shoe, rather than a ball valve, to maximize the diameter of the recovered core.
4. The recovered HYACINTH cores are in plastic liners and the pressure autoclaves mate to a common transfer system so the cores can be manipulated and transferred into other chambers for analysis, storage, and transportation under full pressure.

Fugro Pressure Corer

The HYACINTH percussion corer was developed by Fugro Engineers BV and is known as the Fugro Pressure Corer (Fig. **F18**). The FPC uses a water hammer, driven by the circulating fluid pumped down the drill pipe, to drive the core barrel into the sediment up to 1 m ahead of the drill bit. The core diameter is 57 mm (liner outer diameter = 63 mm). On completion of coring, the drill string is lifted to extract the core barrel from the sediment. Once the core barrel is free from the sediment, the wireline pulls the core barrel liner containing the core into the autoclave. A specially designed flapper valve seals the bottom end of the autoclave after the core has been retrieved. The FPC is designed to retain a pressure of up to 25 MPa. It is suitable for use with unlithified sediments ranging from soft through stiff clays to sandy or gravelly material. In soft sediments it acts like a push corer prior to the hammer mechanism becoming active. It has operated effectively in sediments with shear strengths exceeding 500 kPa.

HYACE Rotary Corer

The HYACINTH rotary corer was developed by the Technical University of Berlin and the Technical University of Clausthal and is known as the HYACE Rotary Corer (Fig. **F18**). HYACE was the name of the original development program. The HRC uses an inverse Moineau motor driven by the circulating fluid pumped down the drill pipe to rotate the cutting shoe up to 1 m ahead of the roller cone bit. A narrow kerf, dry auger design cutting shoe with polycrystalline diamond cutting elements is used on the HRC. This design allows the core to enter into the inner barrel before any flushing fluid can contaminate the material being cored. The core diameter is 51 mm (liner outer diameter is 56 mm). On completion of coring, the tool is lifted off the bottom with the drill string and then the core is retracted into the autoclave by pulling in on the wireline in a similar manner to the FPC. The pressure is sealed by a specially designed flapper valve. The HRC is designed to retain a pressure of up to 25 MPa and was primarily designed for use in sampling lithified sediment or rock. However, in practice we have found that the HRC can also sample much softer formations very effectively, presumably acting as a push corer with minimal rotation.

HYACINTH coring operations

As during Leg 204, the HRC and the FPC were prepared and assembled on tool trestles located on the port side of the piperacker. The normal tool assembly area above the core technician shop was used for PCS tool assembly and was impacted by the presence of the 20 ft HYACINTH van. Stands of drill pipe normally used from the port side were moved to the starboard side to reduce disruption to the tool preparations.

Both tools followed similar operational procedures on the rig floor. They were initially transferred from the piperacker working area into the vertical position. To achieve this, a tugger line from the derrick was attached to the upper end of the tool while the base of the tool was lowered onto the piperacker skate using the port side racker crane. The tool was then hauled into a vertical position using the tugger line and lowered into the rig floor shuck as the strongbacks were removed by hand. Finally, the tool was deployed in the open drill string that was then closed, and the tools were lowered on the wireline while pumping and rotating.

When the tools were recovered to the rig floor, they were placed into the ice water–filled shuck in the moonpool for 30 min, similar to the recovery of the PCS. Once removed from the ice shuck, both the FPC and the HRC followed a reverse procedure back to the trestles on the piperacker, including replacing the strongbacks. Autoclaves were removed from the tools in a timely manner (<15 min) and placed in the HYACINTH cold van. It was once thought that additional ice baths might be necessary to rechill the autoclaves at this point; however, temperature data from the autoclave data loggers proved this to be unnecessary.

HYACINTH core transfer

Between Leg 204 and Expedition 311, the HYACINTH transfer and analysis systems were redesigned and integrated to fit inside a 20 ft refrigerated van, and procedures differ significantly from those described in Tréhu, Bohrmann, Rack, Torres, et al. (2003) and Schultheiss et al. (2005). To remove the core from the pressure corer autoclave, the autoclave was connected to the manipulator/shear transfer

chamber with quick-clamps (Fig. F19B) and then pressure balanced with the autoclave before opening the ball valves. The "technical" end of the pressure core containing the piston and other components was captured by a catcher on the end of the manipulator, and the full core was withdrawn from the autoclave into the shear transfer chamber, the ball valves closed, and the autoclave removed from the system.

The manipulator/shear transfer chamber (STC), now containing the core at full in situ pressure, was attached to the GeoTek MSCL-P (see **"Pressure multisensor core logger measurements on HYACINTH cores"**), pressures were balanced, and ball valves were opened (Fig. F19D). The core was pushed and pulled through the sensors using the manipulator under computer control. Once the analyses were completed, the core was withdrawn to the cutting position (Fig. F19E) and the core was cut free from the manipulator portion of the core system with the shear blades. A storage chamber was then attached to the manipulator/STC and pressures balanced. The core was pushed into this storage chamber (Fig. F19F) for storage at in situ pressure and temperature conditions (5°–7°C) for shore-based analyses.

At the first two sites (U1328 and U1329) cored we used seawater as the pressurizing medium, as had been done on previous expeditions, but at the remaining three sites we used freshwater, which is much less corrosive for long-term storage. The freshwater pressurizing fluid was spiked with fluorescein (1–10 mg/L), and samples of pressurizing fluid were taken when each pressure core was stored so that shore-based investigators might monitor any infiltration of the pressurizing fluid into the core.

Pressure and temperature control

To study the properties of gas hydrate–bearing sediments from sediment cores, an ideal core would retain the in situ effective pressures, the hydrostatic pressure, and the temperature. It is currently only practical to retain the hydrostatic pressure in a coring tool. During Expedition 311, we also made an effort to improve temperature control during the recovery, handling, and analysis of pressure cores.

Pressure control in pressure corers

Pressure cores rarely (if ever) arrive in the laboratory at in situ pressure (Dickens et al, 2003; Tréhu, Bohrmann, Rack, Torres, et al., 2003). The recovery pressure is generally below the in situ pressure, but occasionally the recovery pressure has been higher when there is gas hydrate present. The main causes of pressure loss are

- Seals that do not close immediately,
- Differential volume changes of the tool and its contents caused by changes in temperature, and
- Volume changes in the tool caused by changes in the differential pressure that occurs during recovery.

Volume changes from differential pressure occur mainly from the initial compression of compliant components (O-rings, etc.) as the tool seals, though a small component is caused by the volume expansion of the tool itself as the pressure on the outside falls with respect to the inside pressure.

Even cores recovered at substantially below in situ pressure and those that have been outside the GHSZ for a significant period of time are still of value if the corer sealed soon after coring, capturing all enclosed methane and other core constituents. If pressure losses can be attributed mainly to tool volume changes due to pressure and temperature, although the methane may have changed phase during the retrieval process, the total quantity of methane will remain unchanged and the in situ phases can be calculated. However, cores that have been outside gas hydrate stability cannot be used to investigate the nature and distribution of gas hydrate in the core with confidence using nondestructive techniques (*P*-wave velocity, gamma ray density, and X-ray imaging). The difficulty arises in recognizing the difference between pressure losses due to late sealing of a pressure coring tool versus losses caused by pressure and temperature changes. Thus, the operation of the tools has become an area of ongoing investigation.

To minimize the reduction in pressure caused by differential expansion from temperature and pressure effects, the HRC and FPC systems contain a gas accumulator that is normally set at 80%–90% of the anticipated in situ pressure. This allows the tool to expand slightly without any significant change in pressure, keeping the pressure high and minimizing the chances of the core moving out of the GHSZ. PCS deployments during Expedition 311 generally recovered cores with 50%–60% of the in situ pressure. The PCS could benefit from a gas-filled pressure accumulator connected to the autoclave.

Improvement of temperature control

None of the pressure coring tools have any active temperature control and, hence, the best that can be achieved is to minimize or reverse any adverse rises in temperature during the complete coring and handling processes. To achieve this, we recovered the core to the rig floor on the wireline "as fast as practically possible;" normally at a speed of 100 m/min but up to 250 m/min. After breaking the corer out of the pipe, it was quickly inserted through a rathole in

the rig floor into a newly designed, vertical, 2.5 m deep, insulated ice water–filled shuck suspended in the moonpool (Fig. F20). This ice shuck is deep enough to quickly cool the autoclave containing the core, which is at the bottom of the tools, and was filled by a chute from an ice machine located below the drill floor in the subsea shack. After examining the temperature records for the first few pressure corer deployments, a 30 min ice soak before tool removal and breakdown was deemed optimal. During this chilling period, the next rig floor operation/tool deployment was performed and, hence, the cooling time had little or no impact on drilling activities. The autoclave temperature was 0°–3°C after chilling, and the autoclave slowly warmed during autoclave removal at ambient temperature before it was moved into the refrigerated van. The thermal mass of the core, surrounding fluid, and autoclave was sufficient to keep the core from warming more than a few degrees in 10–20 min. Thereafter, further analyses on the autoclave were conducted in dedicated cold vans.

The inclusion of dedicated cold vans for analysis of pressurized cores was a major change from previous expeditions. During Leg 204, degassing of the PCS cores took place in iced cylinders in the hard rock laboratory, next to the thin section laboratory, while the transfer of HYACINTH cores took place on the walkway above the catwalk with ice bags being used (unsatisfactorily) for cooling. Degassing and logging of the HYACINTH cores took place in very warm conditions in the lab stack hold, with frequent interruptions, despite insulating foam around the pressure chamber, to take the core back into the adjacent cold reefers in an effort to prevent rapid dissociation of the gas hydrate. During Expedition 311, all of these operations took place in two temperature-controlled (5°–7°C) 20 ft containers, one dedicated to PCS degassing experiments and one used for transferring and logging the HYACINTH cores in the MSCL-P, as well as for X-raying the PCS cores before and after degassing. With this procedure, we maximized the chances of keeping the core within the GHSZ during its journey from the seafloor to the laboratory.

Nondestructive measurements on pressure cores

Although pressure cores are particularly valuable for providing accurate methane volumes for gas hydrate concentration calculations, nondestructive measurements made before or during the depressurization process can provide additional information on the nature and distribution of gas hydrate within the sediment and rare data on near in situ physical properties of gas hydrate–bearing sediments. X-ray images of the pressure cores show the overall structure of the core and gas hydrate within them (as well as contributing to the core length estimate), GRA provides accurate densities of sediment/gas hydrate structures, and measurement of *P*-wave velocity on undisturbed gas hydrate–bearing sediments at in situ pressure provides acoustic parameters valuable for analysis of seismic data. Two measurement systems were used during Expedition 311 to collect data on pressure cores: the GeoTek MSCL-P, used on cores under full recovered pressure; and the GeoTek vertical multisensor core logger (MSCL-V), used during degassing experiments.

Measurements on pressure coring system cores

Efforts during Expedition 311 were the first attempt at taking nondestructive measurements on PCS cores while still in the autoclave under pressure. The aluminum core barrels (specially fabricated for this expedition) allowed X-ray analysis of the PCS cores. Being able to "see" the core prior to degassing enabled the original length (and hence volume) of the core to be measured, which is critical in the calculation of gas hydrate content. The density measurements taken during degassing using the MSCL-V provided information similar to that collected on HYACINTH cores during Leg 204, where low-density, potentially gas hydrate–bearing layers could be monitored as the core was depressurized to observe gas hydrate dissociation and gas evolution.

The PCS autoclave was brought to the HYACINTH logging van for X-ray scanning after it was removed from the tool body. The top of the autoclave was mated to the end of an unpressurized HYACINTH manipulator, allowing the MSCL-P software and manipulator to push the PCS autoclave through the X-ray imaging system. Unfortunately, the metal body of the PCS caused distortion of the X-ray images (Fig. F21). As the PCS was moved past the image intensifier, the character of this classic "S"-distortion changed (Fig. F21), probably as a result of the moving steel interacting with the magnetic fields in the image intensifier. An X-ray montage from 0 to 51 cm relative to the top of the PCS inner barrel was created (normally in 0.5 cm increments) for each PCS core. The lower half of the barrel was completely obscured by a steel sleeve (Fig. F17B).

Once the PCS autoclaves were moved to the PCS degassing van atop the lab stack, they were placed in the MSCL-V (Fig. F22) (Tréhu, Bohrmann, Rack, Torres, et al., 2003). The MSCL-V accommodates cores vertically, and the sensor cluster moves up and down along the stationary core. The gamma ray source and detectors are the same as those used on

the MSCL-P and IODP MST (see **"Multisensor track"**), and calibration was performed in a similar fashion (see **"Pressure multisensor core logger measurements on HYACINTH cores"**). The GRA of an aluminum calibration sample of varying, known thickness was measured within a water-filled PCS autoclave to provide the density calibration. The PCS autoclaves were always oriented the same way in the MSCL-V, with the transducer port facing forward, and gamma ray attenuation for the PCS autoclaves, filled with water, was measured so that the data could be corrected as a function of vertical position (Fig. **F17**).

The core densities measured in the upper half of the PCS autoclave had an estimated error of ±0.05 g/cm^3, but because the lower half of the autoclave outer barrel contains a spring and other steel sleeves, the density of the core in the lower half of the PCS autoclave could not be determined as accurately. There was also an unexplained interaction between the PCS and the gamma ray attenuation sensor at 30–55 cm core depth, causing a lowering of the count rate that varied over time in this area (Fig. **F17**). However, the primary use of the tool was to look at density differences that occurred during degassing, and, hence, most of the data were simply plotted as differential density (the initial density profile subtracted from each of the subsequent profiles) to observe the evolution and migration of gas within the core barrel during depressurization.

Pressure multisensor core logger measurements on HYACINTH cores

The MSCL-P (Fig. **F23**) is an automated measurement system for the collection of acoustic *P*-wave velocity, GRA, and X-ray image data on HYACINTH pressure cores under pressures up to 25 MPa. The MSCL-P pressure chamber is constructed of aluminum and contains an internal set of ultrasonic transducers. X-ray and gamma ray sources and detectors are situated outside of the pressure chamber. The system moves pressurized HYACINTH cores incrementally past these sensors, under computer control, with a positional precision of better than 1 mm, allowing detailed gamma ray density and acoustic velocity profiles to be obtained rapidly and automatically along the core as well as creating automated full-core X-ray montages. The manipulator mechanism ensures that the core does not rotate during the linear translation.

Core logging under pressure using the MSCL-P is, in principle, very similar to core logging with the IODP MST or a standard GeoTek MSCL. One exception is the increased distance and varied material between the sensors and the core. Sensors are separated from the core by the plastic liner, the pressurizing fluid (seawater), and, in the case of the gamma and X-ray sensors, the aluminum pressure chamber. To calibrate for measurements of acoustic velocity and gamma ray density, similar techniques are used to those developed for the MST and MSCL (see **"Multisensor track"**), which use distilled water and aluminum as standards. During logging of pressure cores, the inner liner is assumed to have a constant diameter because it cannot be directly measured under pressure.

Gamma ray density was measured using a ^{137}Cs source and NaI detector very similar to those used on the MST (see **"Multisensor track"**). Errors are proportional to the square root of the total counts (generally ~5000 cps), giving a density precision of 2%. Calibration of the gamma ray density measurements was performed by measuring the intensity of the gamma ray beam through a stepped aluminum bar of varying thickness sitting centrally in a core liner filled with and surrounded by saltwater of known salinity. This calibration procedure, using aluminum and water, provides a good approximation for a water-saturated sediment (minerals and water) and has proven to be an excellent calibration protocol for determining density from GRA. Separate calibrations were performed for FPC and HRC liners, and no effect was seen with increasing pressure.

Ultrasonic *P*-wave velocity (V_P) was measured using two 500 kHz acoustic transducers mounted inside the pressure chamber, perpendicular to the core and the gamma ray beam. Traveltimes were measured with a precision of 50 ns, and the error associated with the velocity was ±3 m/s, assuming a core thickness of ~6 cm. To calibrate V_P, the total *P*-wave traveltime was measured when both the core liner and the pressure chamber were filled with water of known velocity (from temperature, pressure, and salinity). Changes in traveltime as a function of pressure were also measured (up to 25 MPa). The measured variation in V_P with pressure was close to the theoretical variation for water, and therefore the traveltimes in the liner material were essentially constant with changing pressure (as was found during Leg 204; Tréhu, Bohrmann, Rack, Torres, et al., 2003).

X-ray images were obtained using a linear X-ray device consisting of a lead-shielded microfocal X-ray source, phosphor image intensifier, and digital camera. An aluminum compensator minimizes the intensity variations that are caused when illuminating round objects. With the geometrical arrangement and typical X-ray spot size of ~8–12 µm used, the intrinsic spatial resolution of the images is ~150 µm. All final core images were obtained by creating mon-

tages from a series of area images taken along the core. The normal spatial interval used for the final image was 0.5 cm, which creates a relatively flat image along the core without any apparent significant spherical distortion. However, an unexpected electromagnetic distortion in the image intensifier, similar to but less intense than that observed with the PCS (Fig. **F21**), limited our ability to create perfectly smoothed montages. The X-ray images were not density calibrated because the GRA measurements give higher accuracy than the polychromatic X-rays. Instead, we varied the X-ray energy and power levels to maximize the qualitative resolution of the image in an effort to examine subtle structures within the core. X-ray energies as much as 110 kV were used depending on the density of the cores being measured.

HYACINTH core analysis at the Pacific Geosciences Centre

The HYACINTH pressure cores were placed in storage chambers for immediate postcruise analysis and sampling at the Pacific Geoscience Centre of the Geological Survey of Canada, Sidney, British Columbia. The cores underwent one of three different subsampling and analysis protocols. Cores to be degassed were degassed at 4°C, in a similar fashion to the PCS, using the same degassing manifold, MicroGC, and the MSCL-V. Cores to be subsampled and placed into Parr vessels were rapidly depressurized by opening a side valve on the storage chamber, and the core was cut using a hacksaw into 20 cm subsections that would fit inside the Parr vessels. The subsections were placed inside the Parr vessels and repressurized with methane. Other pressure cores were held for specialized subsampling under pressure.

Degassing experiments

During Expedition 311, the PCS retrieved pressurized sediments for onboard degassing experiments. Controlled release of pressure from the PCS through a manifold permits

- Collecting all gas discharged from the sediment's free gas and gas hydrate phase for quantitative and qualitative analysis;
- Estimating the in situ abundance of gas hydrate and free gas based on mass balance, methane solubility, and gas hydrate stability considerations (Dickens et al., 1997; see **"Estimating the abundance of gas hydrate and free gas"**);
- Identifying the presence of gas hydrate from volume-pressure-time relations (Hunt, 1979; Dickens et al., 2000b; Milkov et al., 2004); and
- Monitoring the controlled decomposition of gas hydrate with nondestructive methods in the course of the degassing experiment.

Degassing experiments were carried out in the PCS van (Fig. **F24**) after some time (>1 h) had been allowed for the PCS to equilibrate to ambient van temperature (7°C) and a vertical gamma ray scan had been run to determine the initial density distribution within the PCS core (see **"Measurements on pressure coring system cores"**). The PCS was connected to a pressure transducer, a helium-flushed degassing manifold for controlled release of pressure, and through the manifold to a bubbling chamber that allows collection of released gas (Fig. **F25**). We used a liquid leak detector to check the connection between the PCS and the manifold for leakages. Prior to each degassing experiment, we monitored the air quality in the temperature-controlled van and analyzed a blank (i.e., a gas-phase sample taken from the helium-flushed bubbling chamber). If the blank contained traces of O_2 and N_2, we continued flushing of the degassing system with helium and repeated the blank analysis until all air was removed. For the gas analysis, we used the same Agilent 3000A MicroGC and method as for samples (see below). Thereafter, we carefully released and collected a small volume of gas that was usually extruded together with some water from the outer core barrel (~500 mL) to flush the lines connecting the PCS to the manifold. All water that escaped from the PCS was collected by the sampling port on the manifold, quantified, and subsampled for geochemical analysis. We observed a strong decrease in pressure when water was expelled from the PCS during the initial phase of the degassing experiment. In the following steps, gas was released, collected, and subsampled from the bubbling chamber for quantitative and qualitative analysis as outlined in the degassing protocol below. During the degassing procedure, we ran additional gamma ray scans of the PCS to monitor the evolution of gas voids and pathways. Degassing experiments were terminated when the pressure within the PCS had equilibrated to atmospheric pressure, and <5 mL of gas had exsolved from the core within 3 h. At the end of each experiment, we collected a final gas sample and ran a final gamma ray scan. The degassed core was removed from the outer core barrel, X-rayed, extruded, curated, and sampled for IW chemistry, dissolved gases, and physical properties, including parameters critical for calculating methane concentration (see **"Estimating the abundance of gas hydrate and free gas"**).

Degassing was carried out in incremental steps using the following protocol. First, the manifold was

closed with respect to the bubbling chamber and then opened with respect to the PCS. In this manner, a constant volume of gas was allowed to move into the manifold. The pressure inside the manifold was not constant throughout the experiment but equilibrated with the residual pressure of the PCS core. Next, the valve between the manifold and the PCS was closed and the gas inside the manifold was released into the bubbling chamber where its volume expanded as a result of the pressure release.

PCS cores that had strong indications for the presence of gas hydrates were degassed in the following way. During an initial phase, gas and any water that was expelled from the outer core barrel were released in small incremental steps. At this stage degassing caused immediate pressure drops inside the PCS. Once pressure had reached equilibrium conditions for gas hydrate stability, further release of gas caused only relatively small decreases in pressure. The reason for this behavior is twofold:

1. Gas hydrate dissociation releases free gas, which in a closed container, increases pressure until dissociation ceases.
2. Gas hydrate dissociation releases fresh water, which increases the stability of gas hydrate at given pressure and temperature conditions (Dickens et al., 2000b).

During the gas hydrate dissociation phase, depressurization was repeatedly stopped to monitor the pressure response and to carry out gamma ray density scans. Once pressure had dropped below equilibrium conditions for gas hydrate stability, we monitored carefully whether further incremental release of gas was followed by pressure increases from gas hydrate dissociation. When pressure decreases indicated the absence of gas hydrate, depressurization was carried on continuously.

During each degassing experiment, the internal PCS pressure was monitored by analog pressure gauges and recorded by digital pressured transducers connected to a computer. However, because of technical problems, digital pressure records were not available for all degassing experiments conducted during Expedition 311. The released gas was collected in a 1 L bubbling chamber consisting of an inverted graduated cylinder and a plexiglass tube filled with a saturated NaCl solution (Fig. **F25**). The released gas volume was recorded as a function of PCS opening number and pressure. After measuring the volume of collected gas, gas aliquots were sampled from a valve at the top of the inverted cylinder using a syringe. The syringe was thoroughly flushed with gas from the bubbling chamber to minimize dilution of the sample by air that was present in the syringe and valve prior to sampling. After flushing the syringe, one aliquot (6 mL) was taken for immediate analysis of the gas composition (C_1, C_2, CO_2, N_2, and O_2) using an Agilent 3000A MicroGC equipped with Plot U and molecular sieve columns and a TCD that was located in the PCS van. Another aliquot (10 mL) was taken for further shipboard analysis (e.g., low concentrations of C_2 and higher hydrocarbon gases) and for shore-based isotopic analyses. These samples were stored in headspace vials filled with saturated NaCl solution and tightly sealed with untreated blue butyl rubber stoppers and crimp caps. During this expedition, any air measured in gas samples from the PCS was assumed to have been laboratory contamination, and the samples were corrected for air dilution.

Aside from the released gas volume and pressure response inside the PCS, further parameters were documented that are crucial for accurate mass balance calculations and interpretation of the degassing experiments. First, to calculate the quantity of released methane by the ideal gas law, ambient air pressure and air temperature in the PCS van were continuously recorded throughout the experiment using a digital temperature logger inside the PCS van and the barometer on the bridge deck. Second, when pressure is released from the PCS, free gas can evolve in such a way that it forces water out of the core. The total volume of expelled water corresponds to the volume of gas left inside the PCS at the end of depressurization. We accounted for the gas remaining in the PCS by recording the volume of expelled water and assigning the composition of the final gas sample. Third, after degassing was finished, we collected the water remaining in the outer core barrel to account for any additional headspace that might have been present in the PCS. However, we did not include these data in the mass balance calculations presented in this report, because any incomplete recovery of water from the outer core barrel would lead to an overestimation of in situ gas hydrate concentrations. Finally, to account for the total pore water volume, the accurate length of the recovered sediment interval was obtained by an initial gamma ray density scan and the porosity of the sediment was analyzed from solid phase samples taken at the end of the experiment. For mass balance calculations, we used the length obtained prior to degassing (reported as recovered length in each site chapter) rather than the length obtained after degassing from the extruded core (reported as curated length in each site chapter), because any loss of sediment from the inner core barrel during degassing and core extrusion would lead to an overestimation of in situ gas hy-

drate concentrations. In addition, we took samples for HS analysis from the extruded sediment to account for dissolved methane in each PCS core (see "Organic geochemistry").

Estimating the abundance of gas hydrate and free gas

Pressure core degassing experiments allow characterization of the total amount of methane that is present in the PCS as free and dissolved gas phases at shipboard pressure and temperature conditions using the equation

$$n_{\text{tot CH4}} = n_{\text{free CH4}} + n_{\text{diss CH4}}, \quad (5)$$

where

$n_{\text{tot CH4}}$ = total amount of methane in the PCS (moles),
$n_{\text{free CH4}}$ = free methane (moles), and
$n_{\text{diss CH4}}$ = dissolved methane (moles).

We calculated the quantity of free methane from the measured total volume of released gas, the molar fraction of methane in the gas phase known from continuous GC analysis during the degassing experiment, ambient air temperature, and pressure using the ideal gas law

$$n_{\text{free CH4}} = \chi_M \times p_{\text{atm}} \times V/(R \times T), \quad (6)$$

where

χ_M = molar fraction of methane in the headspace gas (GC analysis),
V = volume of released gas (liter),
p_{atm} = ambient air pressure (MPa),
T = ambient air temperature (K), and
R = universal gas constant (0.008314 MPa L/[K·mol]).

The total volume of released gas resulted from the gas volume released into the bubbling chamber, the volume of expelled water, which was assumed to leave a corresponding gas void in the PCS, and from the dead volume of the degassing system (261 mL), which was filled with gas released from the PCS at the end of the degassing experiment.

The amount of dissolved methane was analyzed from sediment samples taken at the end of the experiment using the headspace gas analysis protocol (see "Organic geochemistry") and calculated by

$$n_{\text{diss CH4}} = [\chi_M \times p_{\text{atm}} \times V_H/(R \times T \times \phi \times V_S)] \times V_{\text{pw}}, \quad (7)$$

where

V_H = volume of the sample vial headspace,
V_S = volume of sediment sample in the sample vial, and
V_{pw} = pore water volume (liters).

Pore volume (V_{pw}) is given by

$$V_{\text{pw}} = \pi \times r_{\text{PCS}}^2 \times l_{\text{PCS}} \times \phi, \quad (8)$$

where

r_{PCS} = the radius of the PCS,
l_{PCS} = the recovered core length, and
ϕ = the sediment porosity.

The porosity used in mass balance calculations was the mean of samples taken from the PCS as well as from APC and XCB cores taken at similar depths from the same site.

The total methane concentration (c_{CH4}) in the pore space of the PCS core is given by the total amount of methane and the pore water volume inside the PCS core:

$$c_{\text{CH4}} = n_{\text{totCH4}}/V_{\text{pw}}. \quad (9)$$

To account for the amount of methane that was enclosed in the PCS as free gas or gas hydrate at in situ conditions, we considered the variation of methane solubility with temperature, pressure, and salinity. We calculated methane solubility according to Xu (2002, 2004). Based on the in situ methane saturation, we determined the concentration of methane that could have been dissolved in the pore water volume within the PCS (V_{pw}). If the pore water was oversaturated with methane at in situ conditions, the concentration of nondissolved methane was obtained by subtracting the concentration of dissolved methane $c_{\text{dissCH4, in situ}}$ (i.e., methane saturation) from the total methane concentration in the PCS (c_{CH4}). The amount of nondissolved methane in the PCS was calculated from its concentration and the pore water volume inside the PCS:

$$n_{\text{freeCH4, in situ}} = (c_{\text{CH4}} - c_{\text{dissCH4, in situ}}) \times V_{\text{pw}}. \quad (10)$$

If in situ pressure and temperature were outside the gas hydrate stability field, nondissolved methane was considered to be free gas and the volume of the free gas phase was calculated based on the ideal gas law. If the in situ pressure and temperature indicated gas hydrate stability, nondissolved methane was considered to be gas hydrate and its volume (V_{GH}) was calculated based on and the molecular weight (m_{GH}) and density (δ_{GH}) of gas hydrate using

$$V_{\text{GH}} = n_{\text{free CH4, in situ}} \times m_{\text{GH}}/\delta_{\text{GH}}, \quad (11)$$

where

m_{GH} = 124 g/mol and
δ_{GH} = 0.91 g/cm^3.

Finally, we calculated how much water would have been released and freshened the pore water inside the PCS if the predicted amount of gas hydrate had decomposed during the degassing experiment, assuming that 108 g of water is released per mole of decomposed gas hydrate.

Degassing experiments at Site U1329 were the first ones performed during Expedition 311. They revealed that an initial gas volume of 500 mL needs to be released before all helium is removed from the hoses that connect the PCS port to the bubbling chamber. The hoses and manifold hold a dead volume of 261 mL. Methane that was released within the initial gas volume was included when calculating the total amount of methane released from the core. However, the methane concentration of the helium-diluted initial gas volume was excluded when the average composition of the released gas phase was determined.

Downhole logging

The downhole logging program during Expedition 311 was specifically designed to assess the presence and concentration of gas hydrates at the Cascadia accretionary prism. Several LWD/MWD and wireline logging tools were deployed, as described below. Not all tool strings were run in each hole. Refer to the individual site chapters for details of the tool strings deployed at each site.

Downhole logging aboard the *JOIDES Resolution* is provided by the Lamont-Doherty Earth Observatory Borehole Research Group (LDEO-BRG) in conjunction with Leicester University Borehole Research, the Laboratoire de Mesures en Forages Montpellier, University of Aachen, University of Tokyo, Schlumberger Reservoir Evaluation Services, and Schlumberger Drilling and Measurements.

Logging while drilling

During Expedition 311, six LWD/MWD tools were deployed at the five sites cored and drilled on the Cascadia margin. These tools were provided by Schlumberger Drilling and Measurements Services under contract with the LDEO-BRG.

LWD tools measure in situ formation properties with instruments that are located in the drill collars immediately above the drill bit. MWD tools are also located in the drill collars and measure downhole drilling parameters (weight on bit, torque, etc.). The difference between LWD and MWD tools is that LWD data are recorded into downhole computer memory and retrieved when the tools reach the surface, whereas MWD data are transmitted through the drilling fluid within the drill pipe by means of a modulated pressure wave, or "mud pulsing," and monitored in real time (see below). MWD tools enable both LWD and MWD data to be transmitted uphole when the tools are deployed in conjunction. The term LWD/MWD is used throughout this volume to cover both LWD- and MWD-type measurements.

The Schlumberger LWD/MWD tools used during Expedition 311 include the GeoVISION resistivity (GVR) tool (formerly known as the Resistivity-at-the-Bit [RAB] tool), the EcoScope tool, the SonicVISION tool, the TeleScope MWD tool, the ProVISION nuclear magnetic resonance (NMR) tool, and the ADN-VISION azimuthal density neutron tool. This was the first time the EcoScope, SonicVISION, and TeleScope tools were used during an ODP leg or IODP expedition. Figure **F26** shows the configuration of the LWD/MWD BHA, and Table **T3** lists the set of measurements recorded. LWD/MWD logs complement wireline logs in an integrated interpretation of gas hydrate saturations. LWD/MWD measurements are made shortly after the hole is drilled and before the adverse effects of continued drilling or coring operations. The invasion of drilling fluid into the borehole wall is reduced relative to wireline logging because of the shorter time elapsed between drilling and taking measurements.

The LWD/MWD equipment is powered by batteries or mud motors and uses erasable/programmable read-only memory chips to store logging data until they are downloaded; a limited amount of data is sent to the surface in real time by the MWD tool. The LWD/MWD tools take measurements at evenly spaced time intervals and are synchronized with a system on the drilling rig that monitors time and drilling depth. After drilling, the LWD/MWD tools are retrieved and the data downloaded from each tool. Synchronization of the uphole and downhole clocks allows merging of the time-depth data (from the surface system) and the downhole time-measurement data (from the tools) into depth-measurement data files. The resulting depth-measurement data are transferred to the processing systems in the downhole measurements laboratory (DHML) for reduction and interpretation. For a detailed description of the depth tracking systems, see the Leg 204 *Initial Reports* "Explanatory Notes" chapter (Shipboard Scientific Party, 2003b).

Gas monitoring with real time logging-while-drilling/measurement-while-drilling data

LWD/MWD logs were acquired in the first hole drilled at each site to plan coring and pressure coring operations in subsequent holes. As these holes were drilled without coring, the LWD/MWD data had to be monitored to detect gas entering the borehole. This new procedure supersedes the old standard of using gas ratio measurements for hydrocarbon safety analysis. Results of previous gas hydrate drilling programs, such as ODP Legs 146 (Westbrook, Carson,

Musgrave, et al., 1994), 164 (Paull, Matsumoto, Wallace, et al., 1996), and 204 (Tréhu, Bohrmann, Rack, Torres, et al., 2003), and, more recently, the Chevron/Texaco Gulf of Mexico Gas Hydrate JIP Drilling Program, have shown that gas hydrate–bearing sections do not represent a significant threat to drilling operations and that as long as the hole is advanced at relatively normal drilling rates with mud temperatures near that of the deeper water column there is no significant gas flow from gas hydrate–bearing formations. The main concern of the LWD/MWD monitoring program was the recognition of free-gas zones within the drilled interval that below the GHSZ; these free-gas zones have the potential to flow.

LWD/MWD measurements sensitive to the presence of free gas include borehole fluid pressure (decrease because of less dense fluids), compressional velocity of the borehole fluid and of the formation (strong decrease with free gas), coherence of measured sonic waveforms (decrease with free gas), electrical resistivity (increase with free gas), and neutron and density logs (decrease of density and neutron porosity; e.g., neutron/density crossover). In addition, the gamma ray log indicates whether the changes in the logs are caused by changes in the lithology rather than in the pore fluid, the NMR porosity gives a reference porosity to calibrate the neutron/density crossover, and the caliper measurement can be used to assess the reliability of the measurements and the possible influence of material falling in the borehole.

The primary measurement used in gas monitoring was the annular pressure while drilling (APWD) measured by the EcoScope tool in the borehole annulus (the space between the drill string and the borehole wall). On the basis of a simple calculation of the effect of free gas on the borehole fluid density, it was determined that a pressure decrease of >100 psi (pounds per square inch) from the general trend of fluid pressure would indicate that a significant amount of gas had been released into the drilling fluid. For example, a pressure decrease of 100 psi corresponds to a 25% gas saturation in a borehole drilled to 300 mbsf. It was also decided to monitor sudden pressure increases of >100 psi, which have been reported as precursors to gas flow into the annulus (Aldred et al., 1998).

We also set the SonicVISION tool to process the borehole fluid velocity in real time because previous drilling experience in North Sea wells had shown that the presence of gas caused the coherence of the sonic waveforms to decrease and the inferred value of fluid velocity to become erratic. In practice, we monitored the coherence of the waveforms used to infer the fluid velocity: a low coherence may indicate the presence of gas. Although the pressure and acoustic sensors are located some distance above the drilling bit (6.46 and 17.7 m, respectively) (Fig. **F26**), gas moves rapidly upward in the annulus from the point of entry at the bit and would be detected quickly.

The monitoring procedure followed the decision tree shown in Figure **F27**, which is described below.

1. If a >100 psi pressure decrease is observed, then drilling advancement will cease and relevant personnel will be notified. Seawater will be circulated in the hole and the APWD response will be monitored to obtain the baseline pressure. Duration of monitoring will depend on geologic and drilling conditions at a particular site and depth, based on shipboard personnel experience.
2. An observed pressure decrease of 150 psi will result in terminating the hole and following plug and abandonment procedures.
3. If a <150 psi pressure decrease is observed, drilling can advance at a reduced rate of penetration (ROP) with continued monitoring of pressure and other sensors. Pressure will be maintained within 150 psi of normal using weighted mud, as required. The ability to continue advancing the hole while controlling pressure changes with weighted mud is dependent upon onboard mud capacity and availability.
4. If pressure cannot be controlled with 10.5 pounds per gallon (ppg) mud, the hole will be plugged and abandoned.
5. If pressure can be controlled with 10.5 ppg mud, then drilling advancement may continue.

A pressure decrease caused by gas flow into the borehole may be preceded by a pressure increase as the result of the acceleration of fluids in the annulus (Aldred et al., 1998). If an increase >100 psi is observed, drilling will cease as a precautionary measure and relevant personnel will be notified. Seawater will be circulated in the hole and the APWD response will be monitored to obtain the baseline pressure. Because no overpressure water flow events are expected or likely in this environment, such a pressure increase could be the result of the aforementioned precursor or drilling-induced pressure increases. A drilling-induced pressure increase will be resolved by cleaning the hole, whereas the precursor event will be followed by a pressure decrease, leading to appropriate response as dictated by the procedure above.

GeoVISION tool

The GeoVISION tool (RAB or GVR6) provides resistivity measurements of the formation and electrical images of the borehole wall, similar to the wireline Formation MicroScanner (FMS) but with complete

coverage of the borehole walls and lower vertical and horizontal resolution. In addition, the RAB tool contains a scintillation counter that provides a total gamma ray measurement.

The tool is located directly above the drill bit and uses two transmitter coils and a number of electrodes to obtain several measurements of resistivity:

- Bit resistivity: the lower transmitter coil generates a current that flows through the bit and into the formation, returning to the drilling collar far up the tool string. By measuring the axial current through the bit for a given voltage, resistivity near the bit is determined by Ohm's law.
- Ring resistivity: the upper and lower transmitter coils produce currents in the collar that meet at the ring electrode. In a homogeneous medium, these currents flow perpendicularly to the tool at the ring electrode. In a heterogeneous formation, this radial current flow is distorted, and the current required through the ring electrode to focus current flow into the formation is related to the formation resistivity. The ring electrode is only 4 cm thick and provides a high-resolution resistivity measurement.
- Button resistivity: the same focusing process used in measuring the ring resistivity is applied to determine the resistivity at three 1 inch button electrodes. Button resistivity measurements made about every 6° as the tool rotates in the borehole are stored and processed to produce a resistivity image of the borehole wall. The button electrodes measure resistivity at three depths of investigation and thus generate three resistivity images: shallow, medium, and deep. The tool uses the Earth's magnetic field to refer the resistivity images to magnetic north.

GeoVISION tool programming

For quality control reasons, the minimum data recording density is one measurement per 6 inch (15.2 cm) interval; hence, a balance must be determined between the ROP and the sampling rate. This relationship depends on the recording rate, the number of data channels to record, and the memory capacity (46 MB) of the tool. During the Expedition 311 LWD program, we used a data acquisition sampling rate of 5 s for high-resolution resistivity images. The maximum ROP allowed to produce one sample per 6 in interval is given by ROP_{max} (m/h) = 548/sample rate. This relationship gives 110 m/h maximum ROP for the GeoVISION tool. During Expedition 311, the target ROP was 20–50 m/h, at most ~50% of the maximum allowable ROP for the GeoVISION tool. These reduced rates improved the vertical resolution of the resistivity images to 5–10 cm per rotation. Under this configuration the GeoVISION tool had enough memory to record as much as 6 days of data, which was sufficient to complete the Expedition 311 LWD operations.

EcoScope tool

The EcoScope tool integrates several formation evaluation, well placement, and drilling optimization measurements in a single collar. The EcoScope tool provides a suite of resistivity, thermal neutron porosity, and azimuthal gamma ray and density measurements. The dual-frequency propagation resistivity array (2 MHz and 400 kHz) makes 10 phase and 10 attenuation measurements at several depths of investigation, providing invasion profiling and formation resistivity. For neutron generation, the EcoScope uses a pulsed neutron generator, which eliminates the need for a chemical source; it still uses a ^{137}Cs gamma ray source for density logging. In addition, the EcoScope provides the first commercial LWD measurements of elemental capture spectroscopy, neutron gamma density, photoelectric factor (PEF), and neutron capture cross-section, or sigma. Drilling optimization measurements include APWD, caliper, and shock detection. We used the APWD measurement to monitor gas in the annulus in real time.

SonicVISION tool

The SonicVISION tool records monopole acoustic waveforms in downhole memory and transmits uphole, in real time, acoustic slowness obtained by processing the recorded waveforms. The principle of the SonicVISION tool is similar to that of wireline array sonic tools (Schlumberger, 1989). The monopole source produces a ~13 kHz pulse that travels into the formation and refracts back into the borehole. Sonic waveforms are recorded at four monopole receivers spaced at 10, 10.67, 11.33, and 12 ft (3.05, 3.25, 3.45, and 3.65 m) above the source.

Sonic measurements made while drilling are affected by drilling noise. Because the upward propagation of energy in the formation is synchronized with the transmitter firing and any residual drilling noise is not, averaging the waveforms from various consecutive firings increases the relative amplitude of coherent signals. A stack size of approximately eight waveforms is deemed appropriate for these conditions. The SonicVISION tool must also be kept centralized in the borehole in order to maximize the strength of the formation signal. In large holes and slow sediments, both the formation itself and asymmetry of the annular space in the hole will attenuate the signal.

To monitor for gas, the SonicVISION tool was configured to process and transmit in real time uphole

wave arrivals corresponding to velocity values (1300–1600 m/s) appropriate for the drilling fluid. The SonicVISION tool is configured so that waveform data are stored at 8 s intervals, allowing for 83 h of drilling before the downhole memory is filled. This was sufficient to reach the target depth at each of the Expedition 311 sites at a typical ROP of 25–35 m/h. The maximum ROP allowable to achieve one sample per 6 inch interval is estimated as ROP_{max} = 1800/8 = 225 ft/h (~68 m/h). SonicVISION waveform data were downloaded from the tool, converted to depth, and processed to estimate fluid wave slowness and waveform coherence using the Schlumberger Drilling and Measurements Integrated Drilling Evaluation and Logging system on the *JOIDES Resolution*.

TeleScope tool

The TeleScope tool transmits MWD data uphole by means of a pressure wave through the fluid in the drill pipe. In practice, the TeleScope tool generates a continuous wave within the drilling fluid and changes the phase of this signal (frequency modulation) to transmit relevant bit words representing information from various sensors. Two pressure sensors attached to the standpipe (one near the top and the second near the bottom) on the rig floor measured the pressure wave in the drilling fluid when information was transmitted up the drill pipe by the MWD tool. With the MWD mud pulsing systems, transmission rates can reach 12 bits/s, depending primarily on water depth and mud density. In contrast to real-time data, the downhole memory in the LWD tools records data at a minimum rate of one sample per 15 cm.

ProVISION tool

The basic technology behind the ProVISION NMR tool is similar to modern wireline NMR technology, based on measurement of the relaxation time of the magnetically induced precession of polarized protons. A combination of bar magnets and directional antennas focuses a pulsed, polarizing field into the formation. The ProVISION tool measures the relaxation time of polarized hydrogen nuclei in the formation, which provides information on the formation porosity. By exploiting the nature of the chemical bonds within pore fluids, for hydrogen in particular, the ProVISION tool can provide estimates of the total porosity and bound fluid volume, and thus be useful to determine whether water, gas, or gas hydrates are present in the formation.

During Expedition 311, the ProVISION tool transmitted only limited data to the surface through MWD and acquired additional data in memory. The relaxation time spectra were recorded downhole, and total porosity estimates were transmitted to the surface in real time. These spectra were stacked during postprocessing to improve the measurement precision. The signal probes a 14 inch cylindrical volume around the borehole, and, for an 8 ½ inch bit size, the depth of investigation of the measurement is ~7 cm into the formation. When the tool is static, the vertical resolution is 6 inch (~15 cm); when the tool moves, vertical resolution is decreased because of the need to maintain accuracy by vertical stacking of relaxation time spectra. For example, at a logging speed of 30 m/h, the vertical resolution is 1.2 m. Lateral tool motion may reduce data quality in some circumstances. Therefore, data from accelerometers and magnetometers contained in the downhole tool are used to evaluate data quality and determine the maximum relaxation times that can be resolved. Unfortunately, postcruise processing indicated that a tool malfunction had prevented the recording of any reliable data from the ProVISION tool during the expedition.

ADNVISION tool

The ADNVISION tool operation is similar in principle to the azimuthal density neutron tool used during previous ODP legs (e.g., Leg 196; Mikada, Becker, Moore, Klaus, et al., 2002). The density section of the tool uses a 1.7 Ci ^{137}Cs gamma ray source in conjunction with two gain-stabilized scintillation detectors to provide a borehole-compensated density measurement. The two detectors are located 5 and 12 inch (12.7 and 30.48 cm) below the source and compensate for the effect of fluid in the borehole. The number of Compton scattering collisions (change in gamma ray energy by interaction with the formation electrons) is related to the formation density. Returns of low-energy gamma rays are converted to a PEF value, measured in barns per electron. The PEF value depends on electron density and hence responds to bulk density and lithology. It is particularly sensitive to low-density, high-porosity zones.

The density source and detectors are positioned behind holes in the fin of a full gauge clamp-on stabilizer. This geometry forces the sensors against the borehole wall, thereby reducing the effects of borehole irregularities and drilling. The vertical resolution of the density and PEF measurements is ~15 and 5 cm, respectively. For measurement of tool standoff and estimated borehole size, a 670 kHz ultrasonic caliper is available on the ADNVISION tool. The ultrasonic sensor is aligned with and located just below the density detectors. In this position the sensor can also be used as a quality control for the density measurements. Neutron porosity measurements are obtained using fast neutrons emitted from a 10 Ci

americium oxide-beryllium (AmBe) source. Hydrogen quantities in the formation largely control the rate at which the neutrons slow down to epithermal and thermal energies. The energy of the detected neutrons has an epithermal component because much of the incoming thermal neutron flux is absorbed as it passes through the 1 inch drill collar. Neutrons are detected in near- and far-spacing detector banks, located 12 and 24 inch (30.48 and 60.96 cm), respectively, above the source. The vertical resolution of the tool under optimum conditions is ~34 cm. The neutron logs are affected to some extent by the lithology of the matrix rock because the neutron porosity unit is calibrated for a 100% limestone environment. Neutron logs are processed to eliminate the effects of borehole diameter, tool size, temperature, drilling mud hydrogen index (dependent on mud weight, pressure, and temperature), mud and formation salinities, lithology, and other environmental factors.

In near-vertical drill holes, the ADNVISION tool does not collect quadrant azimuthal data. Data output includes apparent neutron porosity (i.e., the tool does not distinguish between pore water and lattice-bound water), formation bulk density, and PEF. In addition, the ADNVISION tool outputs a differential caliper record based on the standard deviation of density measurements made at high sampling rates around the circumference of the borehole. The measured standard deviation is compared with that of an in gauge borehole, and the difference is converted to the amount of borehole enlargement. A standoff of <1 inch between the tool and the borehole wall indicates good borehole conditions, for which the density log values are considered to be accurate to ±0.015 g/cm^3.

Wireline logging measurements

During Expedition 311, the following three wireline logging tool strings were deployed (Fig. **F28;** Table **T4**):

1. The triple combination (triple combo) tool string (resistivity, density, and porosity measurements), which consisted of the Hostile Environment Gamma Ray Sonde (HNGS), the Phasor Dual Induction–Spherically Focused Resistivity Tool (DIT), the Hostile Environment Litho-Density Tool (HLDT), and the Accelerator Porosity Sonde (APS). The LDEO high-resolution Temperature/Acceleration/Pressure (TAP) tool was attached at the bottom of this tool string.
2. The FMS-sonic tool string, which consisted of the FMS, General Purpose Inclinometer Tool (GPIT), Scintillation Gamma Ray Tool (SGT), and the Dipole Sonic Imager (DSI).
3. The Well Seismic Tool (WST).

Because of difficult sea conditions, some of these tool strings had to be reduced or reconfigured. See individual site chapters for details.

Tool name acronyms, the parameters measured by each tool, the depth of investigation, and the vertical resolution are summarized in Table **T3.** More detailed descriptions of individual logging tools and their geological applications can be found in Ellis (1987), Goldberg (1997), Rider (1996), Schlumberger (1989, 1994), Serra (1984, 1986, 1989), and the LDEO-BRG Wireline Logging Services Guide (2001).

Hostile Environment Spectral Gamma Ray Sonde and Scintillation Gamma Ray Tool

The HNGS measures the natural gamma radiation from isotopes of K, Th, and U and uses a five-window spectroscopic analysis to determine concentrations of radioactive K (in weight percent), Th (in parts per million), and U (in parts per million). The HNGS uses two bismuth germanate scintillation detectors for gamma ray detection with full spectral processing. The HNGS also provides a measure of the total gamma ray emission (in gAPI) and the uranium-free or computed gamma ray emission (in gAPI). HNGS response is influenced by the borehole diameter and the weight and concentration of bentonite or KCl present in the drilling mud. KCl may be added to the drilling mud to prevent freshwater clays from swelling and forming obstructions. The spectral analysis filters out gamma ray energies below 500 keV, eliminating sensitivity to bentonite or KCl in the drilling mud and improving measurement accuracy. All environmental effects are corrected for during processing of HNGS data.

The SGT uses a NaI scintillation detector to measure the total natural gamma ray emission, combining the contributions of K, U, and Th in the formation. The SGT is not a spectral tool but provides high-resolution total gamma ray data for depth correlation between logging strings. It is included in all tool strings (except the triple combo, where the HNGS is used) to provide a reference log to correlate depth between different logging runs. In the FMS-sonic tool string, the SGT tool is placed between the two tools, providing correlation data to a deeper level in the hole.

Hostile Environment Litho-Density Tool

The HLDT consists of a radioactive cesium (^{137}Cs) gamma ray source (622 keV) and far and near gamma ray detectors mounted on a shielded skid, which is pressed against the borehole wall by a hydraulically activated eccentralizing arm. Gamma rays emitted by the source experience both Compton

scattering and photoelectric absorption. Compton scattering involves the ricochet of gamma rays off electrons in the formation via elastic collision, transferring energy to the electron in the process. The number of scattered gamma rays that reach the detectors is directly related to the number of electrons in the formation, which in turn is related to bulk density. Porosity may also be derived from this bulk density if the matrix density is known.

The HLDT also measures the PEF caused by absorption of low-energy gamma rays. Photoelectric absorption occurs when gamma rays reach <150 keV after being repeatedly scattered by electrons in the formation. As the PEF depends on the atomic number of the elements in the formation, it is essentially independent of porosity and varies according to the chemical composition of the sediment. Some examples of PEF values are pure calcite = 5.08, illite = 3.03, quartz = 1.81, and kaolinite = 1.49 b/e$^-$. PEF values can be used in combination with HNGS curves to identify different types of clay minerals. Coupling between the tool and borehole wall is essential for good HLDT logs. Poor contact results in underestimation of density values. Both density correction and caliper measurement of the hole are used to check the contact quality.

Accelerator Porosity Sonde

The APS consists of a minitron neutron generator that produces fast neutrons (14.4 MeV) and five neutron detectors (four epithermal and one thermal) positioned at different spacings along the tool. The tool is pressed against the borehole wall by an eccentralizing bowspring. Emitted high-energy (fast) neutrons are slowed down by collisions with atoms. The amount of energy lost per collision depends on the relative mass of the nucleus with which the neutron collides. The largest energy loss occurs when the neutron strikes a nucleus of equal mass, such as hydrogen, which is mainly present in pore water. Once neutrons degrade to thermal energies (0.025 eV), they may be captured by the nuclei of silicon, chlorine, boron, and other elements, with the associated emission of gamma radiation. The neutron detectors record both the numbers of neutrons arriving at various distances from the source and the neutron arrival times, which are a measure of formation porosity. However, hydrogen bound in minerals such as clays or in hydrocarbons also contributes to the measurement, so the raw porosity value is often an overestimate of formation porosity.

Phasor Dual Induction Tool

The DIT, also known as the spherically focused resistivity tool, provides three different measurements of electrical resistivity, each with a different depth of penetration into the formation. Two induction devices (deep and medium resistivity) transmit high-frequency alternating currents through transmitter coils, creating magnetic fields that induce secondary (Foucault) currents in the formation. These ground-loop currents produce new inductive signals, which are proportional to the conductivity of the formation and which are measured by the receiving coils. The measured conductivities are then converted to resistivity. A third device, a spherically focused resistivity instrument that gives higher vertical resolution, measures the current necessary to maintain a constant voltage drop across a fixed interval

High-resolution Temperature/Acceleration/Pressure tool

The TAP tool is a "dual application" logging tool (i.e., it can operate either as a wireline tool or as a memory tool using the same sensors). Data acquisition electronics are dependent on the purpose and required precision of logging data. During Expedition 311, the TAP tool was deployed as a memory tool in low-resolution mode; data were stored in the tool and downloaded after the logging run was completed. Temperatures determined using the TAP tool do not necessarily represent in situ formation temperatures because water circulation during drilling disturbs temperature conditions in the borehole. However, from the spatial temperature gradient, abrupt temperature changes can be identified that may correspond to contrasts in permeability at lithologic boundaries or that may represent localized fluid flow into the borehole, indicating fluid pathways and fracturing.

Dipole Sonic Imager

The DSI employs a combination of monopole and dipole transducers to make measurements of sonic wave propagation in a wide variety of formations. In addition to a robust measurement of *P*-wave velocity, the DSI uses the dipole source to generate a flexural mode in the borehole that can be used to estimate shear wave (*S*-wave) velocity even in highly unconsolidated formations. When the formation *S*-wave velocity is less than the sonic velocity of the borehole fluid, particularly in unconsolidated sediments, the flexural wave travels at the *S*-wave velocity and is the most reliable way to estimate a shear wave velocity log. Meanwhile, the monopole source generates *P*-, *S*-, and Stoneley waves into hard formations. The configuration of the DSI also allows recording of cross-dipole waveforms. In many cases, the dipole sources can also provide estimates of *S*-wave velocity in hard rocks better than or equivalent to the mono-

pole source. A low-frequency (~800 Hz) source enables Stoneley waveforms to be acquired as well.

The DSI measures the transit times between sonic transmitters and an array of eight receivers with 15 cm spacing, each consisting of four orthogonal elements that are aligned with the dipole transmitters. During acquisition, the output from these 32 individual elements are differenced or summed appropriately to produce in-line and cross-line dipole signals or monopole-equivalent (compressional and Stoneley) waveforms, depending on the operation modes. A detailed description of tool configuration and data processing is provided in the Leg 174B *Initial Reports* "Introduction" chapter (Shipboard Scientific Party, 1998). The velocity data from the DSI, together with the formation density, can be used to generate a synthetic seismogram for correlation with seismic data.

Formation MicroScanner tool

The FMS produces high-resolution images of borehole wall microresistivity that can be used for detailed sedimentologic or structural interpretation. This tool has four orthogonally oriented pads, each with 16 button electrodes (5 mm diameter) that are pressed against the borehole wall (see inset in Fig. F28). Good contact with the borehole wall is necessary for acquiring good-quality data. Approximately 30% of a borehole with a diameter of 25 cm is imaged during a single pass. Coverage may be increased by a second run. The vertical resolution of FMS images is ~5 mm, allowing features such as burrows, thin beds, fractures, veins, and vesicles to be imaged. Resistivity measurements are converted to color or grayscale images for display. FMS images are oriented to magnetic north using the GPIT (see next section). This allows the dip and strike of geological features intersecting the hole to be measured from processed FMS images. FMS images can be used to visually compare logs with the core to ascertain the orientations of bedding, fracture patterns, and sedimentary structures (Serra, 1989; Luthi, 2001).

General Purpose Inclinometer Tool

The GPIT is included in the FMS-sonic tool string to calculate tool acceleration and orientation during logging. The GPIT contains a triple-axis accelerometer and a triple-axis magnetometer. The GPIT records the orientation of the FMS images and allows more precise determination of log depths than can be determined from cable length, as the accelerometer data can be used to correct for cable stretching, tool sticking, and ship heave. Detailed tool motion information is monitored to process the FMS data and obtain accurate images of the formation (Luthi, 2001).

Well Seismic Tool

The WST produces a zero-offset vertical seismic profile and/or check shots in the borehole. The WST consists of a single geophone that records the full waveform of acoustic waves generated by a seismic source positioned just below the sea surface. During Expedition 311, we used a 105 inch^3 generator-injector air gun as a seismic source. This gun was positioned at a water depth of ~2 m and offset from the borehole by ~50 m on the port side of the *JOIDES Resolution*. The WST was clamped against the borehole wall at 5 to 10 m intervals, and the air gun was typically fired between 5 and 15 times at each station. The recorded waveforms were stacked and a one-way traveltime was determined from the median of the first breaks for each station, thus providing check shots for calibration of the integrated transit time calculated from sonic logs. Check shot calibration is required for well-seismic correlation because *P*-wave velocities derived from the sonic log may differ significantly from the velocities determined from seismic data. Causes for this difference include

- Frequency dispersion (the sonic tool operates at 10–20 kHz, with seismic data in the 50–200 Hz range),
- Difference in travel paths between well sonic and surface seismic surveys, and
- Borehole effects caused by formation alterations (Schlumberger, 1989).

In addition, sonic logs cannot be measured through the pipe, so the traveltime down to the uppermost logging point has to be estimated by other means.

Logging data flow and processing

Data for each wireline logging run were recorded and stored digitally and monitored in real time using the Schlumberger MAXIS 500 system. After logging was completed in each hole, data were transferred to the DHML for preliminary processing and interpretation. FMS image data were interpreted using Schlumberger's GeoFrame.

Logging data were also transmitted to LDEO-BRG using a satellite high-speed data link for processing soon after each hole was logged. Data processing at LDEO-BRG consisted of

- Depth-shifting all logs relative to a common datum (i.e., in meters below seafloor),
- Depth-matching successive runs using a common measurement (e.g., gamma radiation),
- Corrections specific to individual tools, and
- Quality control and rejection of unrealistic or spurious values.

Once processed at LDEO-BRG, logging data were transmitted back to the ship, providing near real-time data processing. Processed data were then replotted on board (see the "Downhole logging" section in each site chapter). Further postcruise processing of the logging data from the FMS will be performed at LDEO-BRG. Postcruise-processed data are available directly from the LDEO-BRG web site (**iodp.ldeo.columbia.edu/DATA**) in ASCII format. A summary of "logging highlights" is posted on the LDEO-BRG web site at the end of each expedition.

Wireline logging data quality

Logging data quality may be seriously degraded by changes in hole diameter and in sections where the borehole diameter greatly decreases or is washed out. Measurements that investigate deeper into the borehole wall, such as resistivity and sonic velocity, are least sensitive to borehole conditions. Nuclear measurements (density and neutron porosity) are more sensitive because of their shallower depths of investigation and the effect of drilling fluid volume on neutron and GRA. Corrections can be applied to the original data to reduce some of these effects, but for very large washouts, data cannot be corrected. HNGS and SGT data provide a depth correlation between logging runs. Logs from different tool strings may, however, still have minor depth mismatches caused by either cable stretch or ship heave during recording. Ship heave is minimized by a hydraulic wireline heave compensator designed to adjust for rig motion during logging operations.

Gas hydrate detection and evaluation with downhole logs

With growing interest in natural gas hydrate, it is becoming increasingly important to be able to identify the presence of in situ gas hydrate and accurately assess the volume of gas hydrate and associated free gas within the host sediments. Numerous publications (Mathews, 1986; Collett, 1993, 1998a, 1998b, 2000; Goldberg, 1997; Guerin et al., 1999; Goldberg et al., 2000; Helgerud et al., 2000) have shown that downhole geophysical logs can yield information about the presence of gas hydrate.

Because gas hydrates are characterized by unique chemical compositions and distinct electrical resistivities, physical, and acoustic properties, it is possible to obtain gas hydrate saturation (percent of pore space occupied by gas hydrate) and sediment porosity data by characterizing the electrical resistivity, acoustic properties, and chemical composition of the pore-filling constituents within gas hydrate–bearing reservoirs. Two of the most difficult reservoir parameters to determine are porosity and the degree of gas hydrate saturation. Downhole logs often serve as a source of porosity and hydrocarbon saturation data. Most of the existing gas hydrate log evaluation techniques are qualitative in nature and have been developed by the extrapolation of petroleum industry log evaluation procedures. To adequately test the utility of standard petroleum log evaluation techniques in gas hydrate–bearing reservoirs would require numerous laboratory and field measurements. However, only a limited number of gas hydrate occurrences have been sampled and surveyed with open-hole logging devices.

Reviewed below are downhole logging measurements that together yield useful gas hydrate reservoir information. The downhole measurements considered include density, neutron porosity, electrical resistivity, and acoustic transit time. Most of these measurements are converted to porosity; however, because gas hydrate affects each measurement of porosity in a different fashion, the quantity of gas hydrate can be estimated by comparing porosity measurements made using different techniques.

Density logs

Density logs are primarily used to assess sediment porosities. The theoretical bulk density of a Structure I methane hydrate is ~0.9 g/cm^3 (Sloan, 1998). Gas hydrate can cause a small but measurable effect on density-derived porosities. At relatively high porosity (>40%) and high gas hydrate saturation (>50%), the density log–derived porosities need to be corrected for the presence of gas hydrate (Collett, 1998b).

Neutron porosity logs

Neutron logs are also used to determine sediment porosities. Because Structure I methane hydrate and pure water have similar hydrogen concentrations, it can be generally assumed that neutron porosity logs, which are calibrated to pure water, are not significantly affected by the presence of gas hydrates. At high reservoir porosities, however, the neutron porosity log could overestimate porosities (Collett, 1998b).

Electrical resistivity

Water content and pore water salinity are the most significant factors controlling the electrical resistivity of a formation. Other factors include the concentration of hydrous and metallic minerals, volume of hydrocarbons including gas hydrates, and pore structure geometry. Gas hydrate–bearing sediments exhibit relatively high electrical resistivities in comparison to water-saturated units, which suggests that a downhole resistivity log can be used to identify

and assess the concentration of gas hydrates in a sedimentary section. The relation between rock and pore fluid resistivity has been studied in numerous laboratory and field experiments. From these studies, relations among porosity, pore fluid resistivity, and rock resistivity have been found. Among these findings is the empirical relation established by Archie (1942), which estimates water saturations in gas-oil-water-matrix systems. Research has shown that the Archie relation also appears to yield useful gas hydrate saturation data (reviewed by Collett, 2000).

Acoustic transit time

The velocity of *P*- and *S*-waves in a solid medium, such as gas hydrate–bearing sediment, is usually significantly higher than the velocity of *P*- and *S*-waves in water- or free gas–bearing sediments. Studies of downhole acoustic log data from both marine- and permafrost-associated gas hydrate accumulations have shown that the volume of gas hydrate in sediment can be estimated by measuring interval velocities (Guerin et al., 1999; Helgerud et al., 2000; Collett, 2000). Analysis of sonic logging waveforms has also shown that the presence of gas hydrate can generate significant energy loss in monopole and dipole waveforms (Guerin and Goldberg, 2002).

Interpreting structure from Resistivity-at-the-Bit and Formation MicroScanner images

Structural data were determined from FMS and GeoVISION images using Schlumberger's GeoFrame. GeoFrame presents image data as a planar, "unwrapped" 360° resistivity image of the borehole with depth. The image orientation is referenced to north, which is measured by the magnetometers inside the tool, and the hole is assumed to be vertical. Horizontal features appear horizontal on the images, whereas planar, dipping features are sinusoidal in aspect. Sinusoids are interactively fitted to beds and fractures to determine their dip and azimuth, and the data are exported from GeoFrame for further analysis.

Methods of interpreting structure and bedding differ considerably between core analysis, wireline FMS images, and GeoVISION image analysis. Resolution is considerably lower for GeoVISION image interpretation (5–10 cm at best, compared with millimeters within cores and 0.5 cm for FMS images), and therefore identified features are likely to be different in scale. For example, microfaults ("small faults," <1 mm width) and shear bands (1–2 mm and as much as 1 cm in width) can only be identified in FMS data. This should be taken into account when directly comparing FMS and GeoVISION images. GeoVISION provides 360° coverage at a lower resolution; FMS provides higher resolution data but coverage is restricted to only ~30% of the borehole wall. Fractures are identified within GeoVISION images by their anomalous resistivity or conductivity and from their contrasting dip relative to surrounding bedding trends. Differentiating between fractures and bedding planes can be problematic, particularly if both are steeply dipping and with similar orientations.

Core-log-seismic correlation

We correlated the results of some of the seismic surveys acquired in the area with the Expedition 311 LWD/MWD and wireline logging data. The correlation included core physical properties, wireline logs, and two-dimensional seismic survey images. To ensure accurate correlation of the data, it was important to ascertain the accuracy of the navigation of each of the associated surveys, the hole deviation, the drill string position at the seafloor relative to the sea surface, the accuracy of the depth-converted seismic data, and the vertical and horizontal seismic resolution. Accurate correlation is critical to extend the study of the direct measurements of the subsurface physical properties away from the borehole using seismic data.

References

Akiba, F., 1986. Middle Miocene to Quaternary diatom biostratigraphy in the Nankai trough and Japan trench, and modified lower Miocene through Quaternary diatom zones for middle-to-high latitudes of the north Pacific. *In* Kagami, H., Karig, D.E., Coulbourn, W.T., et al., *Init. Repts. DSDP,* 87: Washington (U.S. Govt. Printing Office), 393–481.

Aldred, W., Cook, J., Bern, P., Carpenter, B., Hutchinson, M., Lovell, J., Rezmer-Cooper, I., and Leder, P.C., 1998. Using downhole annular pressure measurements to improve drilling performance. *Oilfield Rev.,* 10(4):40–55.

Archie, G.E., 1942. The electrical resistivity log as an aid in determining some reservoir characteristics. *J. Pet. Technol.,* 5:1–8.

Balsam, W.L., and Damuth, J.E., 2000. Further investigations of shipboard vs. shore-based spectral data: implications for interpreting Leg 164 sediment composition. *In* Paull, C.K., Matsumoto, R., Wallace, P., and Dillon, W.P. (Eds.), *Proc. ODP, Sci. Results,* 164: College Station, TX (Ocean Drilling Program), 313–324. [**HTML**]

Balsam, W.L., Damuth, J.E., and Schneider, R.R., 1997. Comparison of shipboard vs. shore-based spectral data from Amazon-Fan Cores: implications for interpreting sediment composition. *In* Flood, R.D., Piper, D.J.W., Klaus, A., and Peterson, L.C. (Eds.), *Proc. ODP, Sci. Results,* 155: College Station, TX (Ocean Drilling Program), 193–215. [**PDF**]

Balsam, W.L., Deaton, B.C., and Damuth, J.E., 1998. The effects of water content on diffuse reflectance spectrophotometry studies of deep-sea sediment cores. *Mar. Geol.,* 149:177–189. **doi:10.1016/S0025-3227(98)00033-4**

Barron, J.A., 1992. Paleoceanographic and tectonic controls on the Pliocene diatom record of California. *In* Tsuchi, R., and Ingle, J.C., Jr. (Eds.), *Pacific Neogene: Environment, Evolution, and Events:* Tokyo (Tokyo Univ. Press), 25–41.

Barron, J.A., and Gladenkov, A.Y., 1995. Early Miocene to Pleistocene diatom stratigraphy of Leg 145. *In* Rea, D.K., Basov, I.A., Scholl, D.W., and Allan, J.F. (Eds.), *Proc. ODP, Sci. Results,* 145: College Station, TX (Ocean Drilling Program), 3–19.

Berggren, W.A., Kent, D.V., Swisher, C.C., III, and Aubry, M.-P., 1995. A revised Cenozoic geochronology and chronostratigraphy. *In* Berggren, W.A., Kent, D.V., Aubry, M.-P., and Hardenbol, J. (Eds.), *Geochronology, Time Scales and Global Stratigraphic Correlation.* Spec. Publ.—SEPM (Soc. Sediment. Geol.), 54:129–212.

Blum, P., 1997. Physical properties handbook: a guide to the shipboard measurement of physical properties of deep-sea cores. *ODP Tech. Note,* 26 [Online]. Available from World Wide Web: **http://www-odp.tamu.edu/publications/tnotes/tn26/INDEX.HTM**.

Boetius, A., Ravenschlag, K., Schubert, C.J., Rickert, D., Widdel, F., Gieseke, A., Amann, R., Jørgensen, B.B., Witte, U., and Pfannkuche, O., 2000. A marine microbial consortium apparently mediating the anaerobic oxidation of methane. *Nature (London, U. K.),* 407:623–626. **doi:10.1038/35036572**

Bullard, E.C., 1954. The flow of heat through the floor of the Atlantic Ocean. *Proc. R. Soc. London A,* 222:408–429.

Cande, S.C., and Kent, D.V., 1995. Revised calibration of the geomagnetic polarity timescale for the Late Cretaceous and Cenozoic. *J. Geophys. Res.,* 100:6093–6095. **doi:10.1029/94JB03098**

Collett, T.S., 1993. Natural gas hydrates of the Prudhoe Bay–Kuparuk River area, North Slope, Alaska. *AAPG Bull.,* 77:793–812.

Collett, T.S., 1998a. Well log characterization of sediment porosities in gas-hydrate–bearing reservoirs [paper presented at Annu. Tech. Conf. Exhib. Soc. Pet. Eng., New Orleans, September 1998], Pap. SPE 49298.

Collett, T.S., 1998b. Well log evaluation of gas hydrate saturations. *Trans. SPWLA Annu. Logging Symp.,* 39:MM.

Collett, T.S., 2000. A review of well-log analysis techniques used to assess gas-hydrate-bearing reservoirs: *In* Paull, C.K., and Dillon, W.P. (Eds.), *Natural Gas Hydrates: Occurrence, Distribution, and Detection.* Geophys. Monogr., 189–210.

Davis, E.E., Villinger, H., MacDonald, R.D., Meldrum, R.D., and Grigel, J., 1997. A robust rapid-response probe for measuring bottom-hole temperatures in deep-ocean boreholes. *Mar. Geophys. Res.,* 19:267–281. **doi:10.1023/A:1004292930361**

Davis, E.E., Hyndman, R.D., and Villinger, H., 1990. Rates of fluid expulsion across the northern Cascadia accretionary prism: constraints from new heat flow and multichannel seismic reflection data. *J. Geophys. Res.,* 9:8869–8889.

Dickens, G.R., Borowski, W.S., Wehner, H., Paull, C.K., and the ODP Leg 164 Scientific Party, 2000a. Data report: Additional shipboard information for the pressure core sampler (PCS). *In* Paull, C.K., Matsumoto, R., Wallace, P.J., and Dillon, W.P. (Eds.), *Proc. ODP, Sci. Results,* 164, 439–443 [CD-ROM]. Available from: Ocean Drilling Program, Texas A&M University, College Station, TX 77845-9547, U.S.A. [**HTML**]

Dickens, G.R., Paull, C.K., Wallace, P., and the ODP Leg 164 Scientific Party, 1997. Direct measurement of in situ methane quantities in a large gas-hydrate reservoir. *Nature (London, U. K.),* 385:427–428. **doi:10.1038/385426a0**

Dickens, G.R., Schroeder, D., Hinrichs, K.-U., and the Leg 201 Scientific Party, 2003. The pressure core sampler (PCS) on Ocean Drilling Program Leg 201: general operations and gas release. *In* D'Hondt, S.L., Jørgensen, B.B., Miller, D.J., et al., *Proc. ODP, Init. Repts.,* 201, 1–22 [CD-ROM]. Available from: Ocean Drilling Program, Texas A&M University, College Station TX 77845-9547, USA. [**HTML**]

Dickens, G.R., Wallace, P.J., Paull, C.K., and Borowski, W.S., 2000b. Detection of methane gas hydrate in the pressure core sampler (PCS): volume-pressure-time relations during controlled degassing experiments. *In* Paull, C.K., Matsumoto, R., Wallace, P.J., and Dillon, W.P. (Eds.), *Proc. ODP, Sci. Results,* 164: College Station, TX (Ocean Drilling Program), 113–126. [**HTML**]

Droser, M.L., and Bottjer, D.J., 1986. A semiquantitative field classification of ichnofabric. *J. Sediment. Petrol.,* 56:558–559.

Duan, Z., Møller, N., Greenberg, J., and Weare, J.H., 1992. The prediction of methane solubility in natural waters to high ionic strengths from 0° to 250°C and from 0 to 1600 bar. *Geochim. Cosmochim. Acta,* 56:1451–1460. **doi:10.1016/0016-7037(92)90215-5**

Ellis, D.V., 1987. *Well Logging for Earth Scientists:* New York (Elsevier).

Expedition 301 Scientists, 2005. Methods. *In* Fisher, A.T., Urabe, T., Klaus, A., and the Expedition 301 Scientists, *Proc. IODP,* 301: College Station TX (Integrated Ocean Drilling Program Management International, Inc.). **doi:10.2204/iodp.proc.301.105.2005**

Expedition 307 Scientists, 2006. Methods. *In* Ferdelman, T., Kano, A., Williams, T., Henriet, J.-P, and the Expedition 307 Scientists, *Proc. IODP,* 307: Washington, DC (Integrated Ocean Drilling Program Management International, Inc.). **doi:10.2204/iodp.proc.307.102.2006**

Ford, K.H., Naehr, T.H., Skilbeck, C.G., and the Leg 201 Scientific Party, 2003. The use of infrared thermal imaging to identify gas hydrate in sediment cores. *In* D'Hondt, S.L., Jørgensen, B.B., Miller, D.J., et al., *Proc. ODP, Init. Repts.,* 201 [Online]. Available from World Wide Web: **http://www-odp.tamu.edu/publications/201_IR/chap_04/chap_04.htm**.

Gieskes, J.M., Gamo, T., and Brumsack, H., 1991. Chemical methods for interstitial water analysis aboard *JOIDES Resolution. ODP Tech. Note,* 15 [Online]. Available from

World Wide Web: **http://www-odp.tamu.edu/publications/tnotes/tn15/f_chem1.htm**.

Goldberg, D., 1997. The role of downhole measurements in marine geology and geophysics. *Rev. Geophys.,* 35:315–342. **doi:10.1029/97RG00221**

Goldberg, D., Collett. T.S., and Hyndman, R.D., 2000. Ground truth: in-situ properties of hydrate. *In* Max, M.D. (Ed.), *Natural Gas Hydrate in Oceanic and Permafrost Environments:* Dordrecht (Kluwer Academic Publishers), 295–310.

Graber, K.K., Pollard, E., Jonasson, B., and Schulte, E. (Eds.), 2002. Overview of Ocean Drilling Program Engineering Tools and Hardware. *ODP Tech. Note,* 31 [Online]. Available from World Wide Web: **http://www-odp.tamu.edu/publications/tnotes/tn31/INDEX.HTM**.

Guerin, G., and Goldberg, D., 2002. Sonic waveform attenuation in gas hydrate-bearing sediments from the Mallik 2L-38 research well, MacKenzie Delta, NWT Canada. *J. Geophys. Res.,* 107. **doi:10.1029/2001JB000556**

Guerin, G., Goldberg, D., and Meltser, A., 1999. Characterization of in situ elastic properties of gas-hydrate bearing sediments on the Blake Ridge. *J. Geophys. Res.,* 104:17781–17796. **doi:10.1029/1999JB900127**

Hartman, A., and Villinger, H., 2002. Inversion of marine heat flow measurements by expansion of the temperature decay function. *Geophys. J. Int.,* 148:628–636. **doi:10.1046/j.1365-246X.2002.01600.x**

Helgerud, M.B., Dvorkin, J., and Nur, A., 2000. Rock physics characterization for gas hydrate reservoirs: elastic properties. *In* Holder, G.D., and Bishnoi, P.R. (Eds.), *Gas Hydrates: Challenges for the Future.* Ann. N.Y. Acad. Sci., 912:116–125.

Hoehler, T.M., Borowski, W.S., Alperin, M.J., Rodriguez, N.M., and Paull, C.K., 2000. Model, stable isotope, and radiotracer characterization of anaerobic methane oxidation in gas hydrate–bearing sediments of the Blake Ridge. *In* Paull, C.K., Matsumoto, R., Wallace, P.J., and Dillon, W.P. (Eds.), *Proc. ODP, Sci. Results,* 164: College Station, TX (Ocean Drilling Program), 79–85. [**HTML**]

Horai, K., and Von Herzen, R.P., 1985. Measurement of heat flow on Leg 86 of the Deep Sea Drilling Project. *In* Heath, G.R., Burckle, L.H., et al., *Init. Repts. DSDP,* 86: Washington (U.S. Govt. Printing Office), 759–777.

Hunt, J.M., 1979. *Petroleum Geochemistry and Geology:* San Francisco (W.H. Freeman).

Koizumi, I., 1992. Diatom biostratigraphy of the Japan Sea: Leg 127. *In* Pisciotto, K.A., Ingle, J.C., Jr., von Breymann, M.T., Barron, J., et al., *Proc. ODP, Sci. Results,* 127/128 (Pt. 1): College Station, TX (Ocean Drilling Program), 249–289.

Koizumi, I., and Tanimura, Y., 1985. Neogene diatom biostratigraphy of the middle latitude western north Pacific, Deep Sea Drilling Project Leg 86. *In* Heath, G.R., Burckle, L.H., et al., *Init. Repts. DSDP,* 86: Washington (U.S. Govt. Printing Office), 269–300.

Kristiansen, J.I., 1982. The transient cylindrical probe method for determination of thermal parameters of earth materials [Ph.D. dissert.]. Åarhus Univ.

Lamont-Doherty Earth Observatory–Borehole Research Group, 2001. *ODP Logging Services Electronic Manual,* Version 2.0 [Online]. Available from World Wide Web: <**http://www.ldeo.columbia.edu/BRG/ODP/LOGGING/MANUAL/index.html**>.

Lunau, M., Lemke, A., Walther, K., Martens-Habbena, W., and Simon, M., 2005. An improved method for counting bacteria from sediments and turbid environments by epifluorescence microscopy. *Environ. Microbiol.,* 7:961–968. **doi:10.1111/j.1462-2920.2005.00767.x**

Luthi, S.M., 2001. *Geological Well Logs: Their Use in Reservoir Modeling:* Berlin (Springer-Verlag).

Manheim, F.T., and Sayles, F.L., 1974. Composition and origin of interstitial waters of marine sediments, based on deep sea drill cores. *In* Goldberg, E.D. (Ed.), *The Sea* (Vol. 5): *Marine Chemistry: The Sedimentary Cycle:* New York (Wiley), 527–568.

Mathews, M., 1986. Logging characteristics of methane hydrate. *The Log Analyst,* 27:26–63.

Mazzullo, J.M., Meyer, A., and Kidd, R.B., 1988. New sediment classification scheme for the Ocean Drilling Program. *In* Mazzullo, J.M., and Graham, A.G. (Eds.), Handbook for shipboard sedimentologists. *ODP Tech. Note,* 8:45–67.

Mikada, H., Becker, K., Moore, J.C., Klaus, A., et al., 2002. *Proc. ODP, Init. Repts.,* 196 [Online]. Available from World Wide Web: **http://www-odp.tamu.edu/publications/196_IR/196ir.htm.**

Mikucki, J.A., Liu, Y., Delwiche, M., Colwell, F.S., and Boone, D.R., 2003. Isolation of a methanogen from deep marine sediments that contain methane hydrates, and description of *Methanoculleus submarinus* sp. nov. *Appl. Environ. Microbiol.,* 69:3311–3316. **doi:10.1128/AEM.69.6.3311-3316.2003**

Milkov, A.V., Dickens, G.R., Claypool, G.E., Lee, Y-J., Borowski, W.S., Torres, M.E., Xu, W., Tomaru, H., Tréhu, A.M., and Schultheiss, P., 2004. Co-existence of gas hydrate, free gas, and brine within the regional gas hydrate stability zone at Hydrate Ridge (Oregon Margin): evidence from prolonged degassing of a pressurized core. *Earth Planet. Sci. Lett.,*222:829–843. **doi:10.1016/j.epsl.2004.03.028**

Mincer, T.J., Jensen, P.R., Kauffman, C.A., and Fenical, W., 2002. Widespread and persistent populations of a major new marine Actinomycete taxon in ocean sediments. *Applied Environ. Microbiol.,* 68:5005–5011. **doi:10.1128/AEM.68.10.5005-5011.2002**

Mix, A.C., Tiedemann, R., Blum, P., et al., 2003. *Proc. ODP, Init. Repts.,* 202 [CD-ROM]. Available from: Ocean Drilling Program, Texas A&M University, College Station TX 77845-9547, USA. [**HTML**]

Munsell Color Company, Inc., 1975. *Munsell Soil Color Charts:* Baltimore, MD (Munsell).

Murray, R.W., Miller, D.J., and Kryc, K.A., 2000. Analysis of major and trace elements in rocks, sediments, and interstitial waters by inductively coupled plasma–atomic emission spectrometry (ICP-AES). *ODP Tech. Note, 29* [Online]. Available from World Wide Web: **http://www-odp.tamu.edu/publications/tnotes/tn29/INDEX.HTM.**

Ni, S., and Boon, D.R., 1991. Isolation and characterization of a dimethyl sulfide-degrading methanogen, *Methanolobus siciliae* HI350, from an oil well, characterization of *M. siciliae* T4/MT, and emendation of *M. siciliae*. *Int. J. Syst. Bacteriol.,* 41:410–416.

ODP Science Services, 2006. Shipboard scientist's handbook. *ODP Tech. Note,* 36 [Online]. Available from WorldWideWeb:<**http://www-odp.tamu.edu/publications/tnotes/tn36/INDEX.HTM**>.

Paull, C.K., Matsumoto, R., Wallace, P.J., et al., 1996. *Proc. ODP, Init. Repts.,* 164: College Station, TX (Ocean Drilling Program).

Paull, C.K., and Ussler, W., III, 2000. History and significance of gas sampling during DSDP and ODP drilling associated with gas hydrates. *In* Paull, C.K., and Dillon, W.P. (Eds.), *Natural Gas Hydrates: Occurrence, Distribution, and Detection.* Geophys. Monogr., 124:53–66.

Pettigrew, T.L., 1992. The design and operation of a wireline pressure core sampler (PCS). *ODP Tech. Note,* 17.

Pimmel, A., and Claypool, G., 2001. Introduction to shipboard organic geochemistry on the *JOIDES Resolution*. *ODP Tech. Note,* 30 [Online]. Available from World Wide Web: **http://www-odp.tamu.edu/publications/tnotes/tn30/INDEX.HTM**.

Pribnow, D.F.C., Kinoshita, M., and Stein, C.A., 2000. Thermal data collection and heat flow recalculations for ODP Legs 101–180. Institute for Joint Geoscientific Research, GGA, Hanover, Germany, 0120432. Available from World Wide Web: **http://www-odp.tamu.edu/publications/heatflow/ODPReprt.pdf**.

Rider, M.H., 1996. *The Geological Interpretation of Well Logs* (2nd ed.): Caithness (Whittles Publishing).

Schlumberger, 1989. *Log Interpretation Principles/Applications:* Houston (Schlumberger Educ. Services), SMP–7017.

Schlumberger, 1994. *Log Interpretation Charts:* Sugarland, TX (Schlumberger Wireline and Testing), SMP-7006.

Schultheiss, P.J., Francis, T.J.G., Holland, M., Roberts, J.A., Amann, H., Thjunjoto, Parkes, R.J., Martin, D., Rothfuss, M., Tyunder, F., and Jackson, P.D., 2005. Pressure coring, logging and sub-sampling with the HYACINTH system. *In* Rothwell, R.G. (Ed.), *New Ways of Looking at Sediment Cores and Core Data.* Geol. Soc. Spec. Publ.

Serra, O., 1984. *Fundamentals of Well-Log Interpretation* (Vol. 1): *The Acquisition of Logging Data:* Dev. Pet. Sci., 15A: Amsterdam (Elsevier).

Serra, O., 1986. *Fundamentals of Well-Log Interpretation* (Vol. 2): *The Interpretation of Logging Data.* Dev. Pet. Sci., 15B: Amsterdam (Elsevier).

Serra, O., 1989. *Formation MicroScanner Image Interpretation:* Houston (Schlumberger Educ. Services), SMP-7028.

Shepard, F.P., 1954. Nomenclature based on sand-silt-clay ratios. *J. Sediment. Petrol.,* 24:151–158.

Shipboard Scientific Party, 1998. Introduction. *In* Becker, K., Malone, M.J., et al., *Proc. ODP, Init. Repts.,* 174B: College Station, TX (Ocean Drilling Program), 3–9. [**HTML**]

Shipboard Scientific Party, 2003a. Explanatory notes. *In* D'Hondt, S.L., Jørgensen, B.B., Miller, D.J., et al., *Proc. ODP, Init. Repts.,* 201, 1–103 [CD-ROM]. Available from: Ocean Drilling Program, Texas A&M University, College Station TX 77845-9547, USA. [**HTML**]

Shipboard Scientific Party, 2003b. Explanatory notes. *In* Tréhu, A.M, Bohrmann, G., Rack, F.R., Torres, M.E., et al., *Proc. ODP, Init. Repts.,* 204 [Online]. Available from World Wide Web: **http://www-odp.tamu.edu/publications/204_IR/chap_02/chap_02.htm**.

Sloan, E.D., 1998. *Clathrate Hydrates of Natural Gases* (2nd ed.): New York (Marcel Dekker).

Smith, D.C., Spivack, A.J., Fisk, M.R., Haveman, S.A., and Staudigel, H., 2000. Tracer-based estimates of drilling-induced microbial contamination of deep sea crust. *Geomicrobiol. J.,* 17:207–219. **doi:10.1080/01490450050121170**

Smith, D.C., Spivack, A.J., Fisk, M.R., Haveman, S.A., Staudigel, H., and ODP Leg 185 Shipboard Scientific Party, 2000. Methods for quantifying potential microbial contamination during deep ocean coring. *ODP Tech. Note,* 28 [Online]. Available from World Wide Web: **http://www-odp.tamu.edu/publications/tnotes/tn28/INDEX.HTM**.

Terry, R.D., and Chilingar, G.V., 1955. Summary of "Concerning some additional aids in studying sedimentary formations" by M.S. Shvetsov. *J. Sediment. Petrol.,* 25:229–234.

Tréhu, A.M., 2006. Subsurface temperatures beneath southern Hydrate Ridge. *In* Tréhu, A.M., Bohrmann, G., Torres, M.E., and Colwell, F.S. (Eds.), *Proc. ODP, Sci. Results,* 204 [Online]. Available from World Wide Web: **http://www-odp.tamu.edu/publications/204_SR/114/114.htm.**

Tréhu, A.M, Bohrmann, G., Rack, F.R., Torres, M.E., et al., 2003. *Proc. ODP, Init. Repts.,* 204 [Online]. Available from World Wide Web: **http://www-odp.tamu.edu/publications/204_IR/204ir.htm**.

Tréhu, A.M., Long, P.E., Torres, M.E., Bohrmann, G., Rack, F.R., Collett, T.S., Goldberg, D.S., Milkov, A.V., Riedel, M., Schultheiss, P., Bangs, N.L., Barr, S.R., Borowski, W.S., Claypool, G.E., Delwiche, M.E., Dickens, G.R., Gracia, E., Guerin, G., Holland, M., Johnson, J.E., Lee, Y.-J., Liu, C.-S., Su, X., Teichert, B., Tomaru, H., Vanneste, M., Watanabe, M., and Weinberger, J.L., 2004. Three-dimensional distribution of gas hydrate beneath southern Hydrate Ridge: constraints from ODP Leg 204. *Earth Planet. Sci. Lett.,* 222:845–862. **doi:10.1016/j.epsl.2004.03.035**

Ussler, W., III, Paull, C.K., McGill, P., Schroeder, D., and Ferrell, D., 2002. Estimating in situ sediment gas concentrations in ODP boreholes by continuously monitoring temperature during core recovery. *Proc. 4th Int. Conf. Gas Hydrate,* 1:210–215.

Ussler, W., III, Paull, C.K., McGill, P., Schroeder, D., and Ferrell, D., 2006. A test of the temperature, pressure, and conductivity tool prototype at Hydrate Ridge. *In* Tréhu, A.M., Bohrmann, G., Torres, M.E., and Colwell, F.S. (Eds.), *Proc. ODP, Sci. Results,* 204 [Online]. Available from World Wide Web: **http://www-odp.tamu.edu/publications/204_SR/112/ 112.htm.**

Von Herzen, R.P., and Maxwell, A.E., 1959. The measurement of thermal conductivity of deep-sea sediments by a needle-probe method. *J. Geophys. Res.,* 64:1557–1563.

Wallace, P.J., Dickens, G.R., Paull, C.K., and Ussler III, W., 2000. Effects of core retrieval and degassing on the carbon isotope composition of methane in gas hydrate–and free gas–bearing sediments from the Blake Ridge. *In* Paull, C.K., Matsumoto, R., Wallace, P.J., and Dillon, W.P. (Eds.), *Proc. ODP, Sci. Results,* 164, 101–112 [CD-ROM]. Available from: Ocean Drilling Program, Texas A&M University, College Station, TX 77845-9547, U.S.A. [**HTML**]

Wellsbury, P., Goodman, K., Cragg, B.A., and Parkes, R.J., 2000. The geomicrobiology of deep marine sediments from Blake Ridge containing methane hydrate (Sites 994, 995, and 997). *In* Paull, C.K., Matsumoto, R., Wallace, P.J., and Dillon, W.P. (Eds.), *Proc. ODP, Sci. Results,* 164: College Station, TX (Ocean Drilling Program), 379–391. [**HTML**]

Wentworth, C.K., 1922. A scale of grade and class terms of clastic sediments. *J. Geol.,* 30:377–392.

Westbrook, G.K., Carson, B., Musgrave, R.J., et al., 1994. *Proc. ODP, Init. Repts.,* 146 (Pt. 1): College Station, TX (Ocean Drilling Program).

Xu, W., 2002. Phase balance and dynamic equilibrium during formation and dissociation of methane gas hydrate. *Fourth Int. Conf. Gas Hydrates,* 19023:199–200.

Xu, W., 2004. Modeling dynamic marine gas hydrate systems. *Am. Mineral.,* 89:1271–1279.

Yanagisawa, Y., and Akiba, F., 1998. Refined Neogene diatom biostratigraphy for the northwest Pacific around Japan, with an introduction of code numbers for selected diatom biohorizons. *J. Geol. Soc. Jpn.,* 104:395–414.

Yayanos, A.A., 1995. Microbiology to 10,500 meters in the deep sea. *Annu. Rev. Microbiol.,* 49:777–805. **doi:10.1146/annurev.mi.49.100195.004021**

Publication: 28 October 2006
MS 311-102

Figure F1. Illustrated IODP conventions for naming sites, holes, cores, and samples. CC = core catcher, mbsl = meters below sea level, mbsf = meters below seafloor.

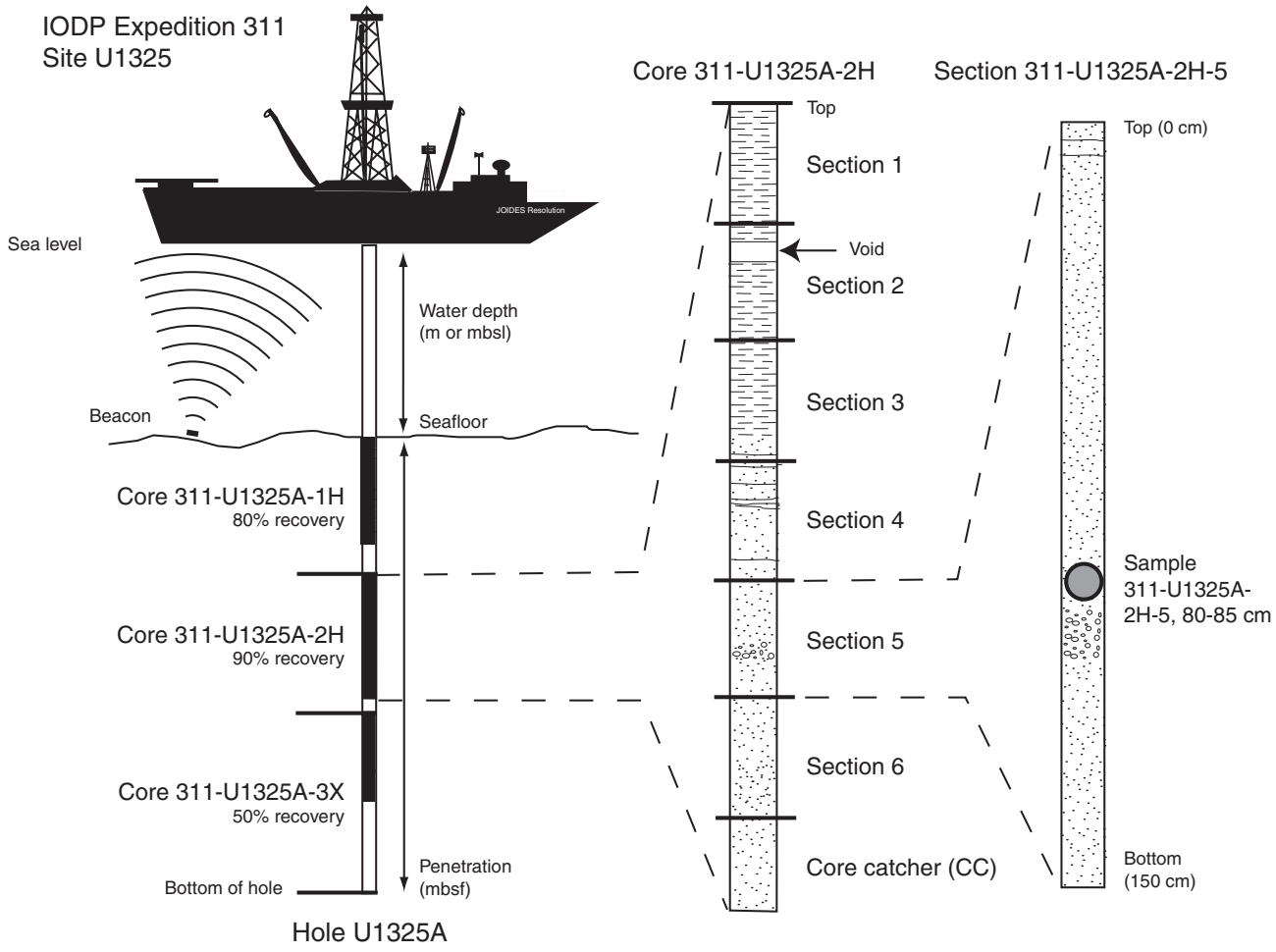

Figure F2. Grain-size classification diagram for siliciclastic sediments (modified after Wentworth, 1922).

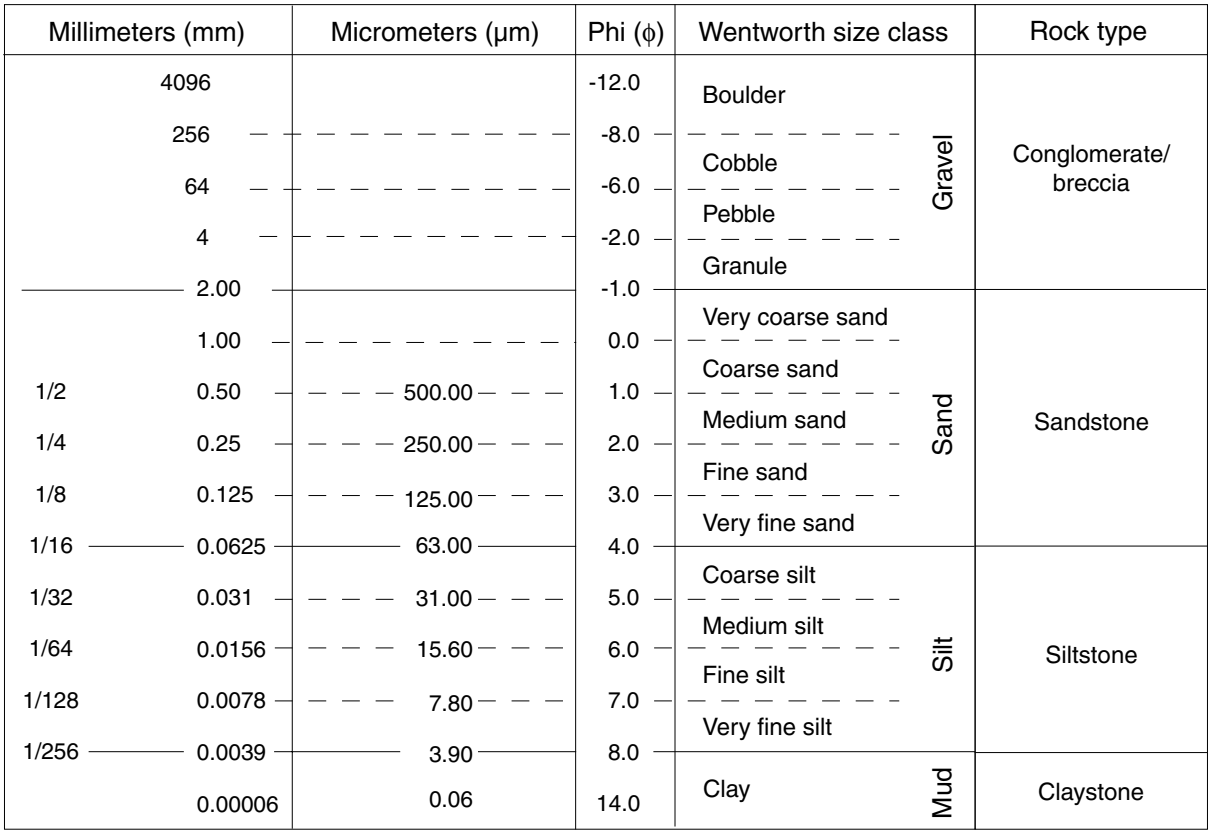

Figure F3. Classification scheme for siliciclastic sediment components (Shepard, 1954).

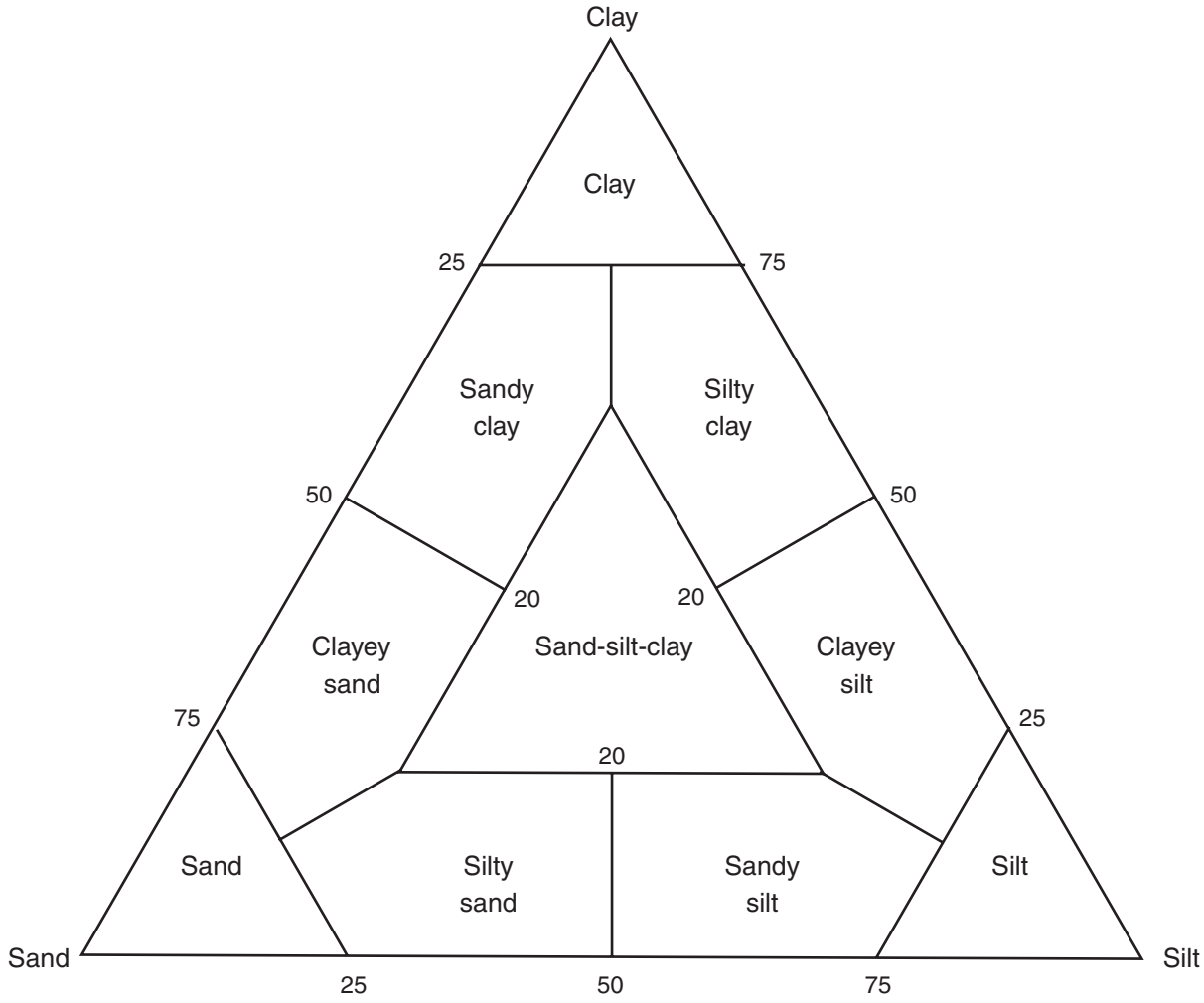

Figure F4. Key to patterns and symbols used in Expedition 311 barrel sheets.

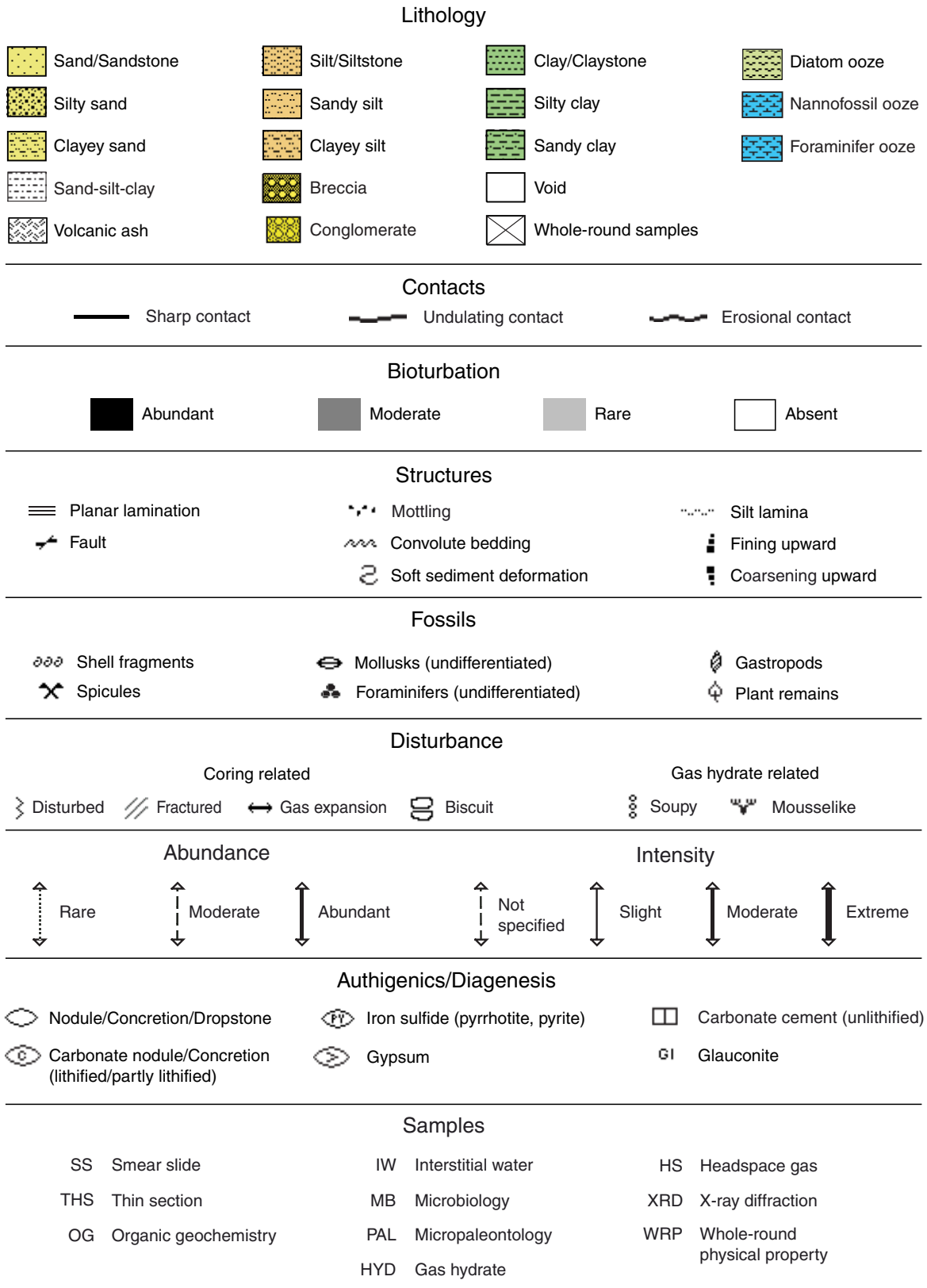

Figure F5. Example of a VCD graphical representation (barrel sheet).

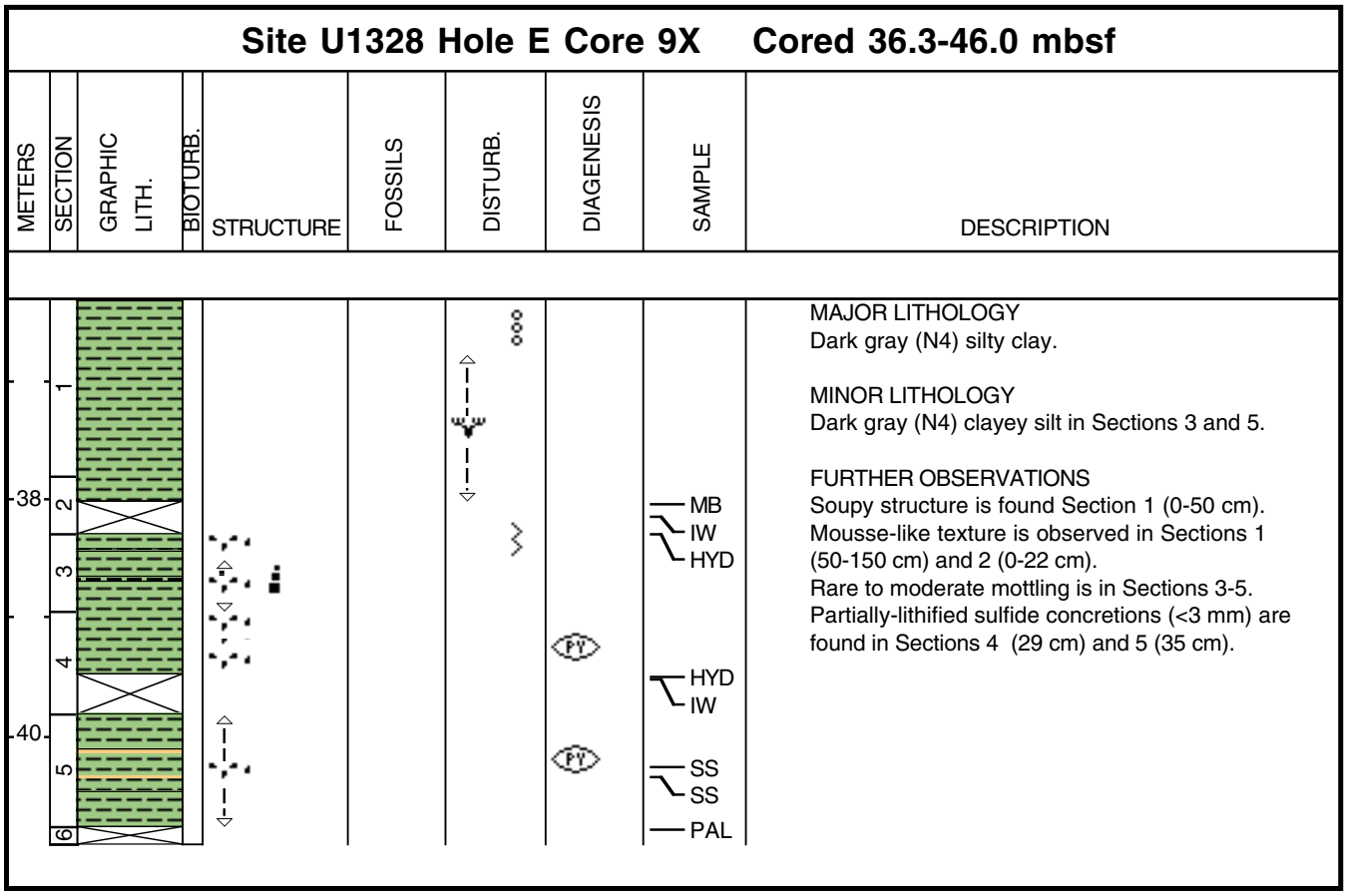

Figure F6. Example of authigenic carbonate facies in smear slides (Sample **311-U1328C-19X-4, 20 cm**).

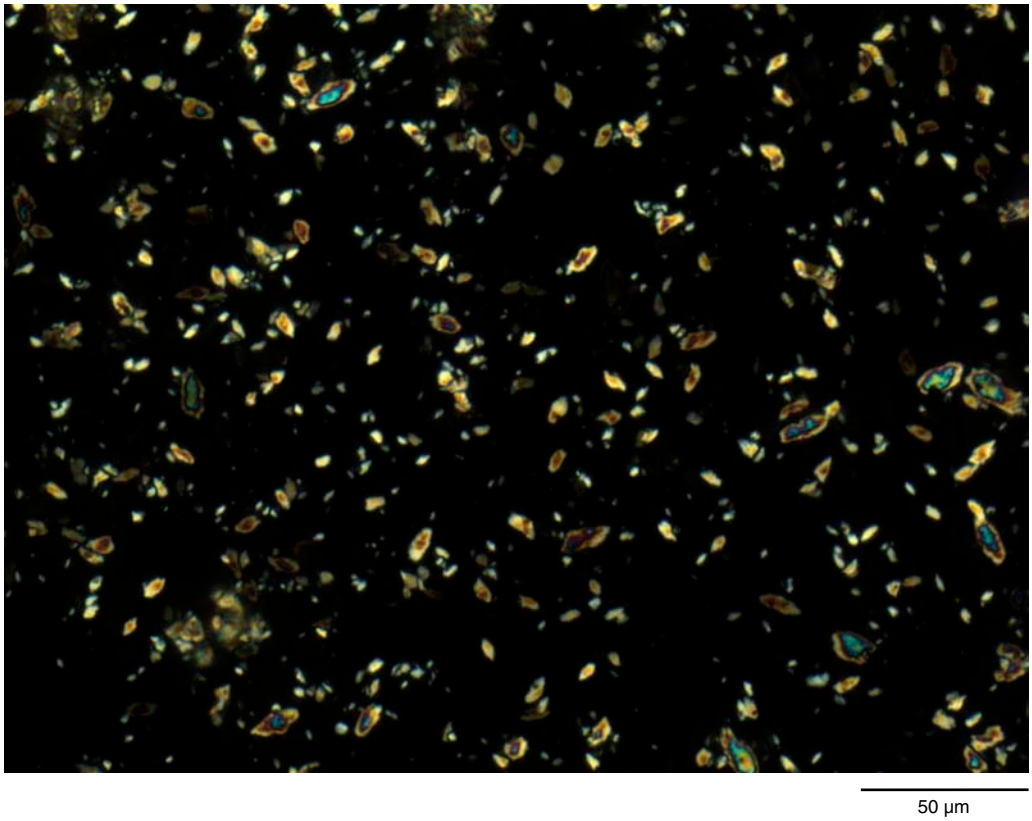

Figure F7. Example of soupy sediment texture (interval 311-U1328B-6X-1, 20–50 cm).

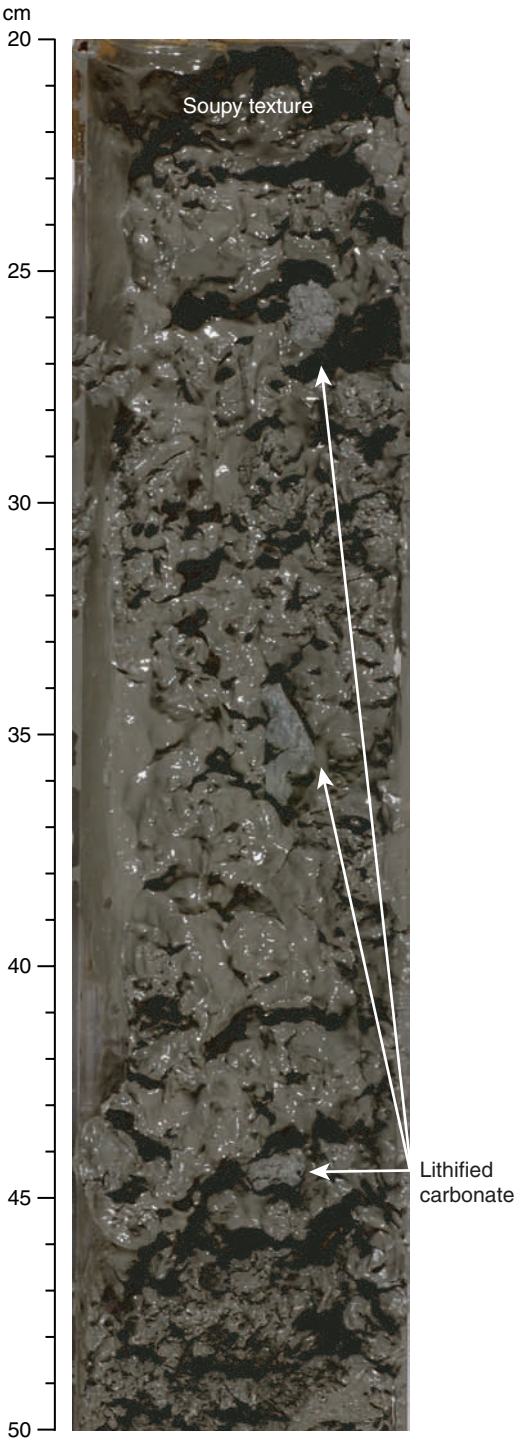

Figure F8. Example of mousselike sediment texture (interval 311-U1328C-10X-1, 119–140 cm).

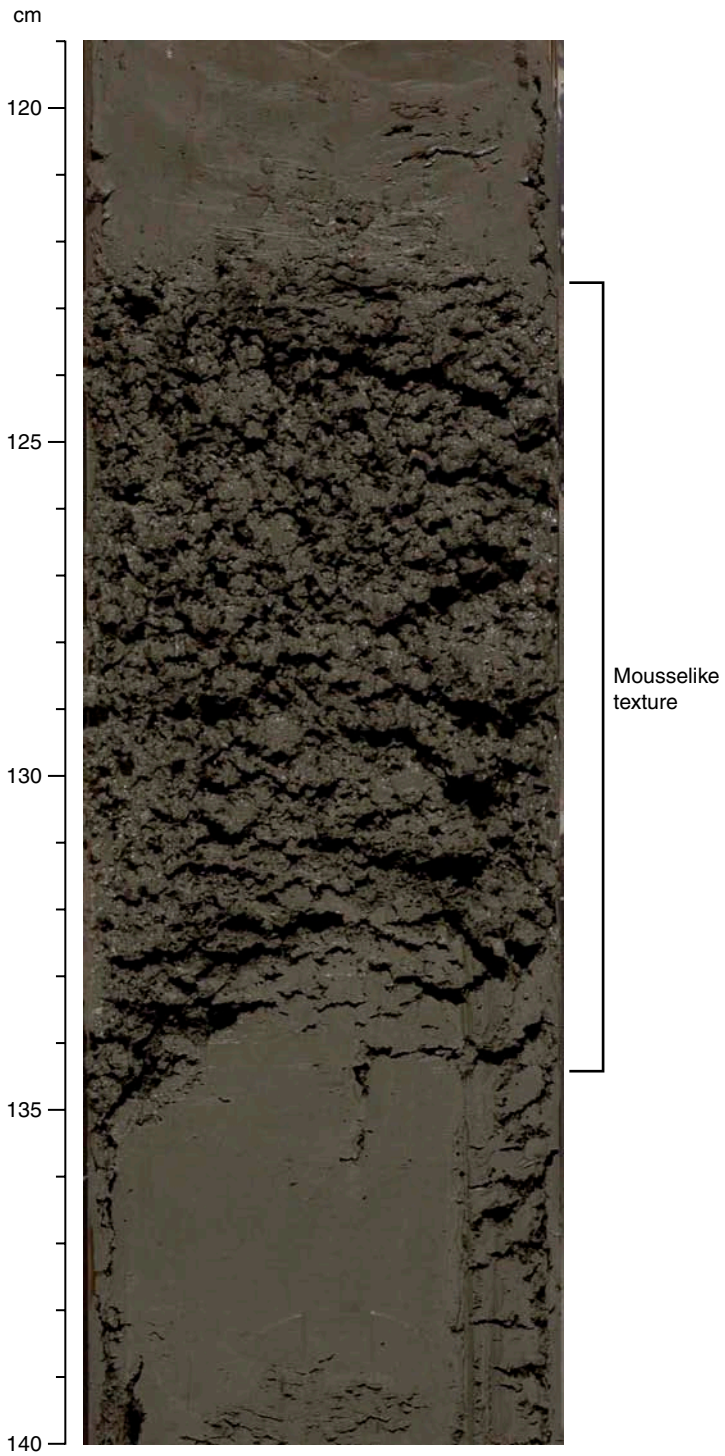

Figure F9. Correlation of the geomagnetic polarity timescale (Cande and Kent, 1995; Berggren et al., 1995) and the diatom biostratigraphic zonations used during Expedition 311. NPD = North Pacific diatom zones (Akiba, 1986; Yanagisawa and Akiba, 1998). FO = first occurrence, LO = last occurrence, LCO = last common occurrence.

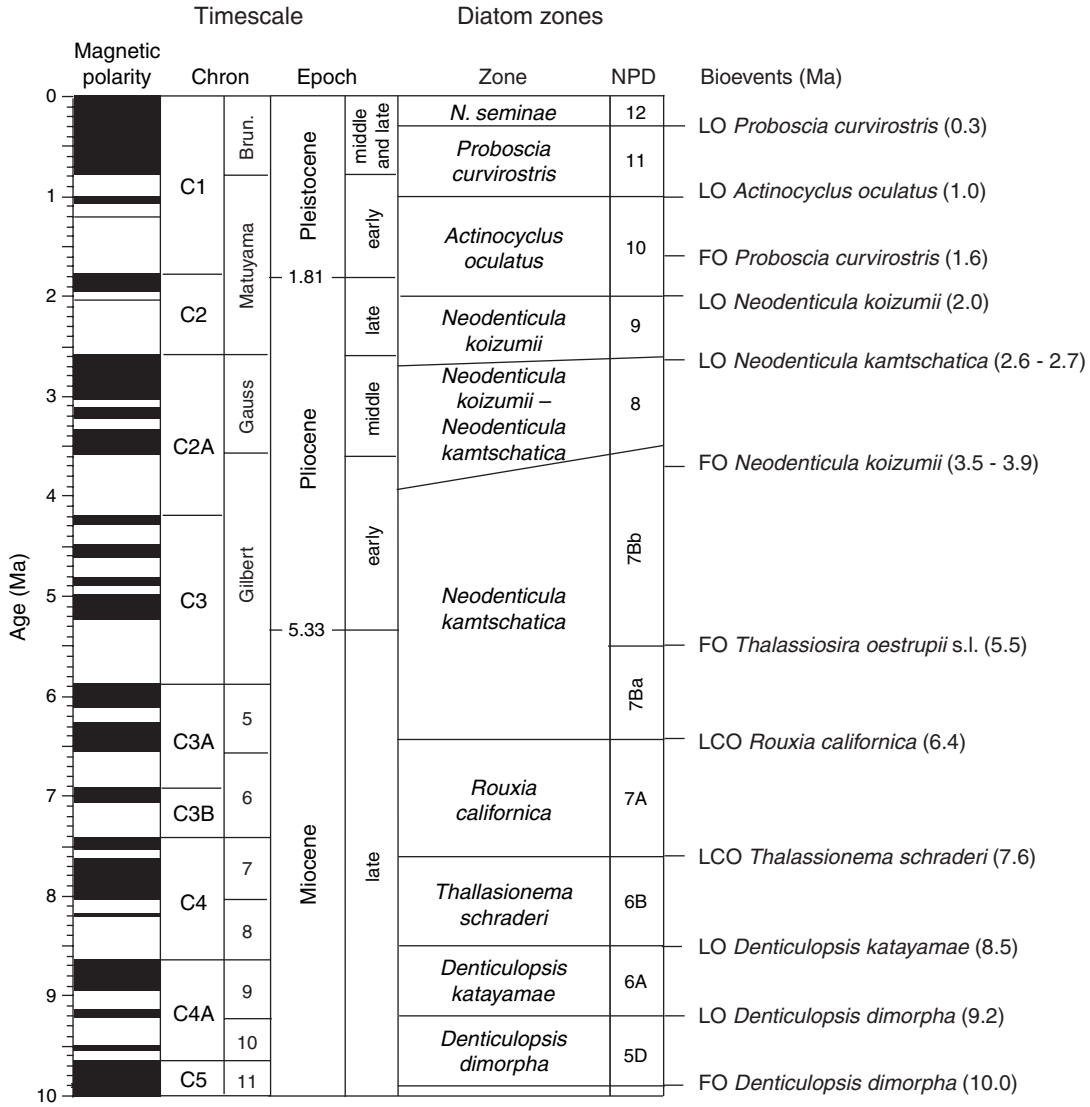

Figure F10. Types of drilling disturbance seen in XCB cores. **A.** Section 311-U1328C-15X-1. **B.** Section 311-U1325C-8X-1. **C.** Section 311-U1328C-20X-3.

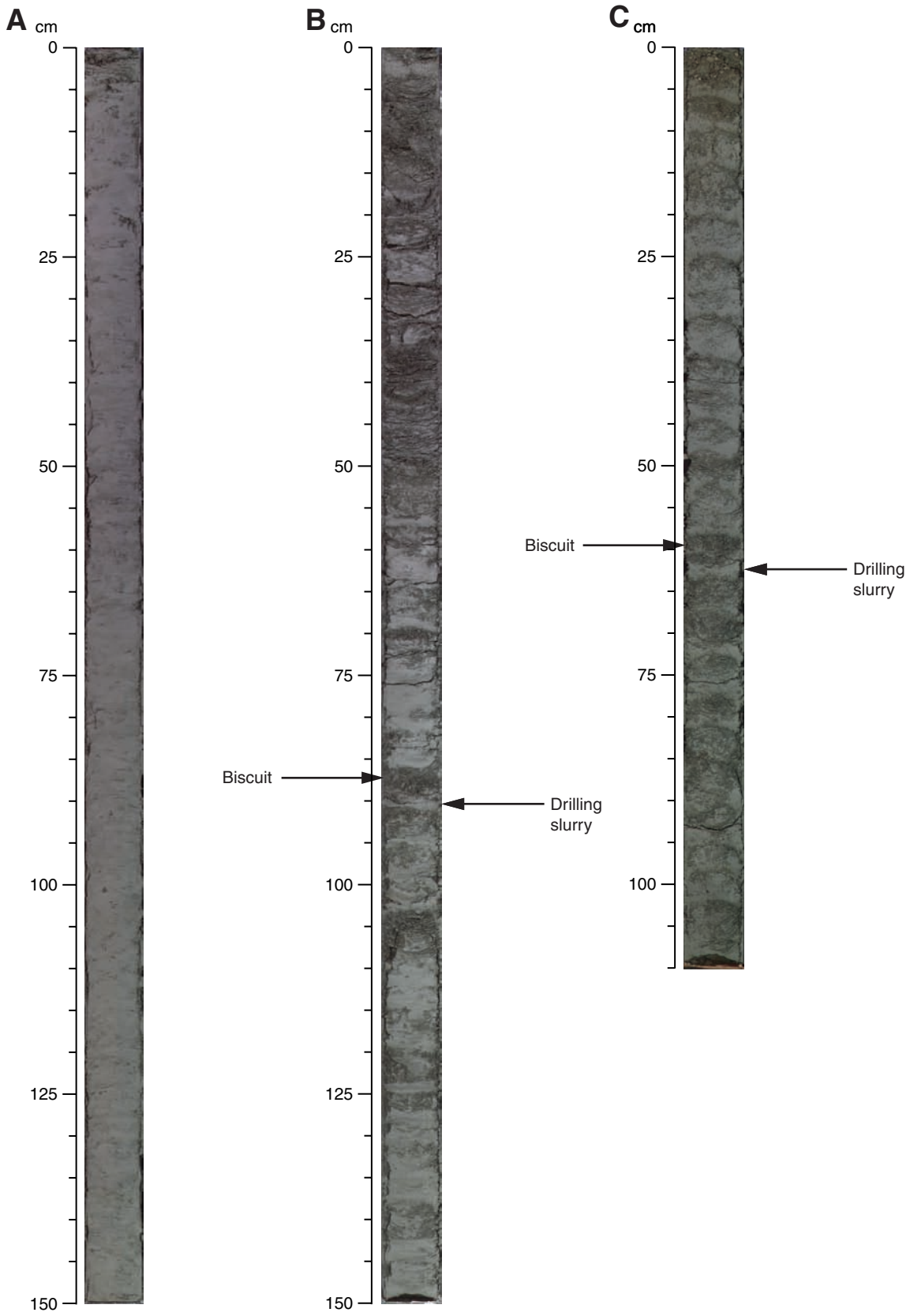

Figure F11. Infrared track-mounted and handheld cameras used during Expedition 311. **A.** IR imaging track system showing camera, monitors, and control system. **B.** Close-up of the track-mounted IR camera. **C.** Handheld IR camera on a wooden stand built to provide a stable platform for imaging core section ends. PVC pipe results in a constant distance between the core end and the camera. **D.** Another view of the handheld IR camera and stand for imaging core ends.

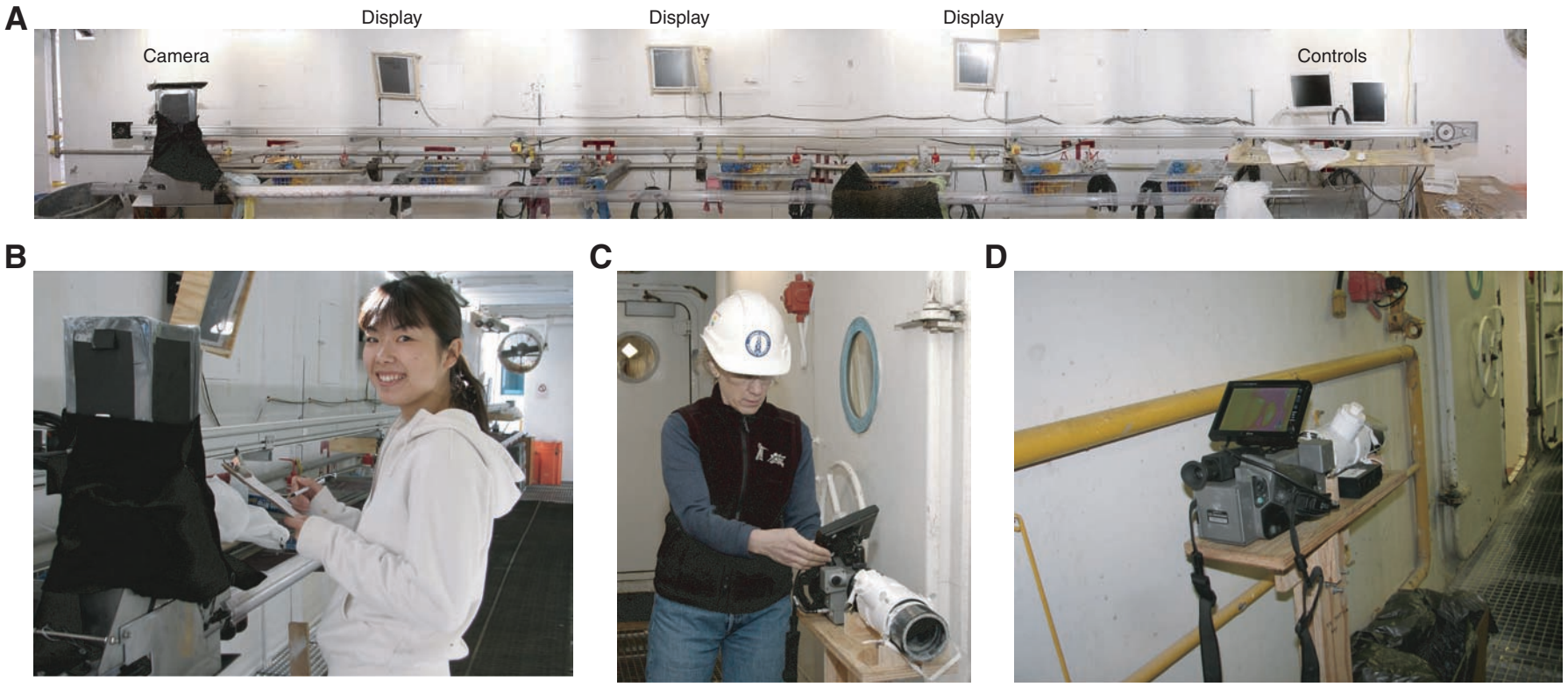

Figure F12. Gamma ray attenuation density calibration.

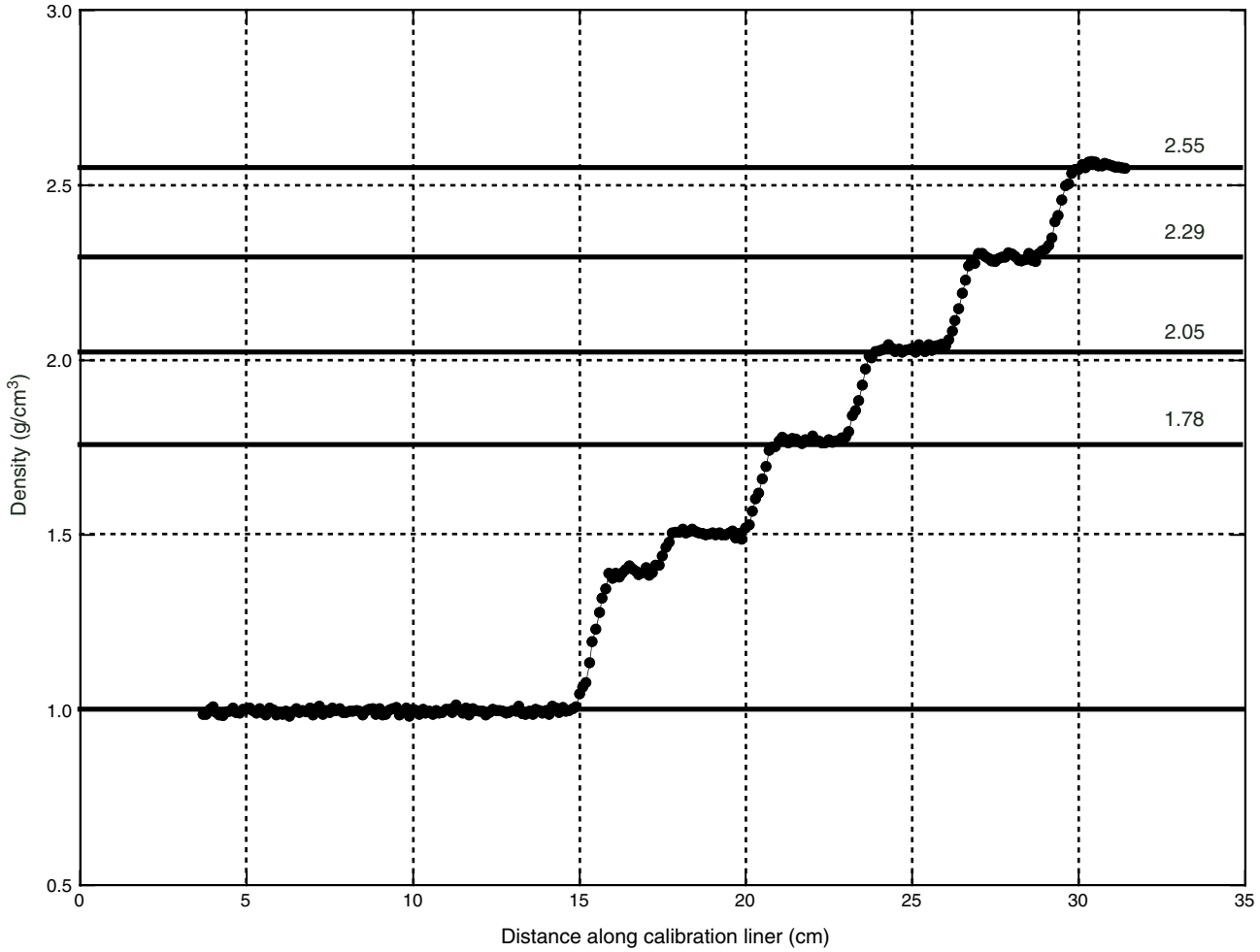

Figure F13. Calibration curves for noncontact resistivity. **A.** Voltage response to a range of salinities (given in parts per thousand). **B.** Best fit of resistivity values to the voltage response.

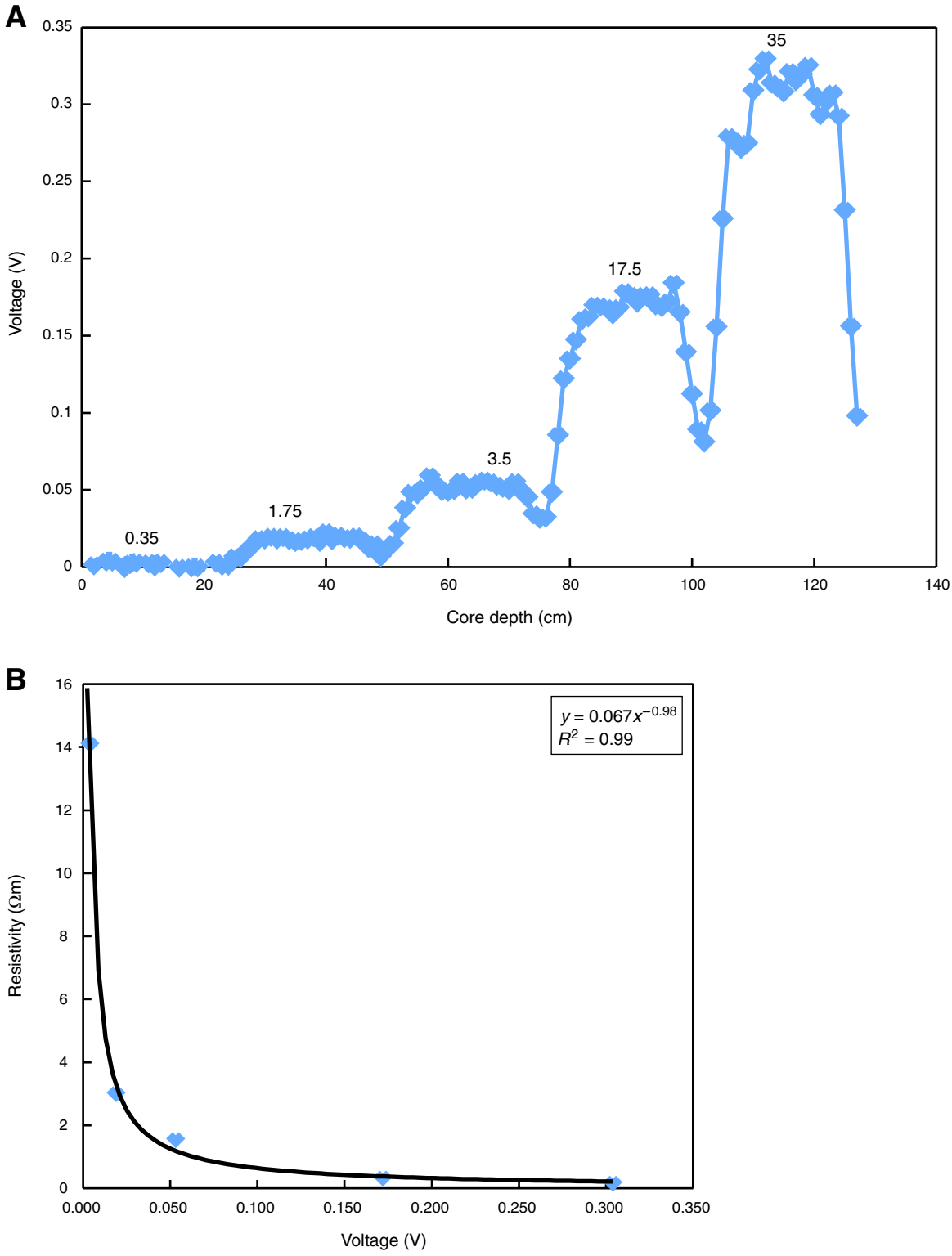

Figure F14. A. Contact method used to measure electrical resistivity. Current is passed between electrodes E1 and E4, and the potential difference is measured between E2 and E3. R1 and R2 are 5 kΩ resistors. **B.** Apparatus used to measure electrical resistivity. Probe is shown perpendicular to the core but can be moved so that it is parallel with the core section.

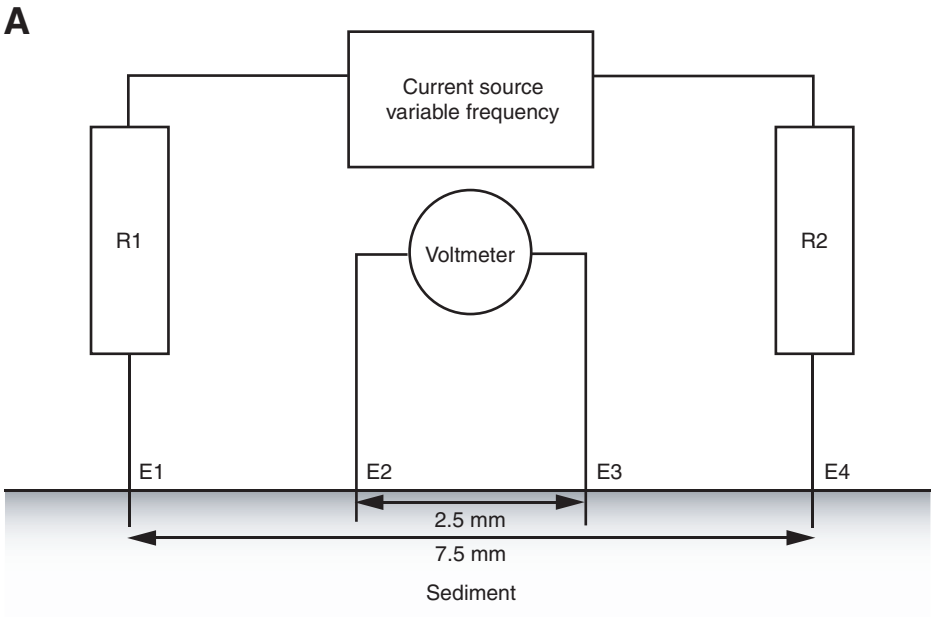

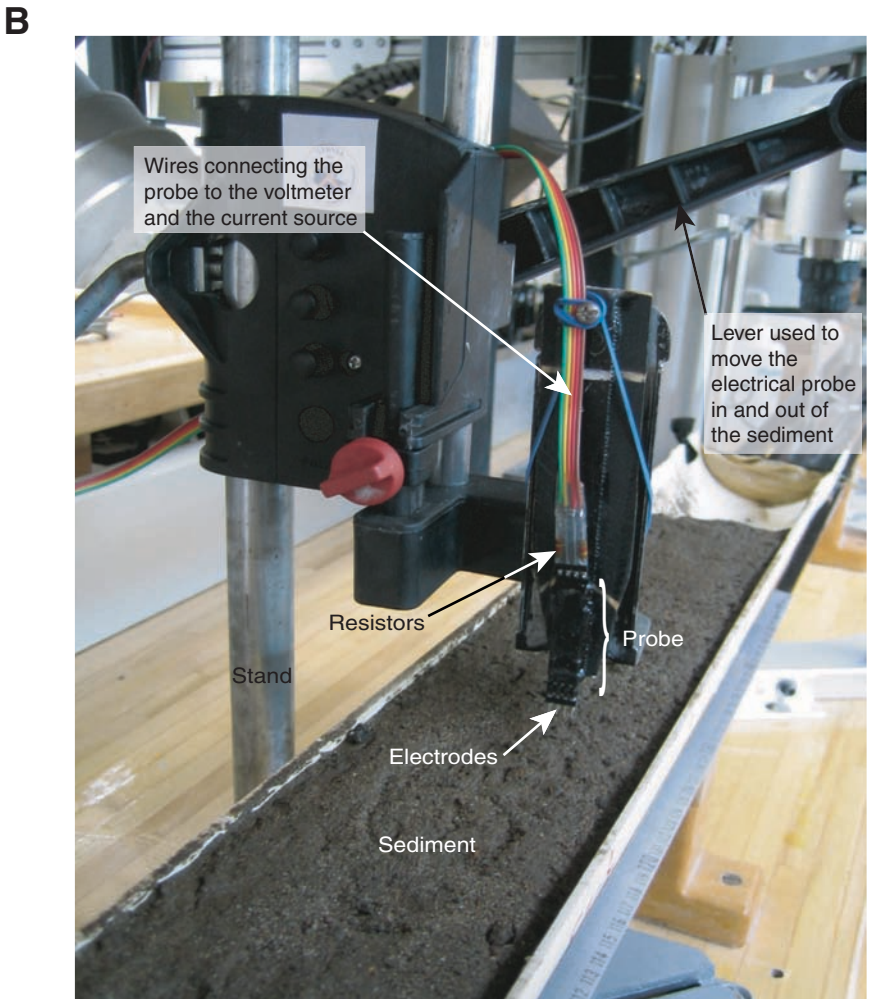

Figure F15. Orientations for *P*-wave velocity measurements on split cores. PWS = *P*-wave sensor.

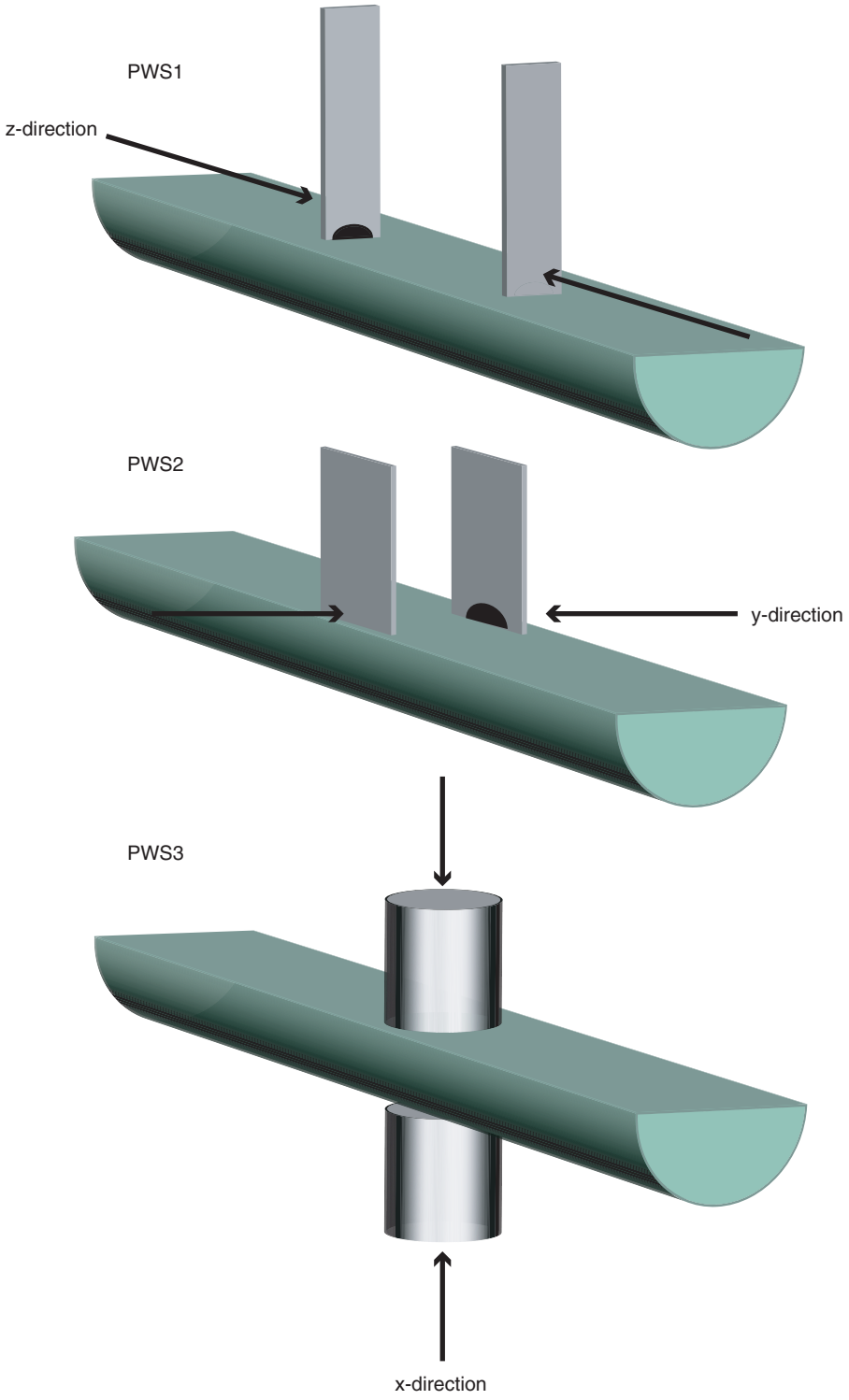

Figure F16. A. Typical advanced piston corer temperature (APCT) tool and third-generation advanced piston corer temperature (APCT-3; APC3 in figure) tool temperature history. **B.** Davis-Villinger Temperature Probe (DVTP) temperature history showing the different responses of the two thermistors (purple = lower, black = upper) on the probe.

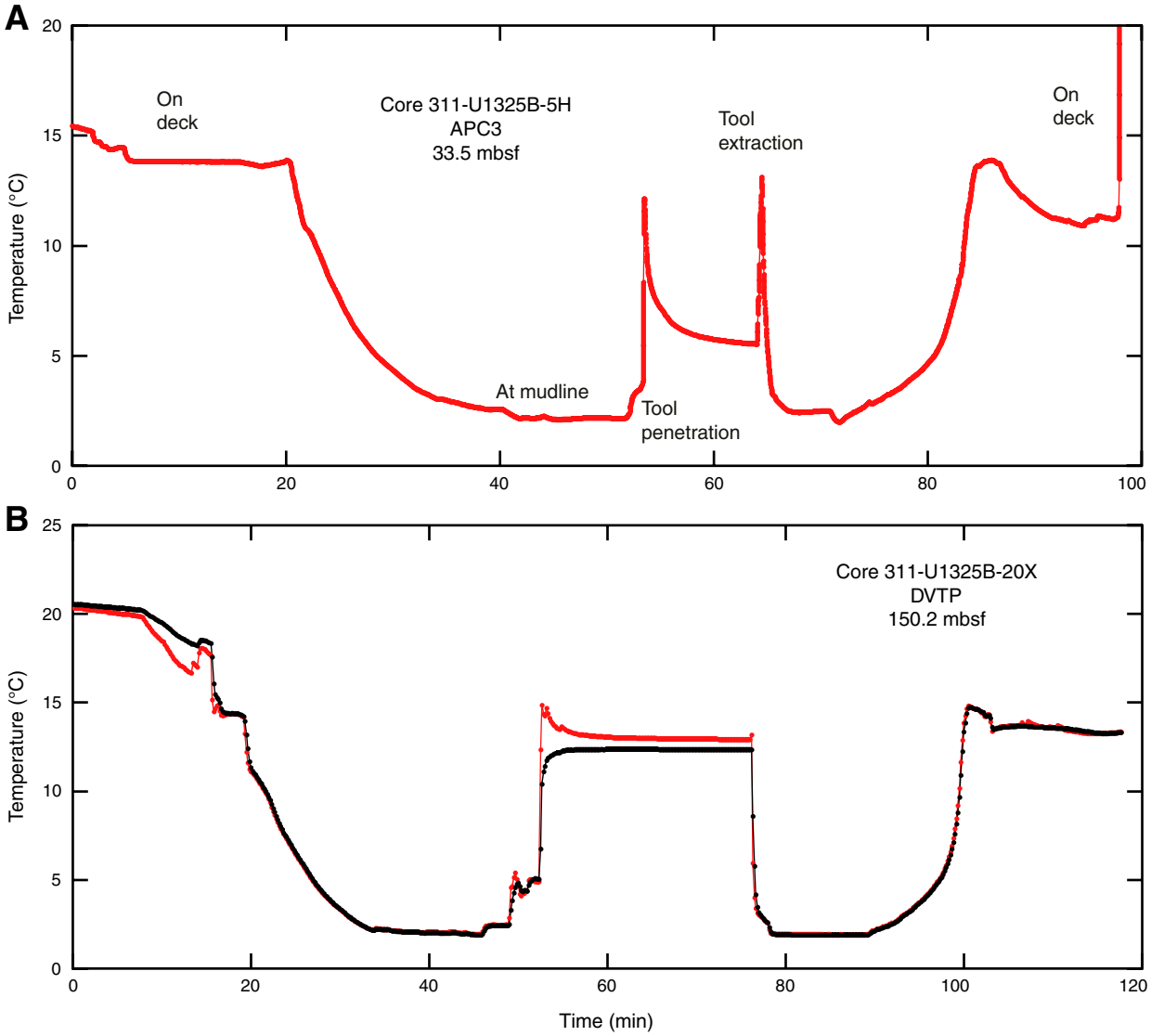

Figure F17. A. Gamma ray density profile (from the MSCL-V) and X-ray image (from the MSCL-P) of a pressure core sampler (PCS) core. The small bulge in the density profile at 44–55 cm depth is an artifact resulting from the interaction of the equipment with the PCS and is variable in size. X-ray data are not possible below a core depth of 51 cm because of the steel components inside the outer barrel. **B.** PCS to scale with A.

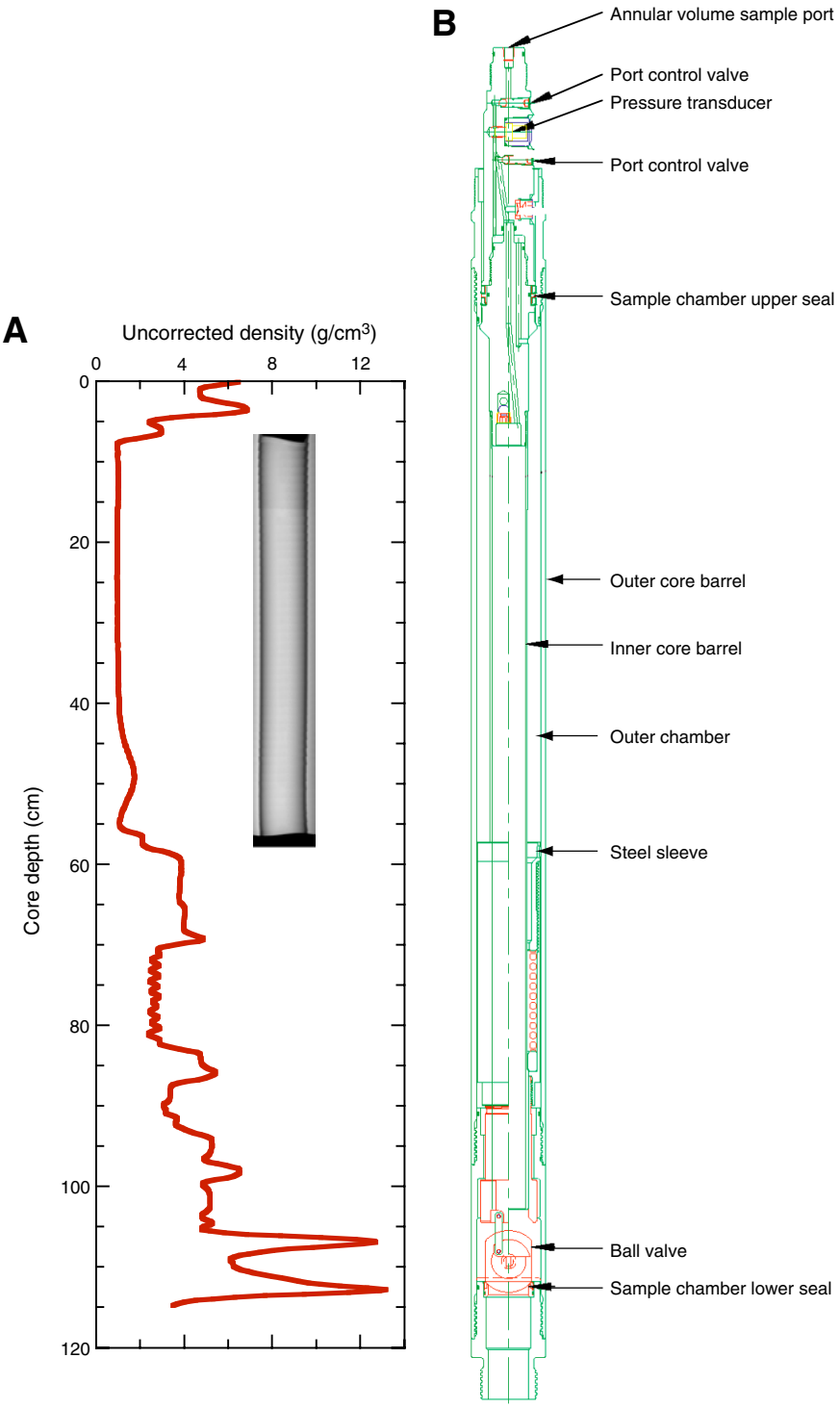

Figure F18. Fugro Pressure Corer (FPC) and the HYACE Rotary Corer (HRC). Common components are shown, where possible. PCD = polycrystalline diamond.

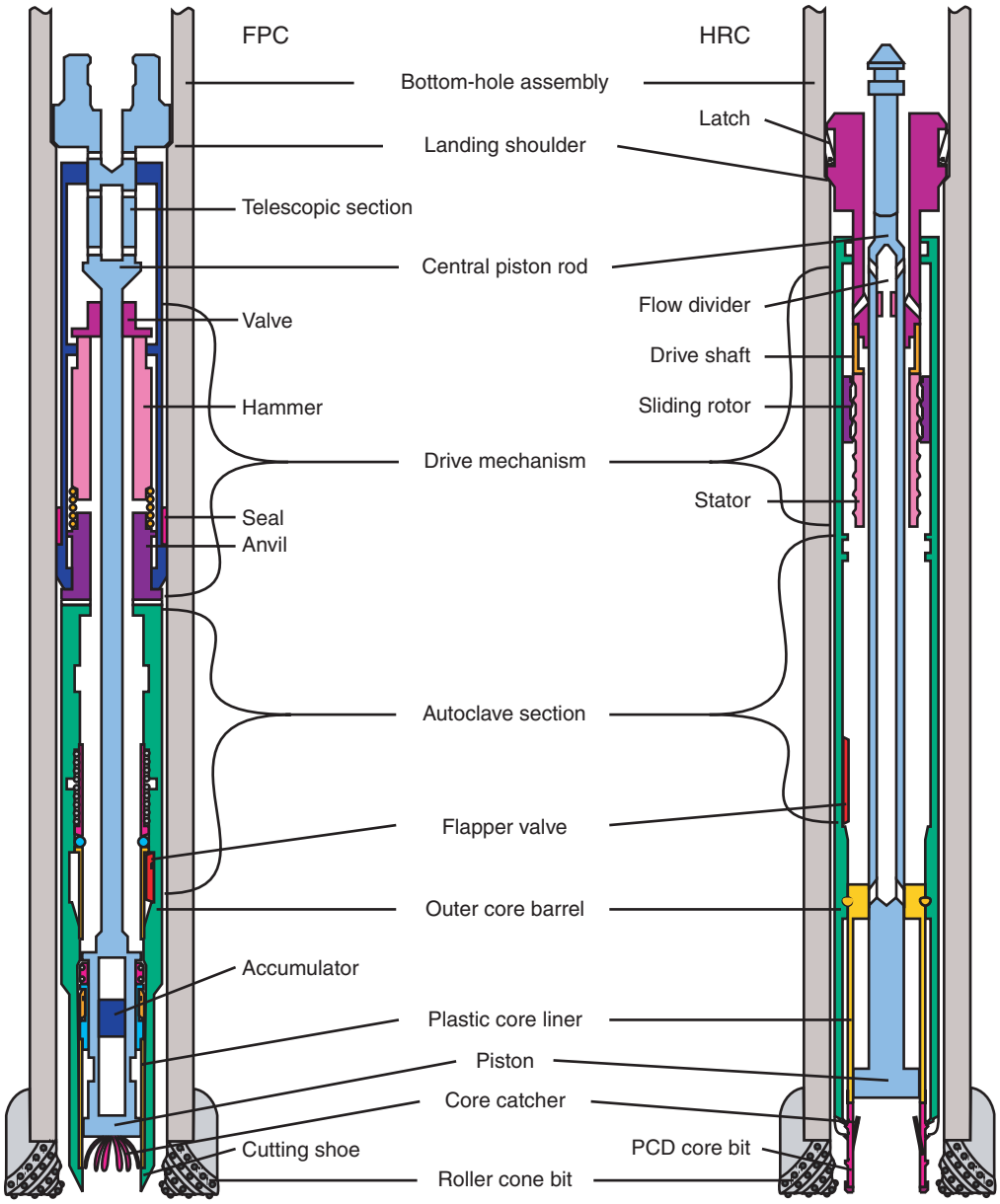

Figure F19. Pressurized HYACINTH core manipulation. **A.** "Start" position. **B.** "Catch" position after the autoclave has been attached with core under pressure. FPC = Fugro Pressure Corer, HRC = HYACE Rotary Corer. **C.** "Retract" position showing the core removed from the autoclave. **D.** "Log" position with the pressure multisensor core logger (MSCL-P) X-ray system in place. **E.** "Cut" position in the shear transfer chamber where the core liner is cut. **F.** "Push" position where the core is pushed into the storage chamber. **G.** "Store" position where the manipulator rod is retracted, the ball valve closed, and the core is free to be transported in the storage chamber.

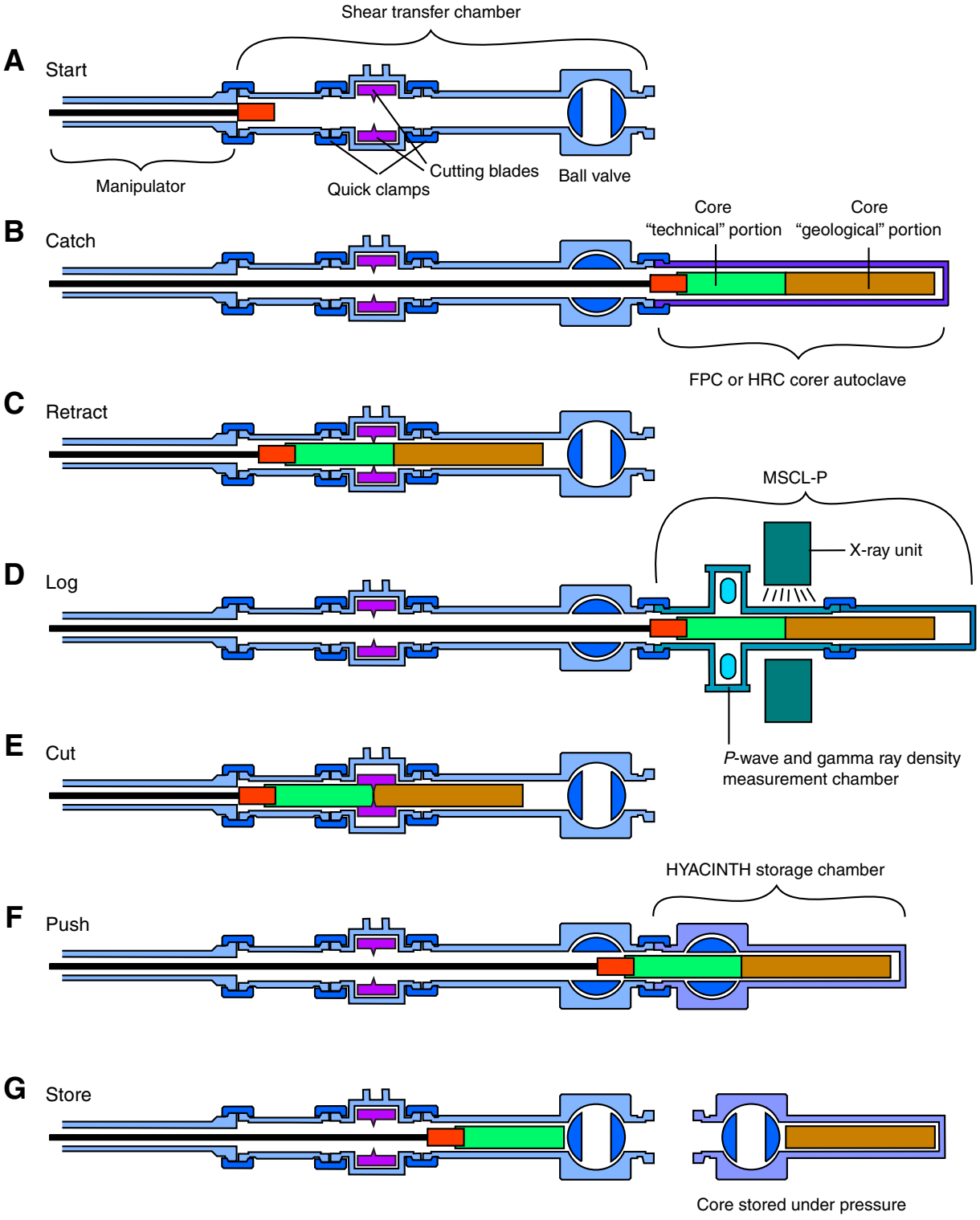

Figure F20. IODP core lab technician pouring water into the ice shuck, which hangs on the moonpool doors. Ice enters the shuck from the chute to the left, which leads to the subsea shack. The cores are lowered into the shuck from the drill floor above and aligned by eye.

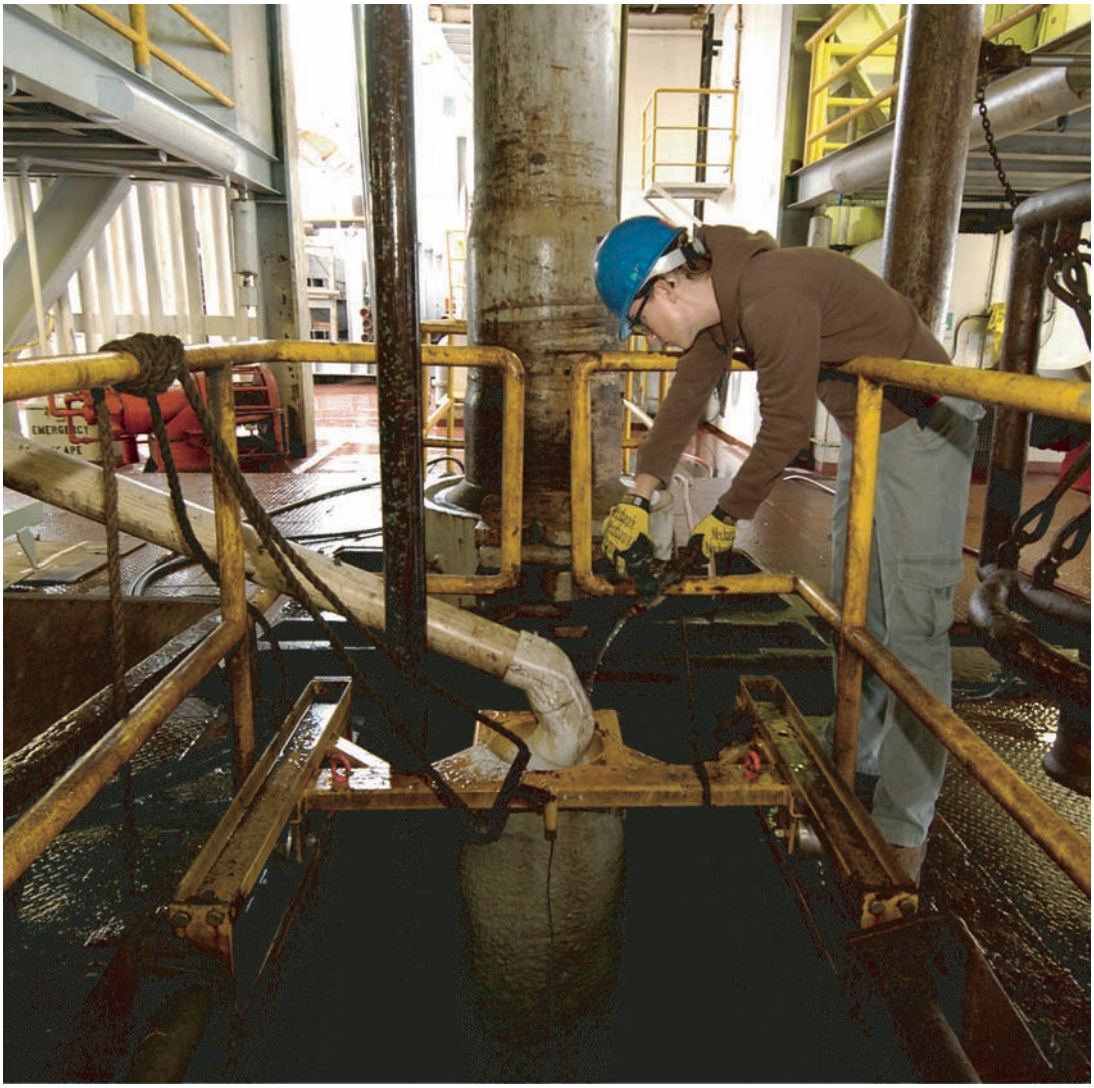

Figure F21. X-ray images of the inner aluminum liner in the PCS, illustrating the S-distortion of the images caused by the massive steel components in the PCS.

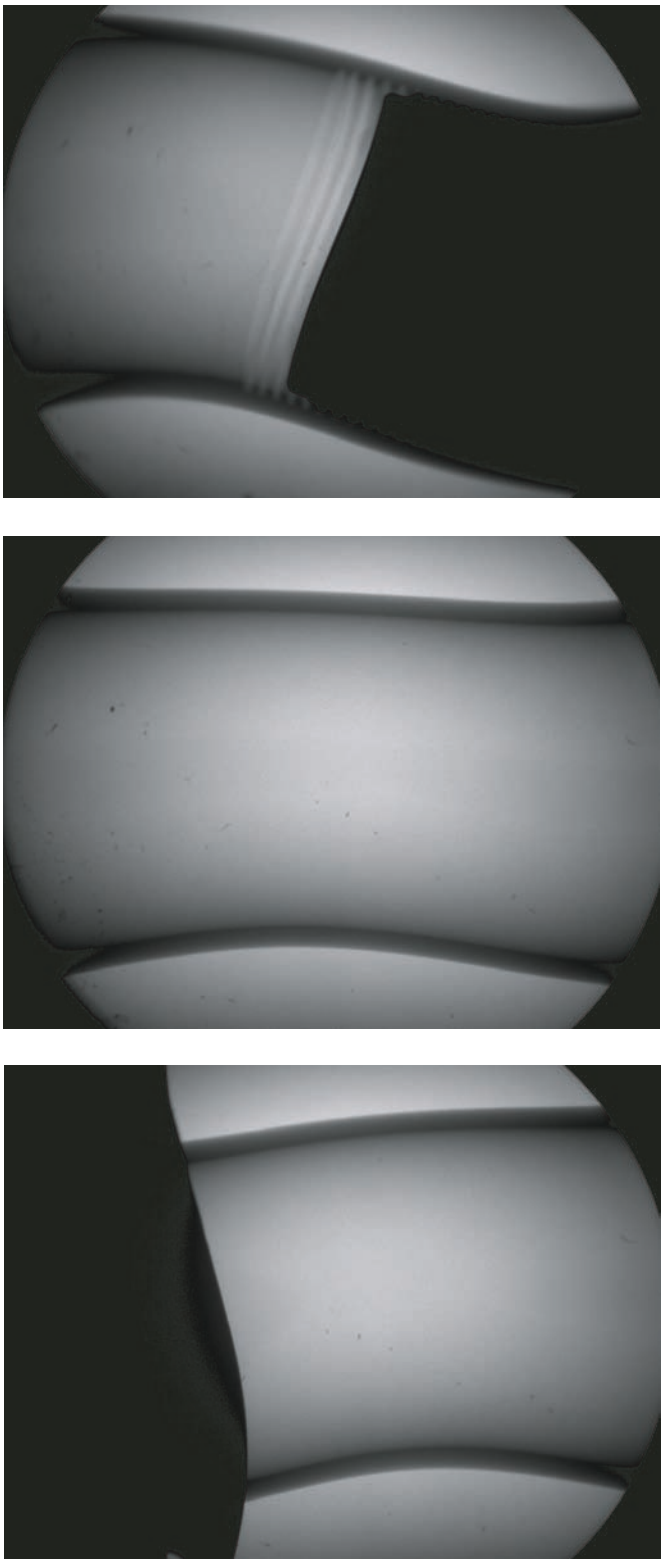

Figure F22. A PCS core being degassed while in the GeoTek vertical multisensor core logger, which is located in the PCS degassing van.

Figure F23. Interior of the HYACINTH logging van showing the long shear transfer chamber in the center with the GeoTek pressure multisensor core logger being adjusted at the far end. The storage chambers can be seen at the rear on the right side.

Figure F24. Interior of the PCS van showing the degassing equipment (bubbling chambers and degassing manifold) and the GeoTek vertical multisensor core logger in the background.

Figure F25. Manifold and bubbling chamber used for degassing experiments. He = helium tank used for flushing the degassing unit, NV = needle valve, BV = constant backpressure valve. For a complete depiction of the pressure coring system (PCS) see Figure **F17.**

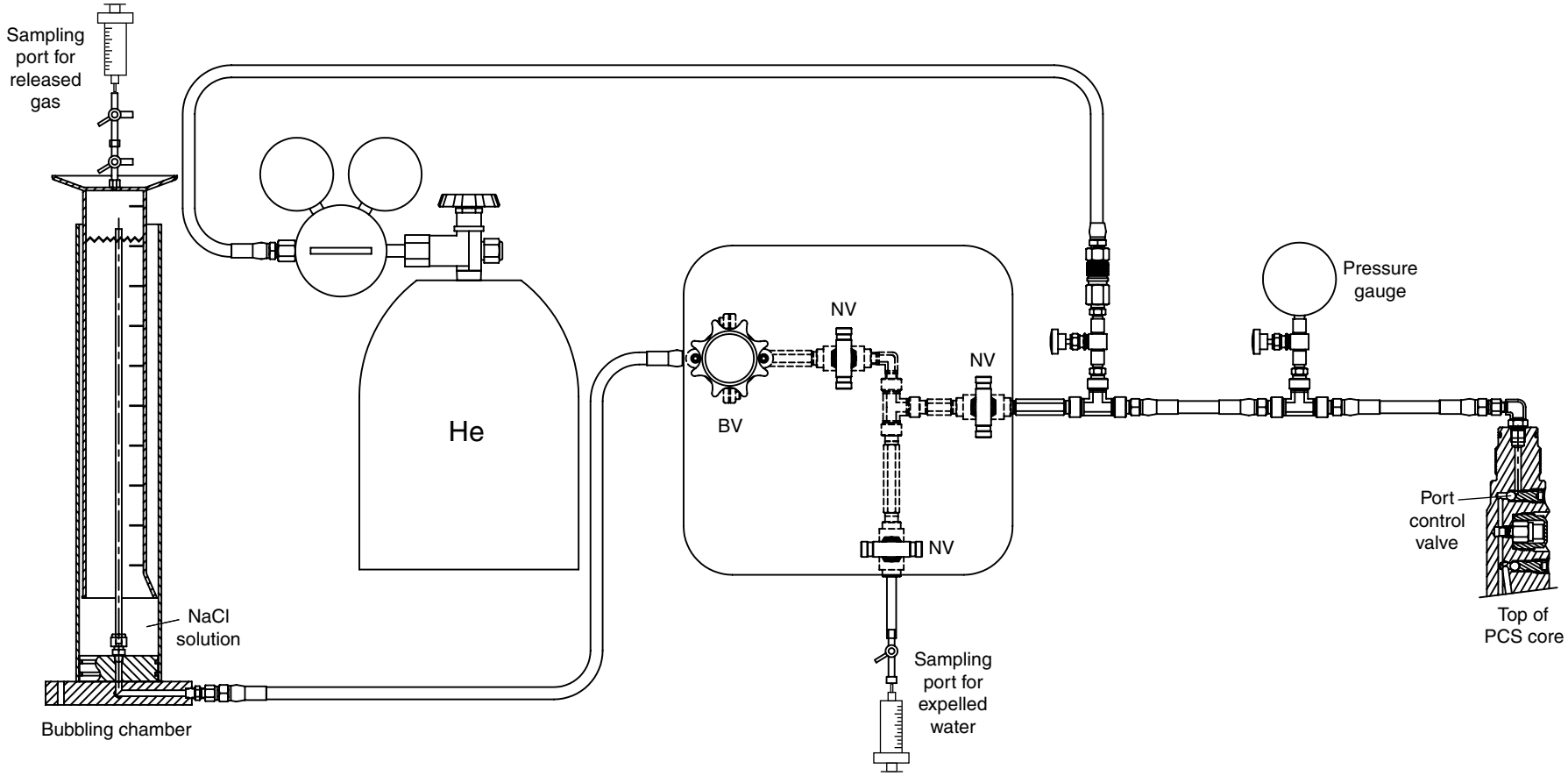

Figure F26. Bottom-hole assembly used for LWD operations. NMR = nuclear magnetic resonance, MWD = measurement while drilling, RAB = resistivity at the bit.

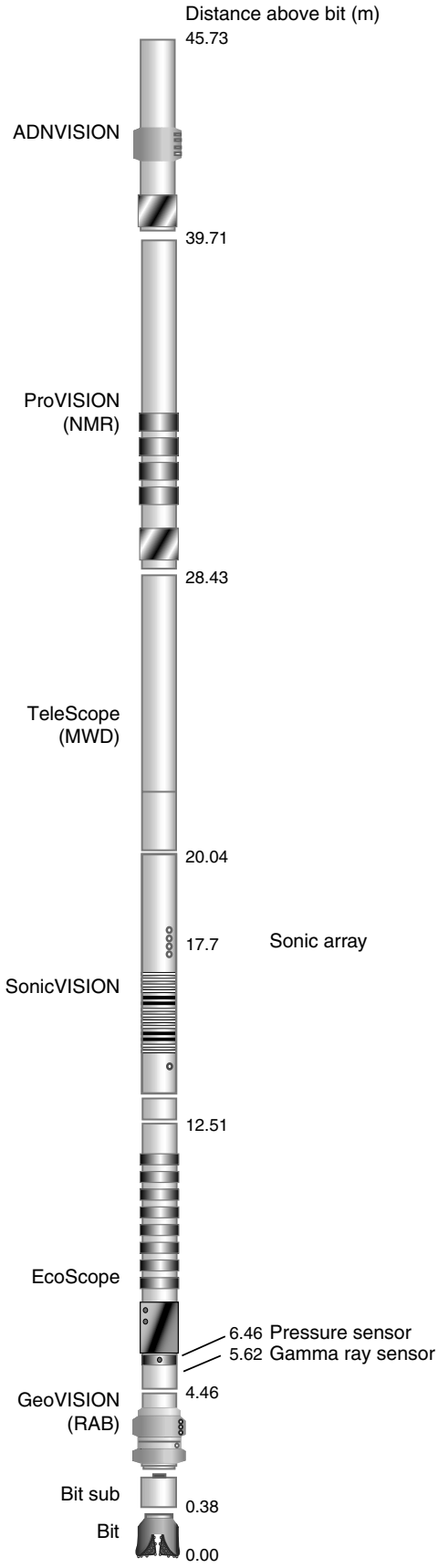

Figure F27. Decision tree used in gas monitoring based on LWD/MWD borehole fluid pressure measurements. Pressure increases were also monitored because they may be precursors to a gas flow pressure decrease. ROP = rate of penetration.

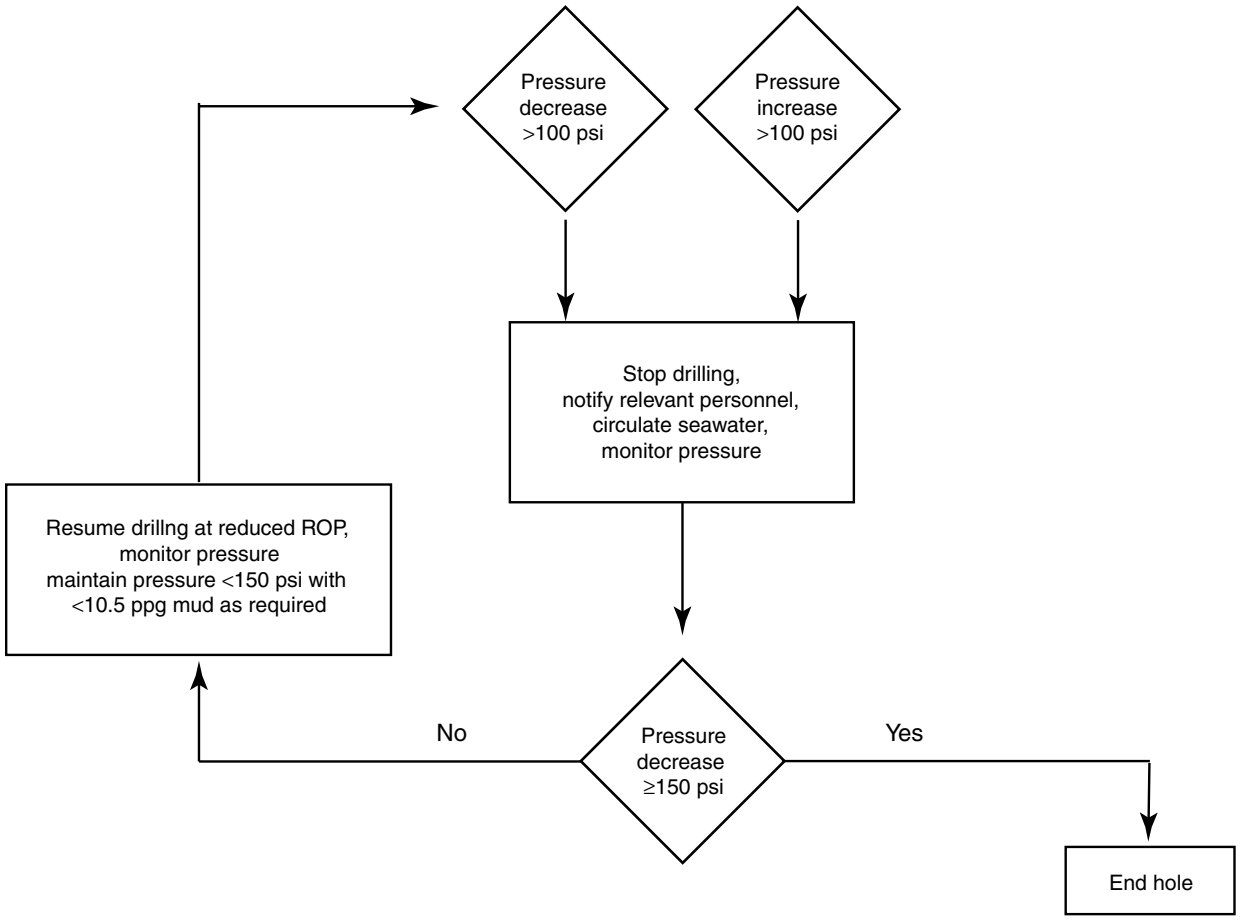

Figure F28. Tool strings used in wireline logging operations.

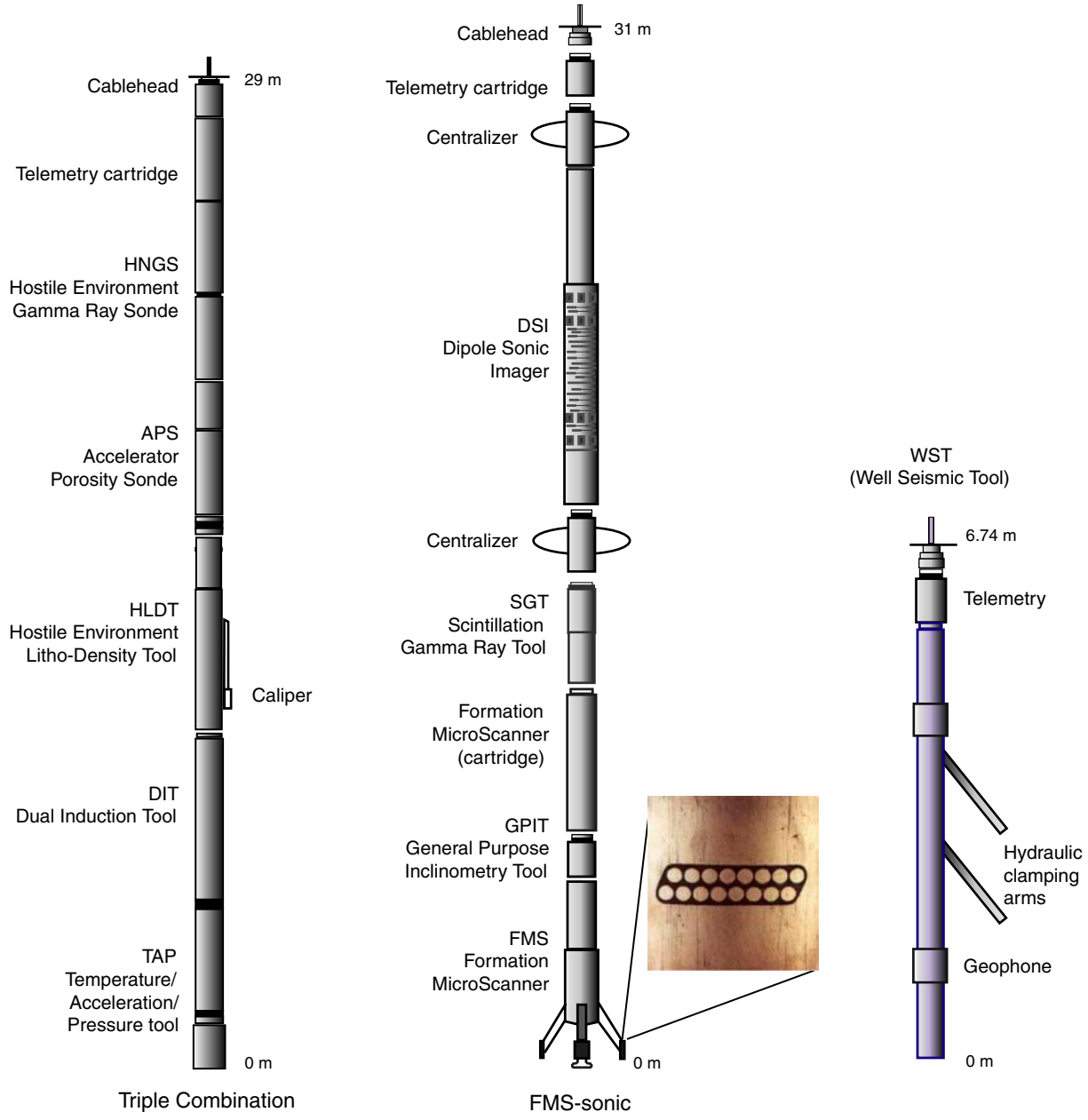

Table T1. Sample spreadsheet used for smear slide and thin section analyses.

Sample reference									Texture %			Biogenic %								Mineral %													Comments
Expedition	Site	Hole	Core	Type	Section	Top (cm)	Depth (mbsf)	Lithology	Sand	Silt	Clay	Diatoms	Foraminifers	Nannofossils	Radiolarians	Siliceous spicules & others	Silicoflagellates	Organic debris	Shell debris	Quartz	Feldspar	Volcanic glass	Muscovite	Biotite	Glauconite	Clay minerals	Carbonate	Calcite	Dolomite	Opaques	Pyrite	Accessory minerals	Rock fragments	
311	U1328	B	1	H	1	68	0.68	M	0	1	99									1						14	85							Semi-lithified carbonate concretion (1–5 µm crystals)
311	U1328	B	1	H	1	71	0.71	D	1	20	79	1	1					1		5	2	3				79	3			3		2		
311	U1328	B	1	H	2	123	2.73	M	16	28	56	1	5				1			17	8				8	56				1		3		
311	U1328	B	2	H	2	25	5.75	D	1	6	93			2						2	1					93	1			1				
311	U1328	B	4	P	1	15	14.65	D	1	8	91									3	2			1		91	1			1		1		
311	U1328	B	5	H	1	30	16.80	D	1	14	85		2	1						5	3			1		85	1			1		1		
311	U1328	B	6	X	1	30	18.70	D	1	22	77		4							8	3					77	2			5		1		
311	U1328	B	6	X	1	103	19.43	D	0	21	79	2		1		1				8						77	2			1	2	6		
311	U1328	B	6	X	2	128	20.83	M	60	40	0									60	20			2						6		12		Sand
311	U1328	B	8	H	2	40	29.90	D	0	20	80									10	7			1		80				1		1		
311	U1328	B	8	H	4	70	33.20	M	80	20	0									58	21			2	2		1			6		6	4	Sand
311	U1328	B	9	H	1	40	37.90	D	1	25	74	1	2	2		1				12	5			1		72	2			1		1		
311	U1328	B	9	H	3	70	41.01	M	80	18	2									55	25			3		2				4		6	5	
311	U1328	B	9	H	5	70	44.01	D	1	25	74	1	7	3						6	3	1				74	3			1		1		
311	U1328	B	9	H	5	143	44.74	M	95	5	0											93		1								1	5	Ash
311	U1328	B	10	H	1	55	47.55	D	2	25	73		15	7						6	2					66				3				
311	U1328	B	10	H	2	55	49.05	M	92	3	5									60	20			2			1					17		
311	U1328	B	10	H	3	55	50.55	D	1	25	74									9	5	2				74	2			3		5		
311	U1328	C	1	H	2	70	58.66	D	1	25	74	1	1					1		13	7			1		74				1		1		
311	U1328	C	1	H	4	61	61.54	M	55	45	0									55	25			5						4		5	6	
311	U1328	C	1	H	6	118	65.11	M	80	20	0									50	25			2						5		8	10	
311	U1328	C	2	H	1	25	66.25	M	60	40	0									51	26			3						3		7	10	
311	U1328	C	2	H	5	70	72.70	D	0	40	60	20						1		10	6			1		60				1		1		
311	U1328	C	3	H	1	80	76.30	D	2	23	75	3								6	4	3		2		75	2			3		2		
311	U1328	C	3	H	1	129	76.79	M	0	90	10									50	25											15	10	Sand
311	U1328	C	3	H	3	80	79.30	M	0	8	92							1		2	1	1				92	1			2				
311	U1328	C	3	H	5	79	82.29	D	2	27	71									13	7	2		2		71	2			1		2		
311	U1328	C	4	X	1	126	86.26	D	3	37	60									17	10			3		60	2			3		5		
311	U1328	C	4	X	3	72	88.72	M	20	45	35									24	15					35				6		10	10	Soupy
311	U1328	C	4	X	3	130	89.30	M	90	10	0									45	30									5		15	5	Sand
311	U1328	C	5	P	1	54	92.54	D	0	40	60	2				1		3		20	7			1		60				2		3	1	
311	U1328	C	6	H	1	77	94.77	D	0	8	92	1								3	2	1				92				1				
311	U1328	C	6	H	1	132	95.32	M	0	5	95									3										97				
311	U1328	C	6	H	3	80	97.70	D	0	21	79	1						1		6	3	2		1		80	3			2		1		
311	U1328	C	6	H	6	80	99.80	D	0	10	90	1								3	1	1		1		90	2			1				
311	U1328	C	6	H	CC	20	102.79	D	2	17	81	1	3	3				1		4	1					81	2			3		1		
311	U1328	C	7	X	1	80	104.30	D	1	9	90	2	1	9		1		1		1	1					81	1			1		1		
311	U1328	C	7	X	1	134	104.84	M	70	20	10	1		1				4		46	26	2				10				3		2	5	

Note: M = minor lithology, D = dominant lithology.

Table T2. Error statistics for shipboard ICP-AES measurements.

Error	Ca (mM)	K (mM)	Mg (mM)	Na (mM)	B (µM)	Ba (µM)	Li (µM)	H_4SiO_4 (µM)	Sr (µM)
Average	10.46	10.60	53.59	476	1849	204	577	1279	680
Actual	10.55	10.44	54.00	480	1850	205	577	1282	686
Error (%)	–1	2	–1	–1	0	0	0	0	–1
1σ	0.21	0.27	2.35	11.75	19.00	5.73	9.20	13.50	9.61
Variance (%)	0.02	0.03	0.04	0.02	0.01	0.03	0.02	0.01	0.01

Table T3. Measurement acronyms, units, vertical resolutions, and depths of investigation (where available) of LWD tools deployed during Expedition 311.

Tool	Output	Tool name/Explanation of output	Unit	Vertical resolution (cm)	Depth of investigation (cm)
ADNVISION		Azimuthal Density Neutron tool			
	DCAV	Density caliper	inches		
	TNPH	Thermal neutron porosity	%	31	
	PEF	Photoelectric factor	b/e^-		
	RHOB	Density	g/cm^3	15	
	IDRO	Image-derived density	g/cm^3		
		Oriented density images of borehole wall			
EcoScope		Multifunction tool			
	AXXH, AXXL, AXXB	Attenuation resistivity at source-receiver spacing XX, where XX = 16, 22, 28, 34, 40 inches	Ωm	55–122	48–102
	PXXH, PXXL, PXXB	Phase-shift resistivity at source-receiver spacing XX, where XX = 16, 22, 28, 34, 40 inches	Ωm	21–30	33–79
	GRMA_FILT	Calibrated, filtered gamma ray	gAPI	46	
	DCAV	Density caliper	inches		
	UAV	Ultrasonic caliper	inches		
	IDPE	Image-derived photoelectric factor	b/e^-		
	TNPH	Thermal neutron porosity	%	31	
	BPHI	Best thermal neutron porosity	%		
	RHOB	Density	g/cm^3	15	
	IDRO	Image-derived density	g/cm^3		
		Oriented density images of borehole wall			
GeoVISION		Resistivity-at-the-Bit tool			
	GR_RAB_FILT	Calibrated, filtered gamma ray	gAPI	46	
	RBIT	Bit resistivity	Ωm	30–61	81
	RING	Ring resistivity	Ωm	8–10	55–64
	BDAV	Deep button resistivity average	Ωm	5–8	44–61
	BMAV	Medium button resistivity average	Ωm	5–8	38–53
	BSRAV	Shallow button resistivity average	Ωm	5–8	28–41
		Oriented resistivity images of the borehole wall		5–8	
ProVISION		Nuclear Magnetic Resonance tool			
	MRP	Magnetic resonance porosity	%	15–120	7
	BFV	Bound fluid volume	%		
	FFV	Free fluid volume	%		
	T2LM	Log mean T2 relaxation time	ms		
	T2	T2 distribution (30 values at each depth)	%		
SonicVISION		Sonic tool			
	DTCC	Compressional wave slowness	µs/ft	61	~10

Note: Output: H = 2 MHz resistivity, L = 400 kHz resistivity, B = blended resistivity. For the complete list of acronyms used in IODP and for additional information about tool physics, consult IODP-USIO Science Services, LDEO, at **iodp.ldeo.columbia.edu/TOOLS_LABS/tools.html.**

Table T4. Measurement acronyms, units, vertical resolutions, and depths of investigation (where available) of wireline logging tools deployed during Expedition 311.

Tool	Output	Tool name/Explanation of output	Unit	Vertical resolution (cm)	Depth of investigation (cm)
APS		Accelerator Porosity Sonde			
	APLC	Near array porosity (limestone calibrated)	%	43	
	SIGF	Formation capture cross section	Capture unit	31	
	STOF	Tool standoff (distance from borehole wall)	inch		
DIT		Dual Induction Tool			
	IDPH	Deep induction resistivity	Ωm	246	122–158
	IMPH	Medium induction resistivity	Ωm	185	66–79
	SFLU	Spherically focused resistivity	Ωm	61	41
DSI		Dipole Sonic Imager			
	DTCO	Compressional wave slowness	µs/ft	107	~10
	DTSM	Shear wave slowness	µs/ft	107	~10
	DTST	Stoneley wave slowness	µs/ft	107	~10
FMS		Formation MicroScanner			
	C1, C2	Orthogonal hole diameters	inch		
	P1AZ	Pad 1 azimuth	Degree		
		Oriented resistivity images of borehole wall		0.5	2
GPIT		General Purpose Inclinometer Tool			
	DEVI	Hole deviation	Degree		
	HAZI	Hole azimuth	Degree		
	F_x, F_y, F_z	Earth's magnetic field (three orthogonal components)	Oersted		
	A_x, A_y, A_z	Acceleration (three orthogonal components)	m/s^2		
HLDT		Hostile Environment Litho-Density Tool			
	RHOB	Bulk density (corrected)	g/cm^3	46	
	PEF	Photoelectric effect	b/e^-		
	CALI	Caliper (borehole diameter)	inch		
	DRHO	Bulk density correction	g/cm^3		
HNGS		Hostile Environment Gamma Ray Sonde			
	HSGR	Standard (total) gamma ray	gAPI	51	
	HCGR	Computed gamma ray (minus uranium contribution)	gAPI	51	
	HFK	Potassium	wt%	51	
	HTHO	Thorium	ppm	51	
	HURA	Uranium	ppm	51	
SGT		Scintillation Gamma Ray Tool			
	ECGR	Environmentally corrected gamma ray	gAPI	46	
TAP		Temperature/Acceleration/Pressure	°C, m/s^2, psi		
WST		Well Seismic Tool			

Note: For the complete list of acronyms used in IODP and for additional information about tool physics, consult IODP-USIO Science Services, LDEO, at **iodp.ldeo.columbia.edu/TOOLS_LABS/tools.html.**